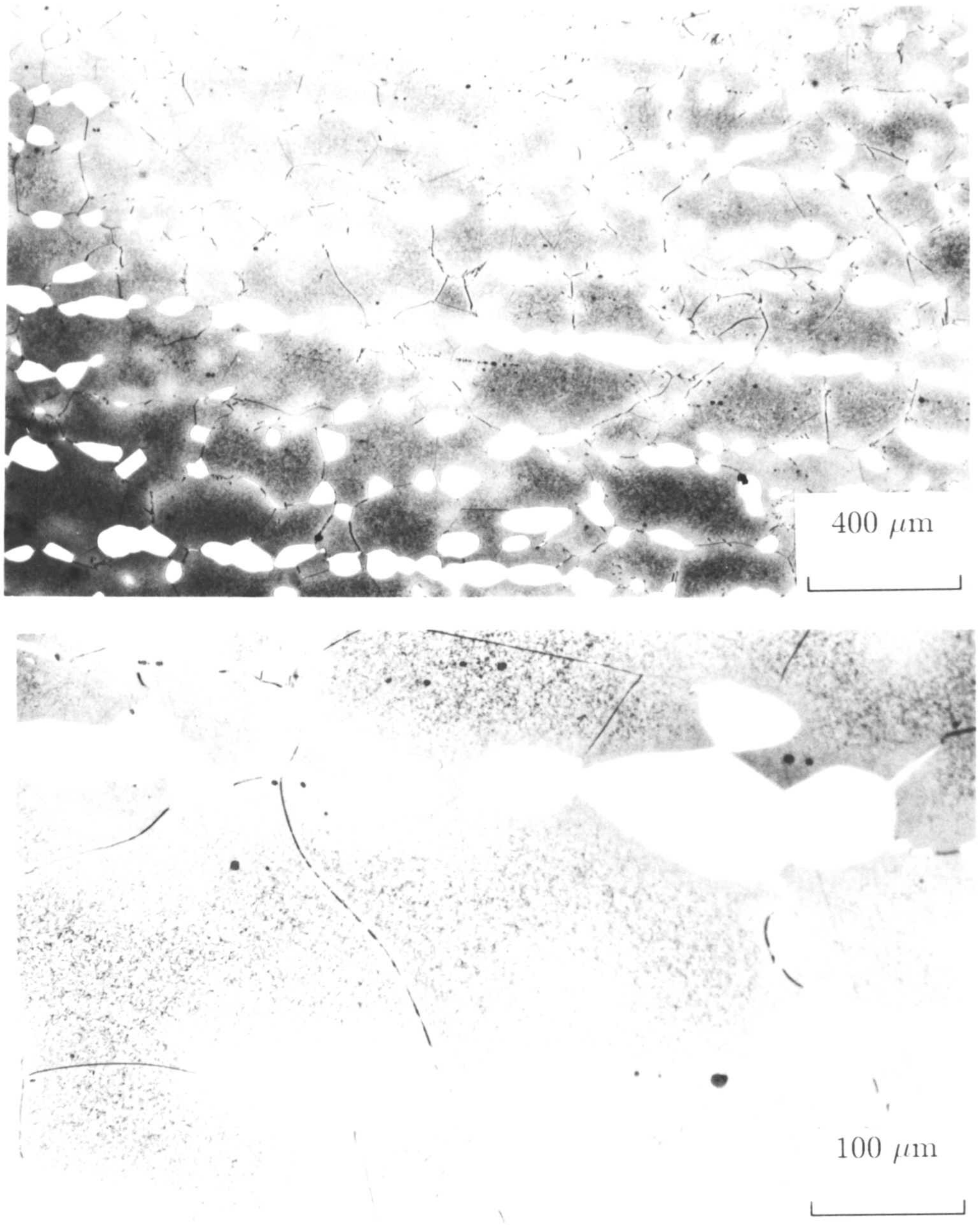

Figure 5.19. Light micrographs showing the microstructure of duplex rolled metal IC381 solution treated at 1300 °C for 26 hours and then quenched into water. The light phase is austenite and the dark one is ferrite. TEM observations (Figure 5.22) show that the fine particles inside the ferrite grains are austenite formed during quenching. The measured volume fraction of austenite (excluding fine particles) is about 0.19.

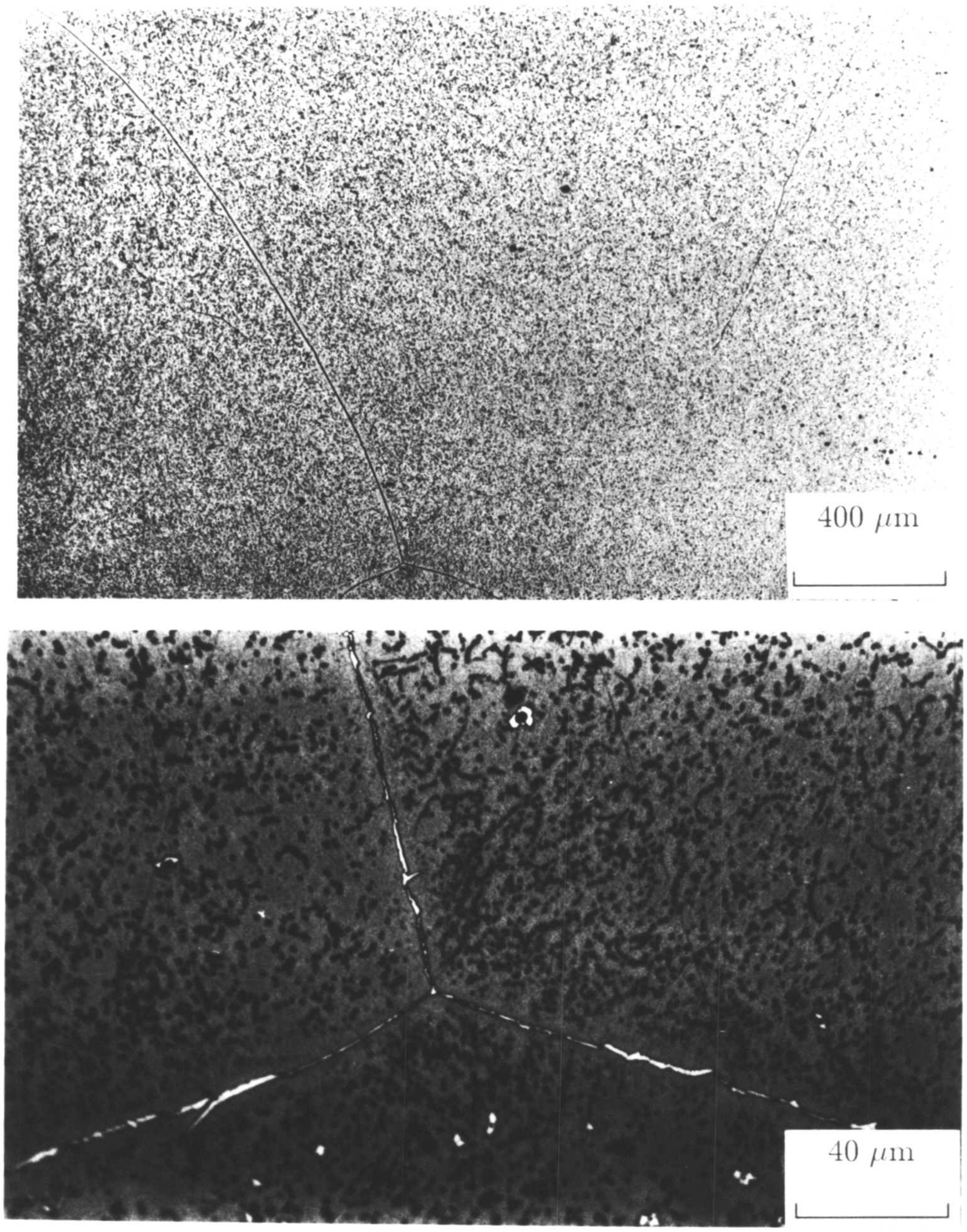

Figure 5.20. Light micrographs showing the microstructure of duplex rolled metal IC373 solution treated at 1300 °C for 26 hours and then quenched into water. Austenite has precipitated mainly at grain boundaries and on inclusions at the elevated temperature. The fine particles inside the ferrite grains are austenite formed during quenching. The measured volume fraction of austenite (excluding fine particles) is less than 0.05.

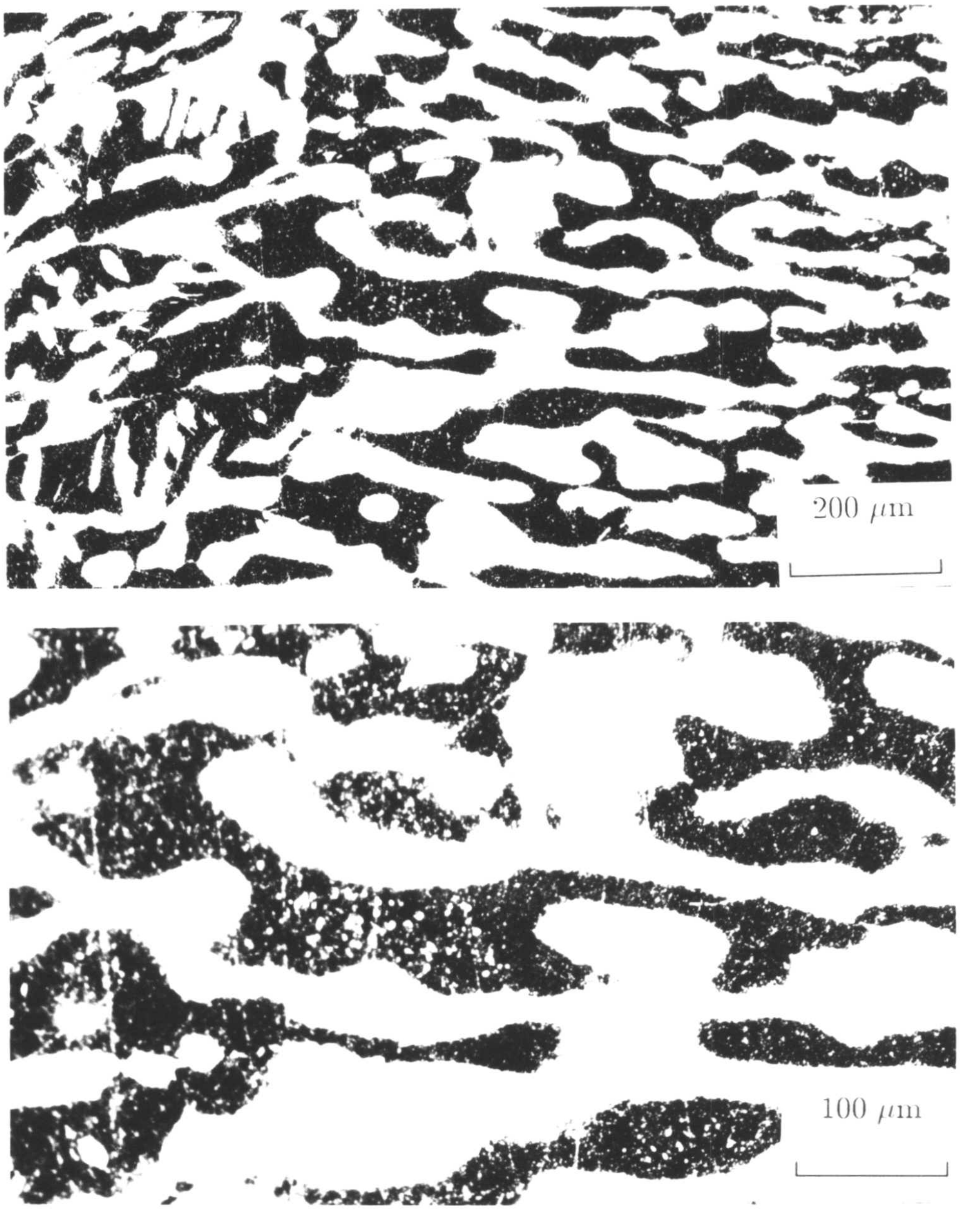

Figure 5.21. Light micrographs showing the microstructure of super duplex weld metal A219 solution treated at 1300 °C for 26 hours and then quenched into water. The measured volume fraction of austenite (excluding fine particles) is less than 0.53.

Figure 5.20 shows the microstructure of duplex rolled metal IC373 is almost wholly ferritic at 1300 °C. Note again that the TEM observations (Figure 5.22) show that the fine precipitates inside the ferrite grains are austenite formed during quenching. Figure 5.23 confirms that the matrix has a b.c.c crystal structure whereas the particle (Figure 5.24) has an f.c.c crystal structure. Figure 5.25 shows clusters of fine austenite particles in the same specimen, the clusters presumably being due to autocatalytic nucleation in which the formation of one particle stimulates others. TEM EDX microanalysis shows that the chemical composition of these precipitates (Table 5.3) is the same as the matrix as far as the substitutional alloying elements are considered. This contrasts with the partitioning of alloying elements between the coarser ferrite and austenite grains (see chapter six).

Table 5.3. TEM EDX microanalysis of δ-ferrite matrix and fine austenite in duplex rolled metal IC373 solution treated for 26 hour (concentrations are in wt.%).

Phase	Fe	Cr	Ni	Mo	Mn	Si
δ-ferrite	62.40±0.94	27.50±0.95	5.13±0.27	2.85±0.64	1.69±0.82	0.43 ±0.11
fine austenite	62.20±0.46	27.24±0.25	5.48±0.24	2.04±0.46	2.50±0.26	0.54 ±0.17

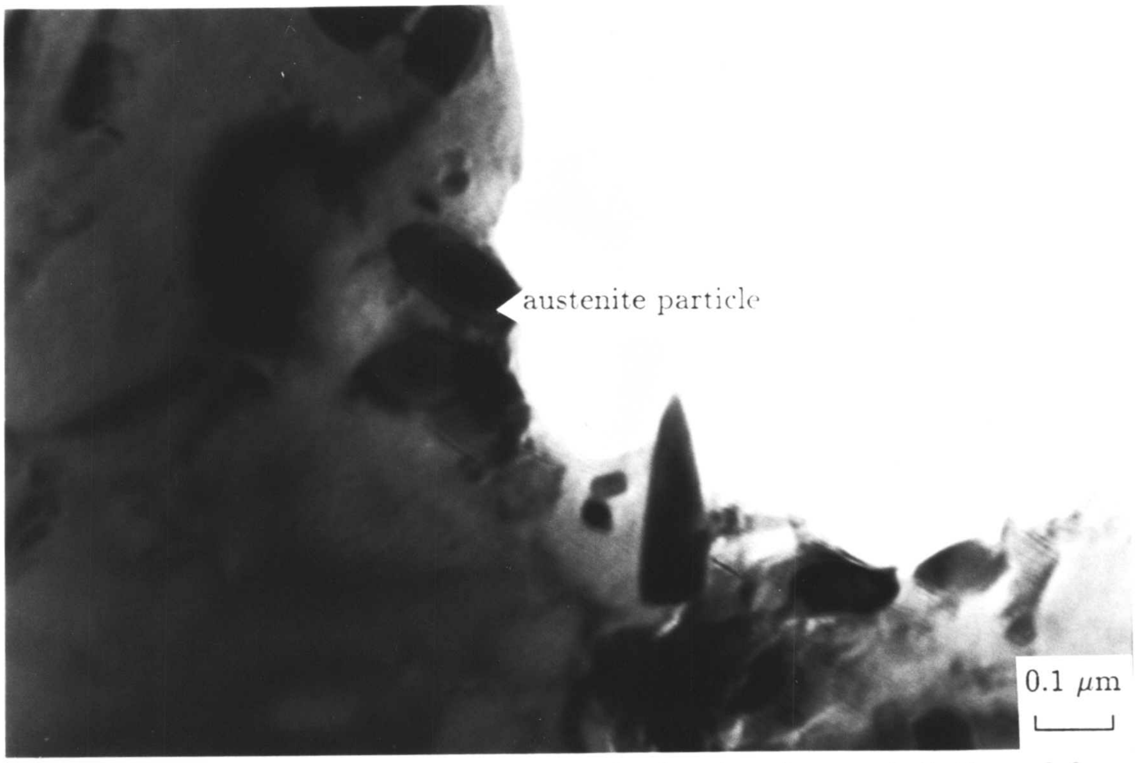

Figure 5.22. TEM bright field micrograph showing the precipitation of fine austenite particles inside δ-ferrite grain in duplex rolled metal IC373 solution treated at 1300 °C for 26 hours.

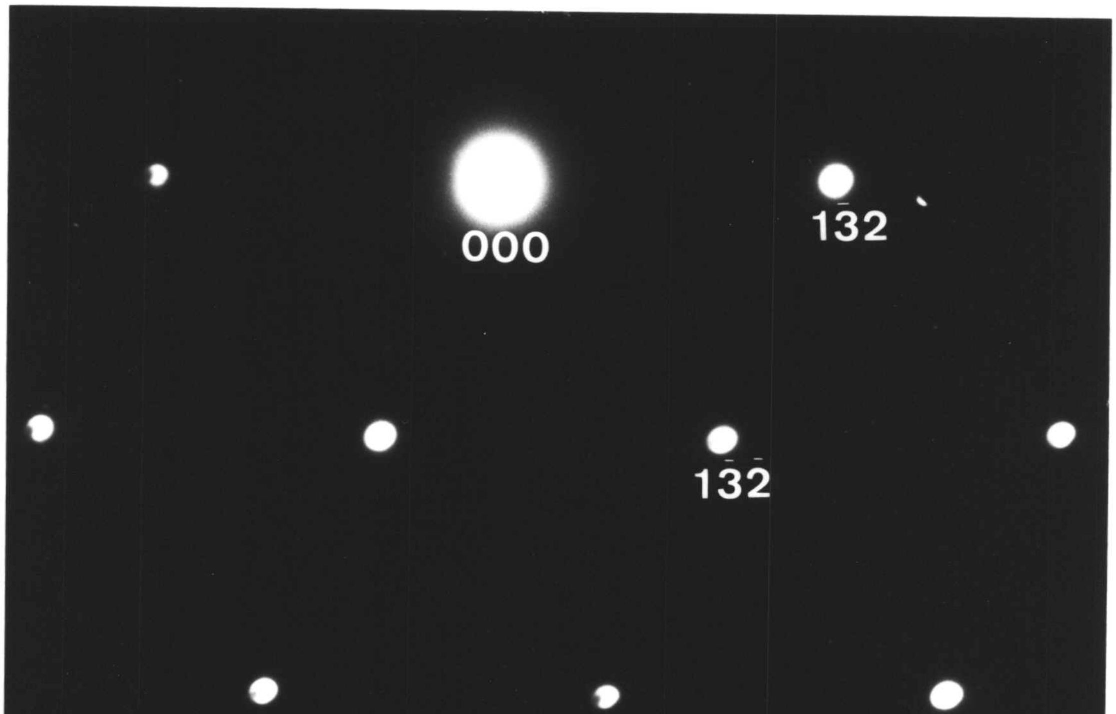

Figure 5.23. SADP of the matrix (δ-ferrite grain in Figure 5.22) showing that its crystal structure is b.c.c. The zone direction of diffraction pattern is [310].

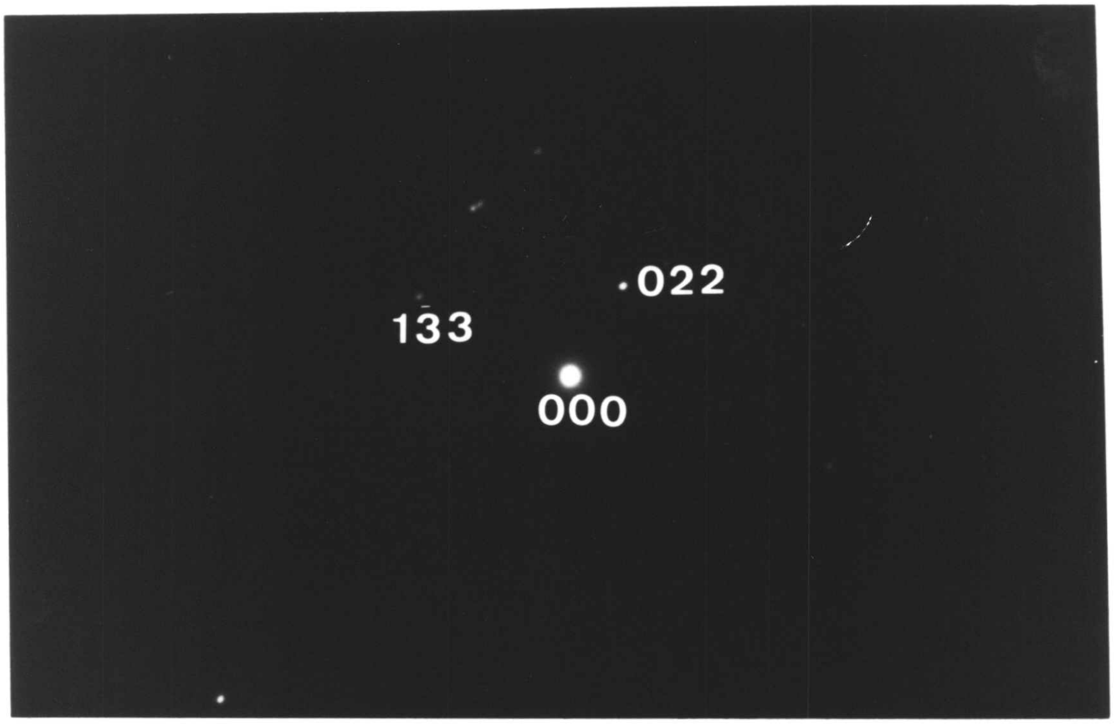

Figure 5.24. SADP of the particle (indicated in Figure 5.22) showing that it has an f.c.c. crystal structure. The zone direction of diffraction pattern is [61$\bar{1}$].

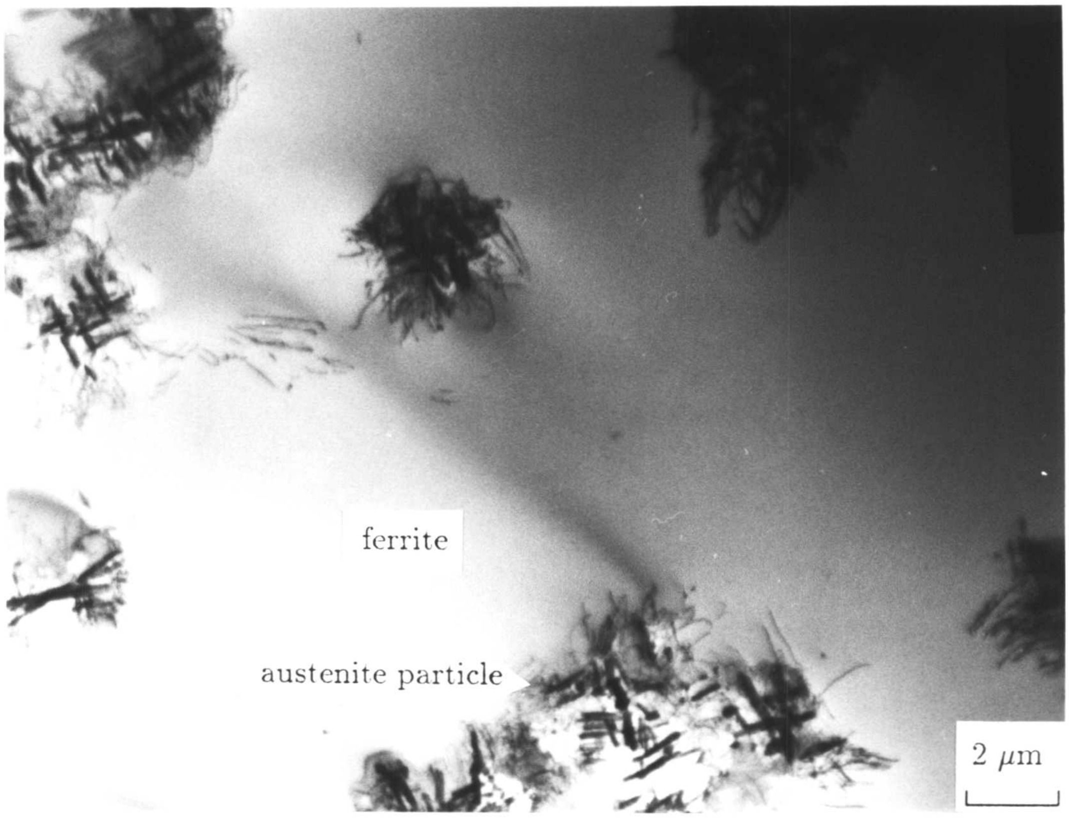

Figure 5.25. TEM bright field micrograph showing the precipitation of fine austenite in cluster form in duplex rolled metal IC373 solution treated at 1300 °C.

5.6 Laser Welding

To investigate the solidification mode of different types of stainless steels and to elucidate the role of austenite and ferrite nucleation on the solidification behaviour a series of laser welds traversing stainless steels of different chemical compositions was studied. Table 5.4 shows the steel grades used in this investigation. The solidification modes shown in the table are those predicted according to the Suutala (1983) model. The chemical compositions of the steels are listed in Table 2.1 and the welding conditions are presented in section 2.3. To ensure full penetration during welding the thickness of the plates was reduced to 0.5 mm by rolling. The welds were made on thin sheet couples of stainless steels of two different compositions butted together (e.g. 904L/IC373), the weld starting on a sheet of one composition and running into the other across the junction (Figure 2.1).

Figure 5.26 to 5.28 show the microstructures of laser weld metals of these alloys in the undiluted regions far from the junctions. The microstructure of laser weld metal of 904L (Figure 5.26) consists of austenite dendrites with interdendritic δ-ferrite showing that the solidification mode is austenitic-ferritic. Figure 5.27 shows that the microstructure of laser weld metal of A219 consists of dendritic and Widmanstätten austenite and ferrite grains. This confirms that the solidification mode is ferritic-austenitic. The ferrite dendrites are invisible as the result of solid state transformation (δ-ferrite to austenite). The microstructure of laser weld metal of IC373 (Figure 5.28) consists of elongated ferrite grains in the weld direction with precipitation of austenite mainly at the grain boundaries. This confirms that the solidification mode is fully ferritic.

5.6.1 Dilution

For the dissimilar joint configuration examined in this study, in which the weld starts from alloy A (Figure 2.1) and the weld direction is normal to the metal junction, dilution in weld pool will start as the front of the weld pool crosses the interface between alloys A and B. To measure the variation of composition with distance from the metal junction a scanning electron microscope equipped with an energy dispersive X-ray analysis system was used (see section 2.10). The differences in composition of the individual phases present in the microstructure did not influence the measurements since the compositions were evaluated over a rastered area (about 0.9×0.12 mm) that was very large compared with the scale of the microstructure (a few micrometres). Measurements were made along the welding direction at the centre of the weld. Only the major constituents were analysed, namely Fe, Cr, Ni, Mo, Mn and Si, and the concentrations of these elements were normalised to 100 wt.%. In addition, limited measurements were also made on the individual phases present in microstructure in order to identify them. The variation of composition with distance for different welds are plotted in Figure 5.29 to 5.31. All the profiles show a rather steep initial change in composition followed by a more gradual decline to the composition of the undiluted alloy (alloy B). With the welding conditions used (see section 2.3) the length of the transition zone (the zone that the composition changes completely from alloy A to alloy B) was found to be not greater than 5-6 mm.

Table 5.4. Steel grades used in this investigation and their solidification modes predicted according to Suutala (1983) model. The Cr_{eq}/Ni_{eq} ratios are calculated according to Hammar and Svensson (1979) equation.

Steel Grade	Cr_{eq}/Ni_{eq}	Solidification mode
IC373	4.15	fully ferritic
A219	2.20	mixture of fully ferritic and ferritic-austenitic
904L	0.98	austenitic-ferritic

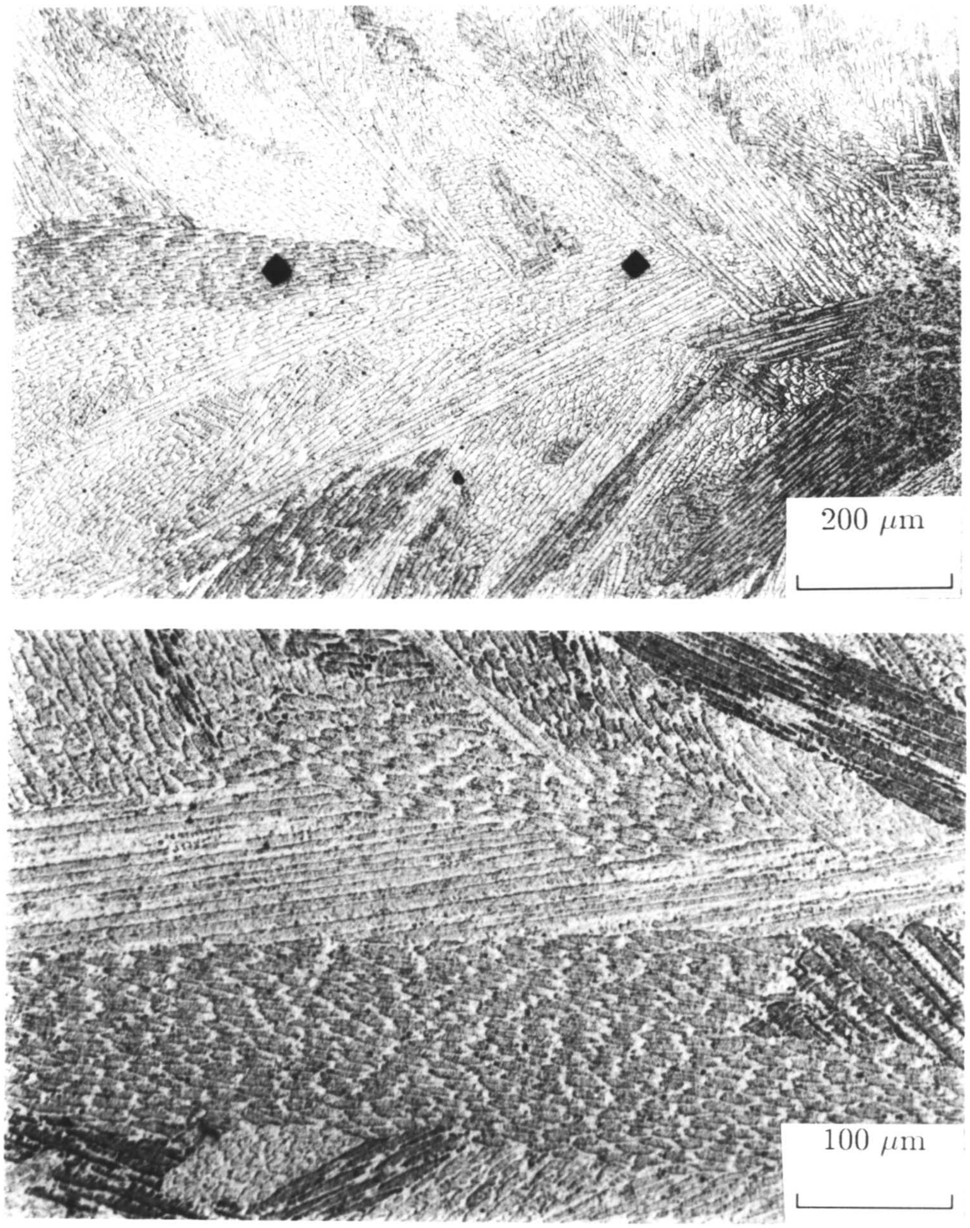

Figure 5.26. Microstructure of laser weld metal of alloy 904L showing the austenite dendrites with interdendritic δ-ferrite. The solidification mode is austenitic-ferritic.

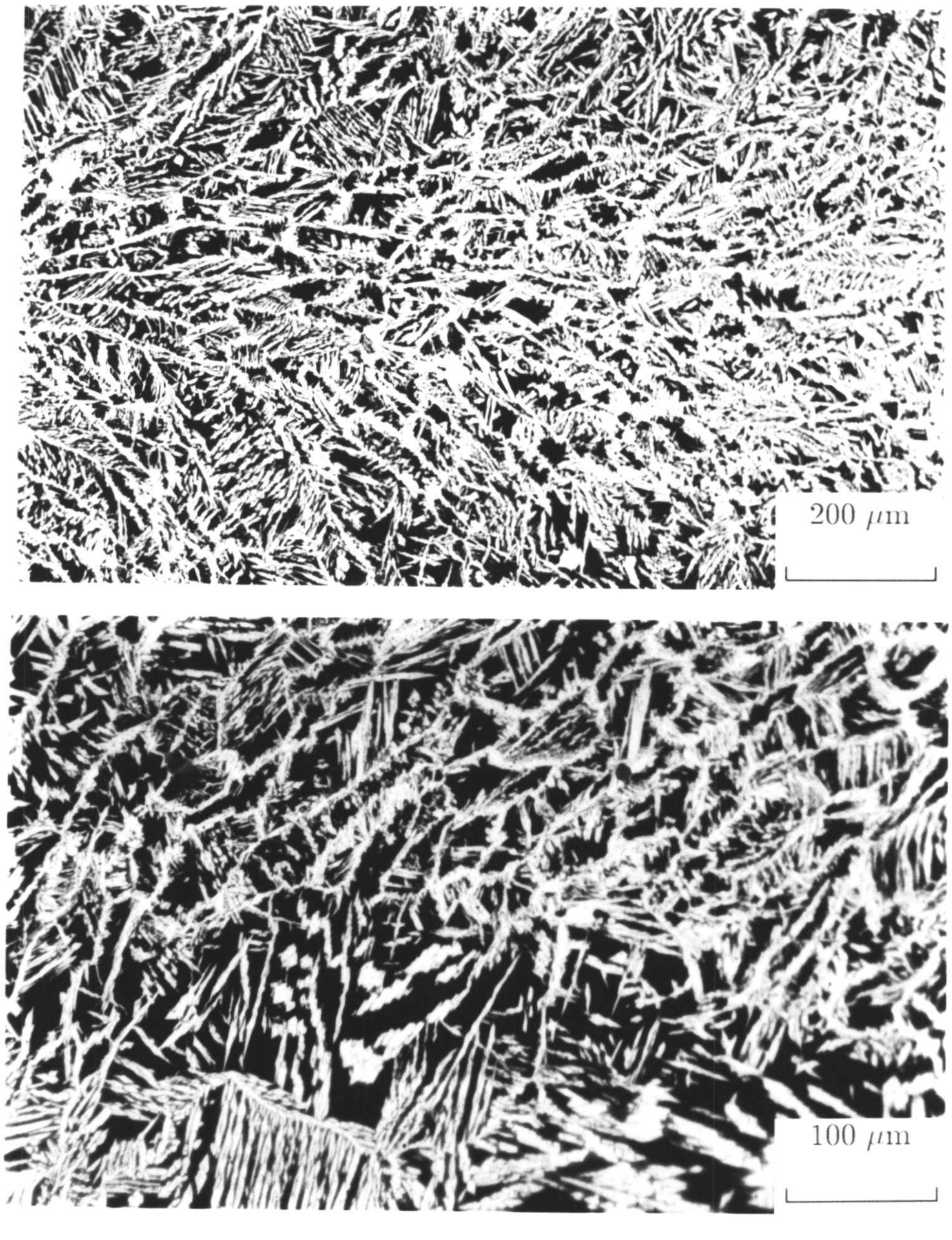

Figure 5.27. Microstructure of laser weld metal of alloy A219. It consists of dendritic and Widmanstätten austenite plus ferrite grains. This confirms that the solidification mode is ferritic-austenitic. The ferrite dendrites are invisible as the result of solid state transformation (δ-ferrite to austenite).

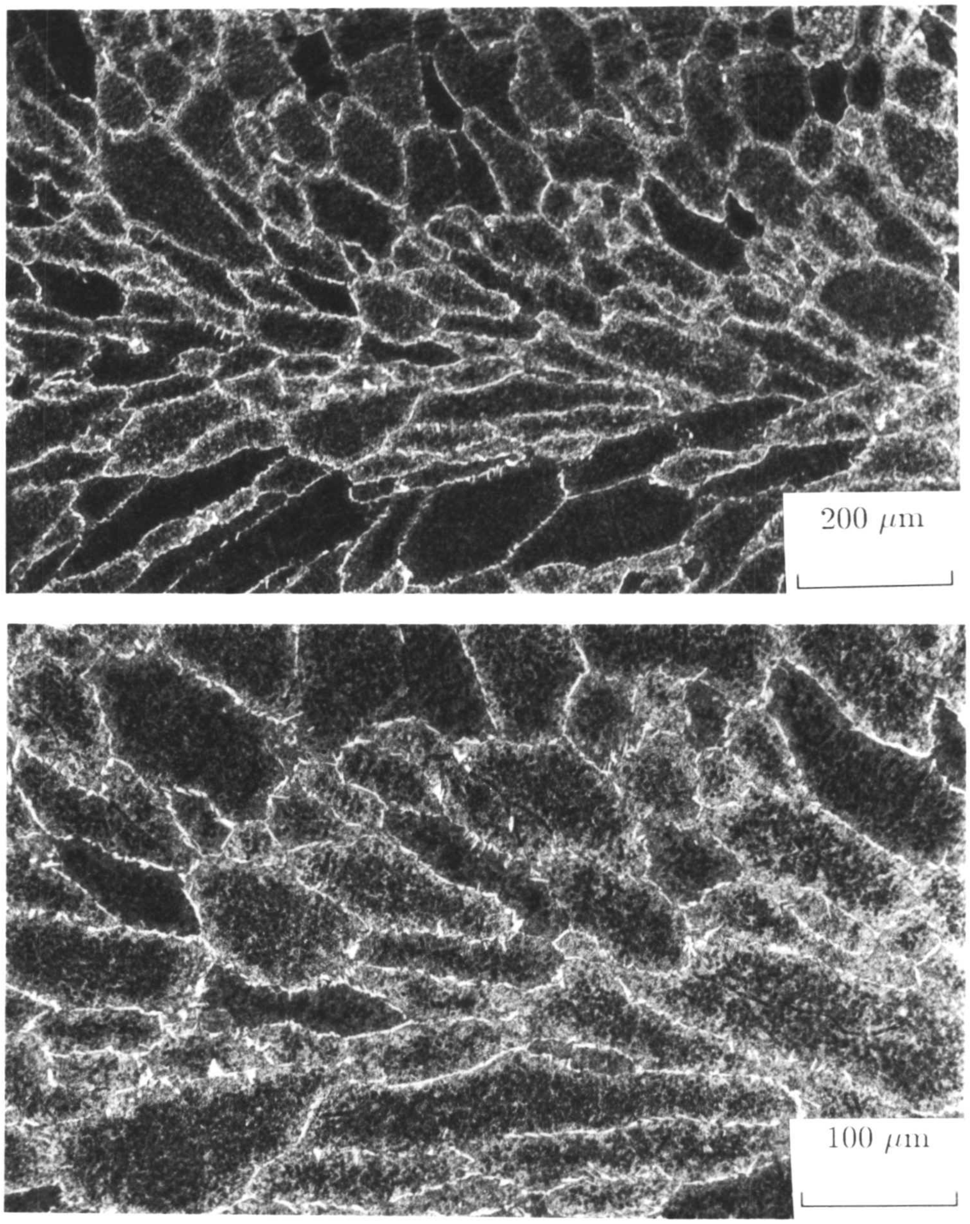

Figure 5.28. Microstructure of laser weld metal of alloy IC373. It consists of ferrite grains elongated in the weld direction with precipitation of austenite mainly at grain boundaries. This confirms that the solidification mode is fully ferritic.

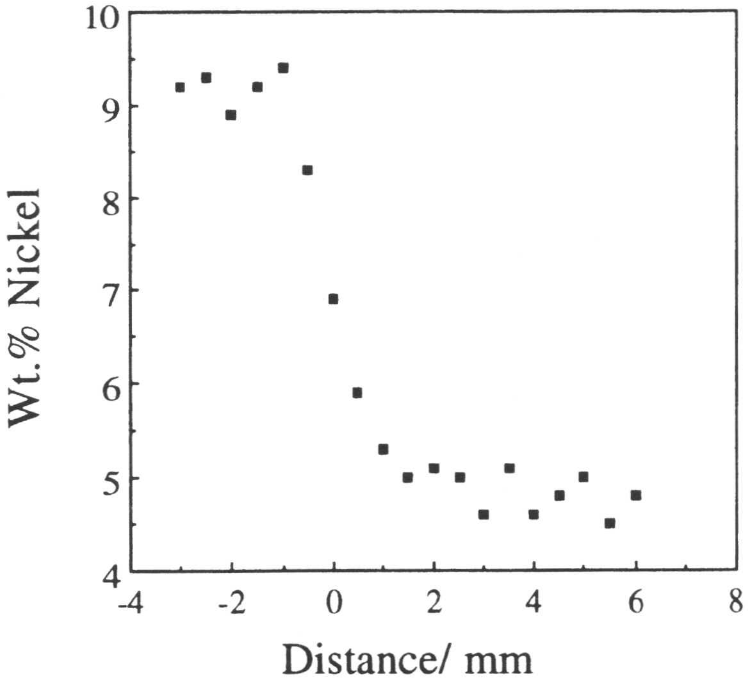

Figure 5.29. SEM EDX data illustrating the extent of dilution associated with dissimilar metal joint between alloys A219 and IC373, as a function of distance normal to dissimilar metal junction. The data show the change in Ni concentration at the centre of the weld. The welding direction is from alloy A219 (wt.%Ni=9.4) to alloy IC373 (wt.%Ni=5.1).

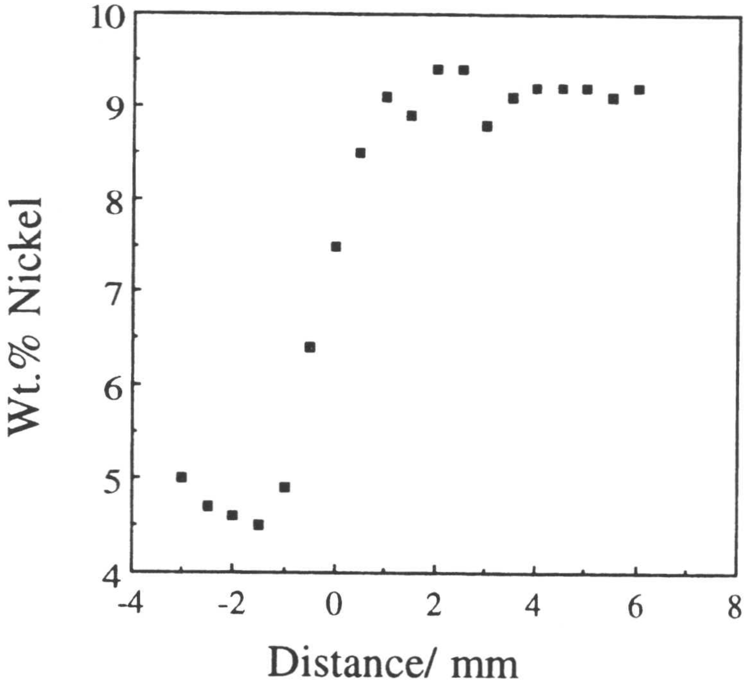

Figure 5.30. Same as Figure 5.29 except that the welding direction is from alloy IC373 to alloy A219.

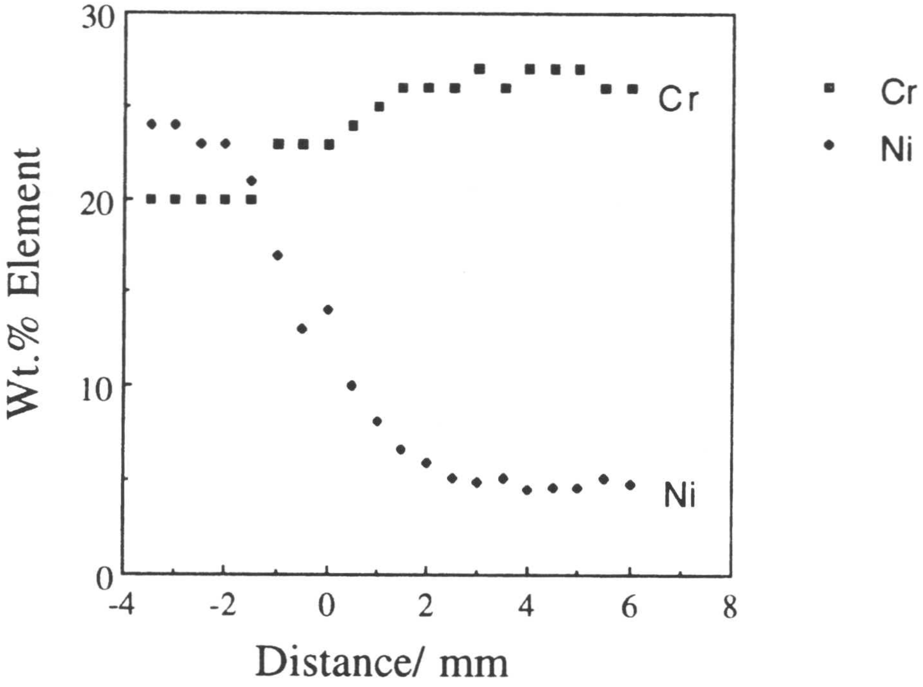

Figure 5.31. SEM EDX data illustrating the extent of dilution associated with dissimilar metal joint between alloys 904L and IC373, as a function of distance normal to dissimilar metal junction. The data show the changes in Ni and Cr concentrations at the centre of the weld. The welding direction is from alloy 904L (24.7 wt.%Ni, 20.0 wt.%Cr) to alloy IC373 (5.1 wt.%Ni, 25.9 wt.%Cr).

5.6.2 Variation of solidification mode in the transition zone

As the solidification front of the weld pool crosses the interface between dissimilar alloys A and B, the chemical composition of the weld pool will change. This obviously can affect the solidification mode, depending on the degree of dilution in the transition zone. Bhadeshia *et al.* (1991) have reported a change of solidification mode from ferritic-austenitic (FA) to austenitic-ferritic (AF) in the transition zone. When the Cr_{eq}/Ni_{eq} ratios for the two alloys do not differ much this change was found to persist far from the transition zone. The Cr_{eq}/Ni_{eq} ratios of alloys that they have used were in the range of 1.30-1.75, which makes the degree of dilution low. Starting the laser weld from the steel with the lower Cr_{eq}/Ni_{eq} ratio (AF solidification mode) they removed the need for the nucleation of austenite in the transition zone and even in undiluted metal of alloy with higher Cr_{eq}/Ni_{eq}. As the result austenite dendrites penetrated into undiluted regions and the alloy solidified to metastable austenite rather than the thermodynamically stable δ-ferrite.

In the present work the difference between the Cr_{eq}/Ni_{eq} of the steels used (Table 5.4) is much greater than those studied by Bhadeshia *et al.* (1991) and no change of solidification mode was observed beyond the transition zone. This confirms that the solidification mode of stainless steels depends essentially on the composition of steel and the effect of solidification conditions is of secondary importance in the present context.

Figure 5.32 shows the microstructure of a dissimilar metal junction between alloys 904L and IC373. The welding direction is from alloy 904L with austenitic-ferritic solidification mode (Cr_{eq}/Ni_{eq}=0.98) to alloy IC373 with fully ferritic solidification mode (Cr_{eq}/Ni_{eq}=4.15). Austenite dendrites penetrated into the transition zone. As the difference between the Cr_{eq}/Ni_{eq} is very high solidification mode changed from austenitic-ferritic to ferritic-austenitic and then to fully ferritic as soon as the transition zone was exceeded.

Figure 5.33 shows the microstructure of a dissimilar metal junction between alloys A219 and IC373. The welding direction is from alloy A219 with ferritic-austenitic solidification mode (Cr_{eq}/Ni_{eq}=2.20) to alloy IC373. Again austenite dendrites penetrated into the transition zone but failed to penetrate undiluted regions of IC373. Figure 5.34 shows the microstructure of dissimilar metal junctions between the same alloys as in Figure 5.33 but with the opposite welding direction. Again the change in solidification mode (this time from fully ferritic to ferritic-austenitic) only occurred in the transition zone.

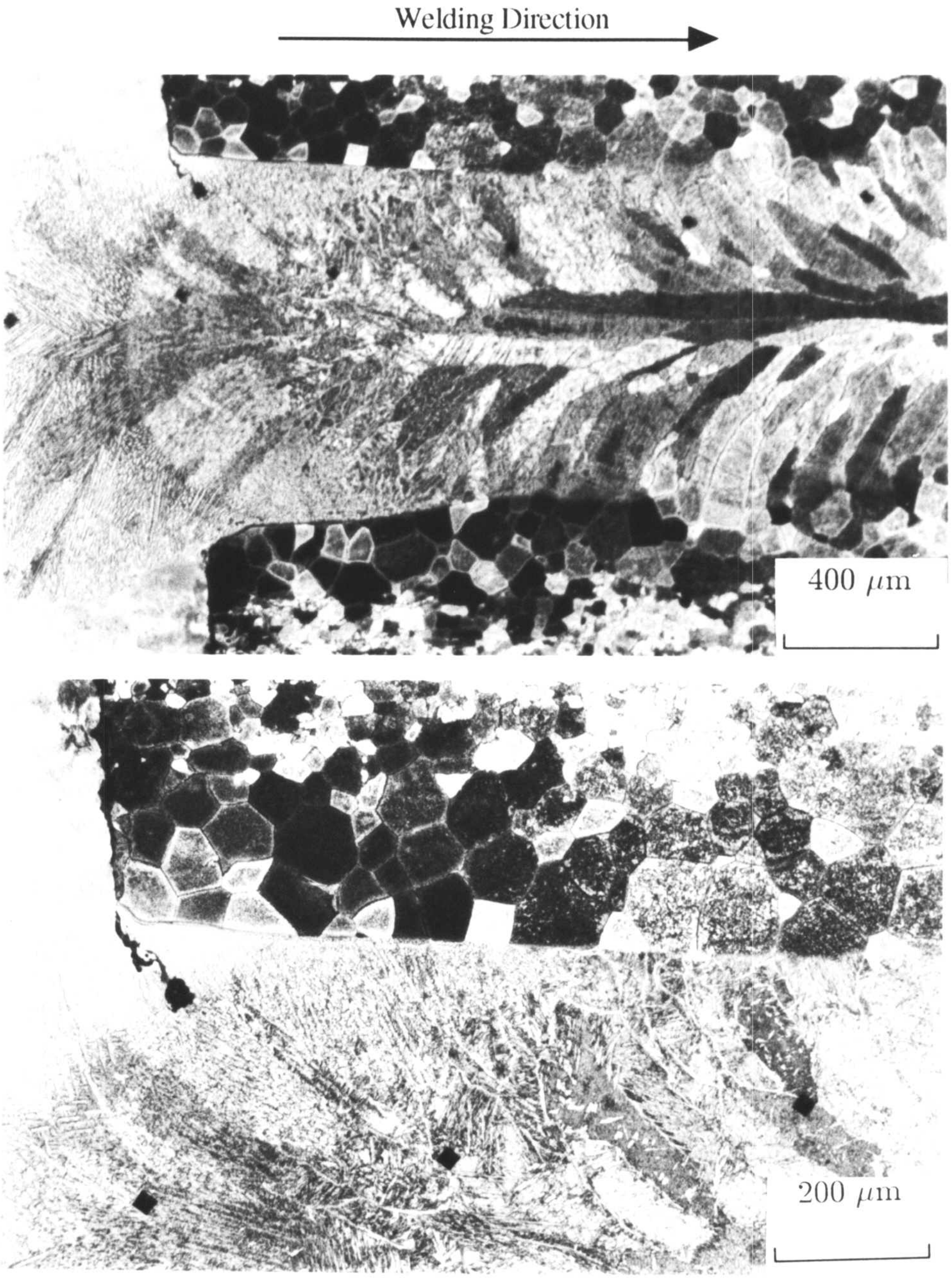

Figure 5.32. microstructure of dissimilar metal junction between alloys 904L and IC373. The weld direction is from alloy 904L (AF solidification mode) to alloy IC373 (fully ferritic solidification mode). A change of solidification mode from AF to FA and then to fully ferritic can be seen in transition zone due to dilution effect.

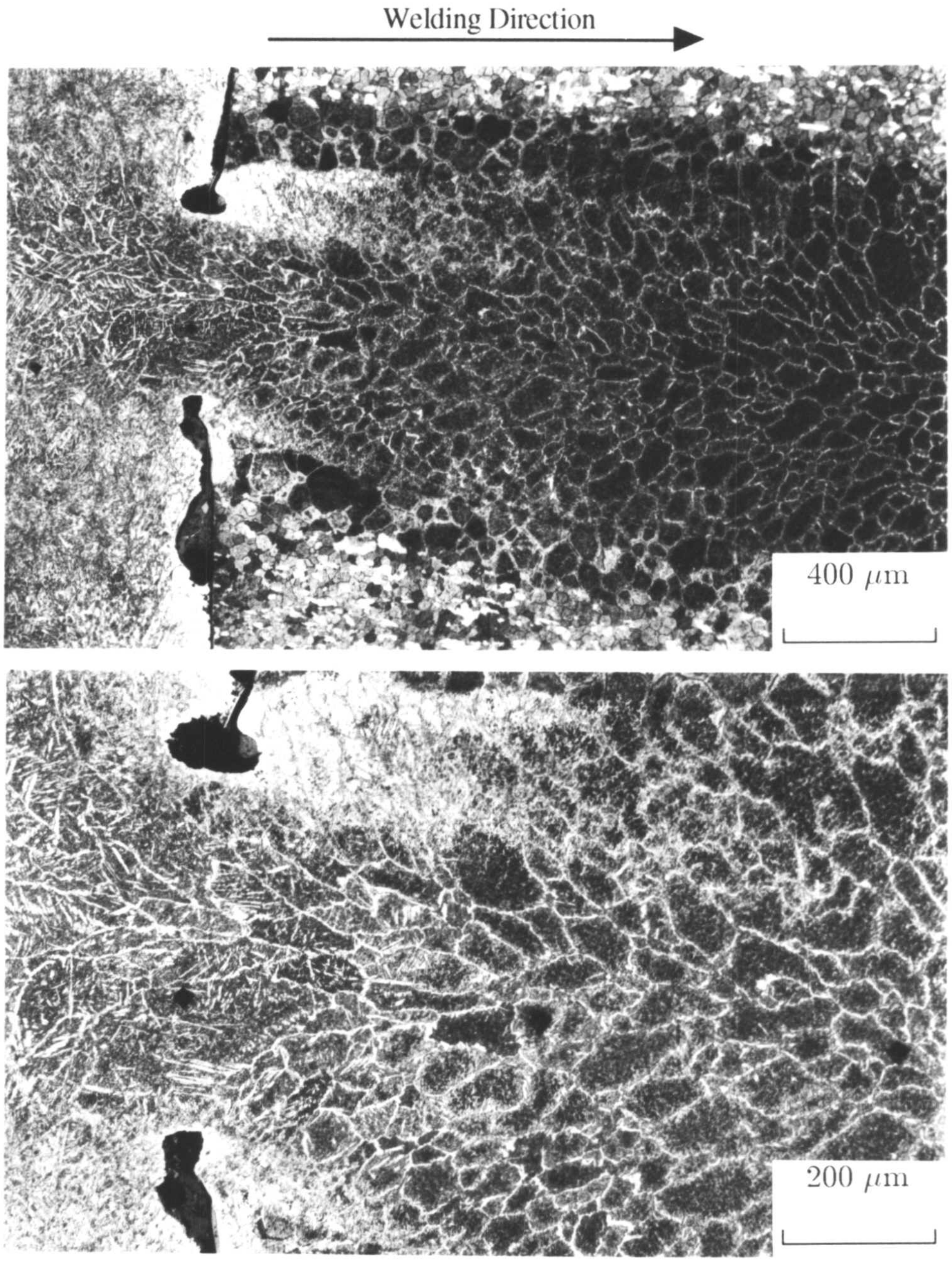

Figure 5.33. microstructure of dissimilar metal junction between alloys A219 and IC373. The weld direction is from alloy A219 (FA solidification mode) to alloy IC373 (fully ferritic solidification mode). A change of solidification mode from FA to fully ferritic can be seen in transition zone due to dilution effect.

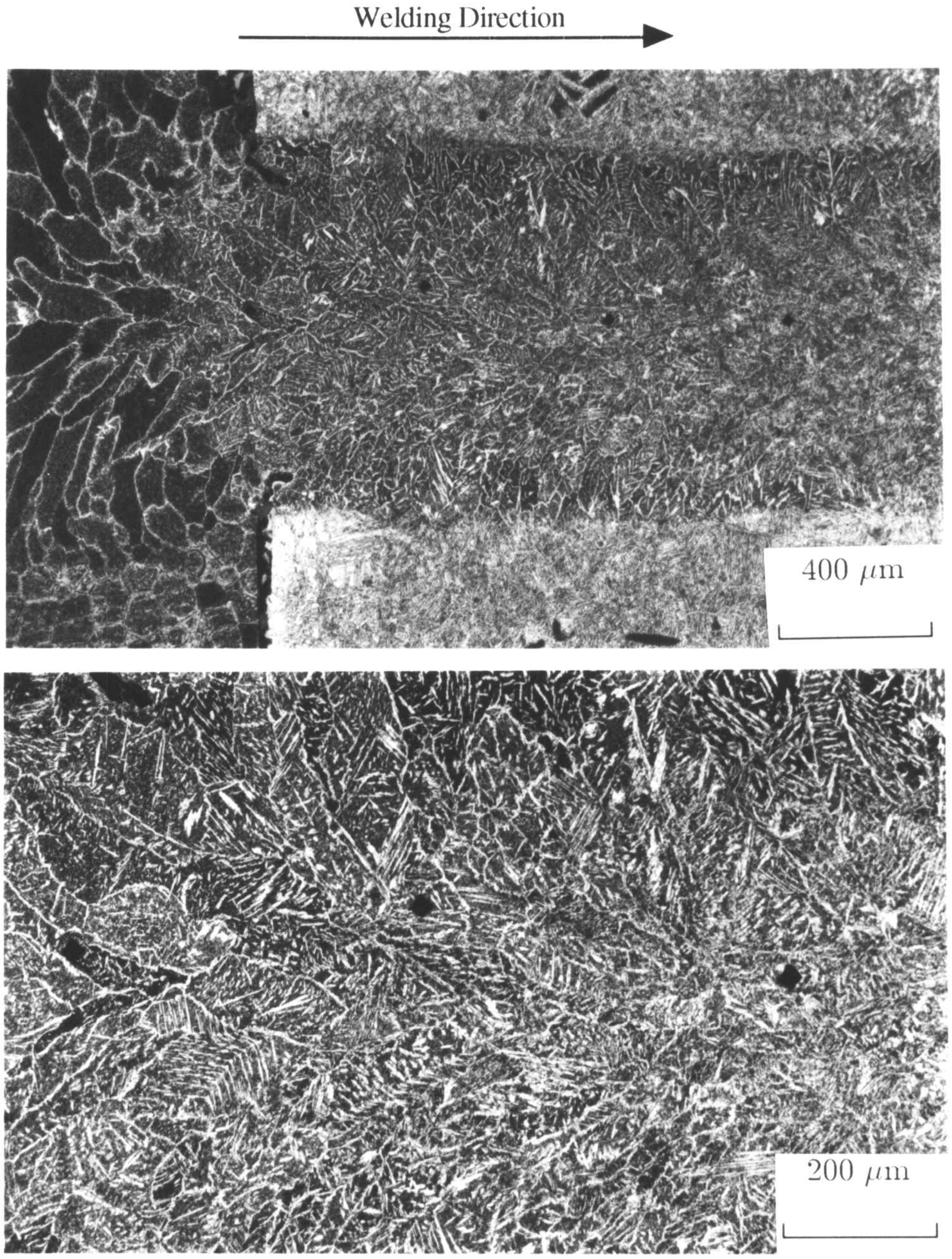

Figure 5.34. microstructure of dissimilar metal junction between alloys IC373 and A219. The weld direction is from alloy IC373 (fully ferritic solidification mode) to alloy A219 (FA solidification mode). A change of solidification mode from fully ferritic to FA can be seen in transition zone due to dilution effect.

5.7 Conclusions

1. Phase diagram calculations of the solidification mode have been found to be consistent with estimates using the Cr_{eq}/Ni_{eq} approach of the Suutala model. Of the five different steel grades investigated only one (ZERON100) shows different solidification mode other than predicted by model. This indicates that the model needs some modification for super duplex stainless steels.

2. Thermodynamic calculations indicate that the suppression of the austenite phase in super duplex weld metal A219 would lead to the persistence of liquid to incredibly low temperatures showing that fully ferritic solidification of this alloy is impossible. This was confirmed experimentally by the failed attempts to induce the alloy to solidify into a fully ferritic state using laser welds which traverse dissimilar metal junctions.

3. The results of long time solution treatments at 1300 °C show that duplex rolled metal IC373 has a wholly ferritic microstructure above this temperature indicating that the solidification mode is fully ferritic as predicted by calculations. In the case of steel grades IC381 and A219 the microstructure is a mixture of ferrite and austenite at 1300 °C . The volume fraction of austenite that forms at all temperatures in grade A219 is much larger than in grade IC381 as predicted by calculations.

4. The melting point of steel decreases with increasing the amount of alloying elements.

5. The melting point of steel increases with increasing heating rate.

6. The solidus temperature on heating is much higher than on cooling and this difference increases with increasing the heating and cooling rates. This is due to the superheating of solid and undercooling of liquid.

7. During the quenching of these steels from an elevated temperature (i.e. 1300 °C) very fine austenite particles (some of them in cluster forms) will precipitate inside the δ-ferrite grains. These fine austenite particles have the same chemical composition as far as substitutional alloying elements are concerned. This is presumably because they form at a low temperature during the quench, where diffusion becomes sluggish.

8. Although from published data (e.g. Bhadeshia *et al.*, 1991) the solidifi-

cation conditions can change the solidification mode from ferritic-austenitic to austenitic-ferritic when the Cr_{eq}/Ni_{eq} of steel be near to the critical value corresponding to the mode change, but the solidification mode depends essentially on the chemical composition of steel (present by Cr_{eq}/Ni_{eq}) and the effect of solidification conditions is of secondary importance.

Chapter 6

ISOTHERMAL HEAT TREATMENT AND ITS EFFECT ON THE FERRITE/AUSTENITE BALANCE

6.1 Introduction

The essential reason for the success of duplex stainless steels is their higher strength and better corrosion resistance when compared with austenitic stainless steels. Moreover, they also have a good weldability. These good properties are to some extent attributable to the microstructure which contains approximately 50 vol.% each of ferrite and austenite (the super duplex grades might have about 60 vol.% austenite). The relative fractions of the phases can be controlled both by the composition of the steel or by heat treatment. The effect of chemical composition on the balance between ferrite and austenite was discussed in chapter three. The influence of heat treatment is presented in this chapter.

6.2 Thermodynamic calculations

Phase calculations using MTDATA are present in Figure 6.1. The calculations take into account the phases liquid, ferrite, austenite, sigma and the carbides $M_{23}C_6$ and M_7C_3. They cover a temperature range over which only liquid, ferrite and austenite coexist. The purpose of these calculations was to enable a comparison against experimental measurements presented in the subsequent sections. The calculations have been done for a typical duplex wrought metal (IC381), duplex composition overalloyed with Cr (IC373), duplex weld metal (UNS31), super duplex wrought metal (ZERON100) and super duplex weld metal (A219). Their chemical compositions are listed in Table 5.1 and Table 5.2 shows their $\mathrm{Cr_{eq}/Ni_{eq}}$ ratios calculated according to the Hammar and Svensson (1979) equation. Comparing the results of these calculations shows that duplex weld metal UNS31 (which has the lowest $\mathrm{Cr_{eq}/Ni_{eq}}$) has the highest volume fraction of austenite.

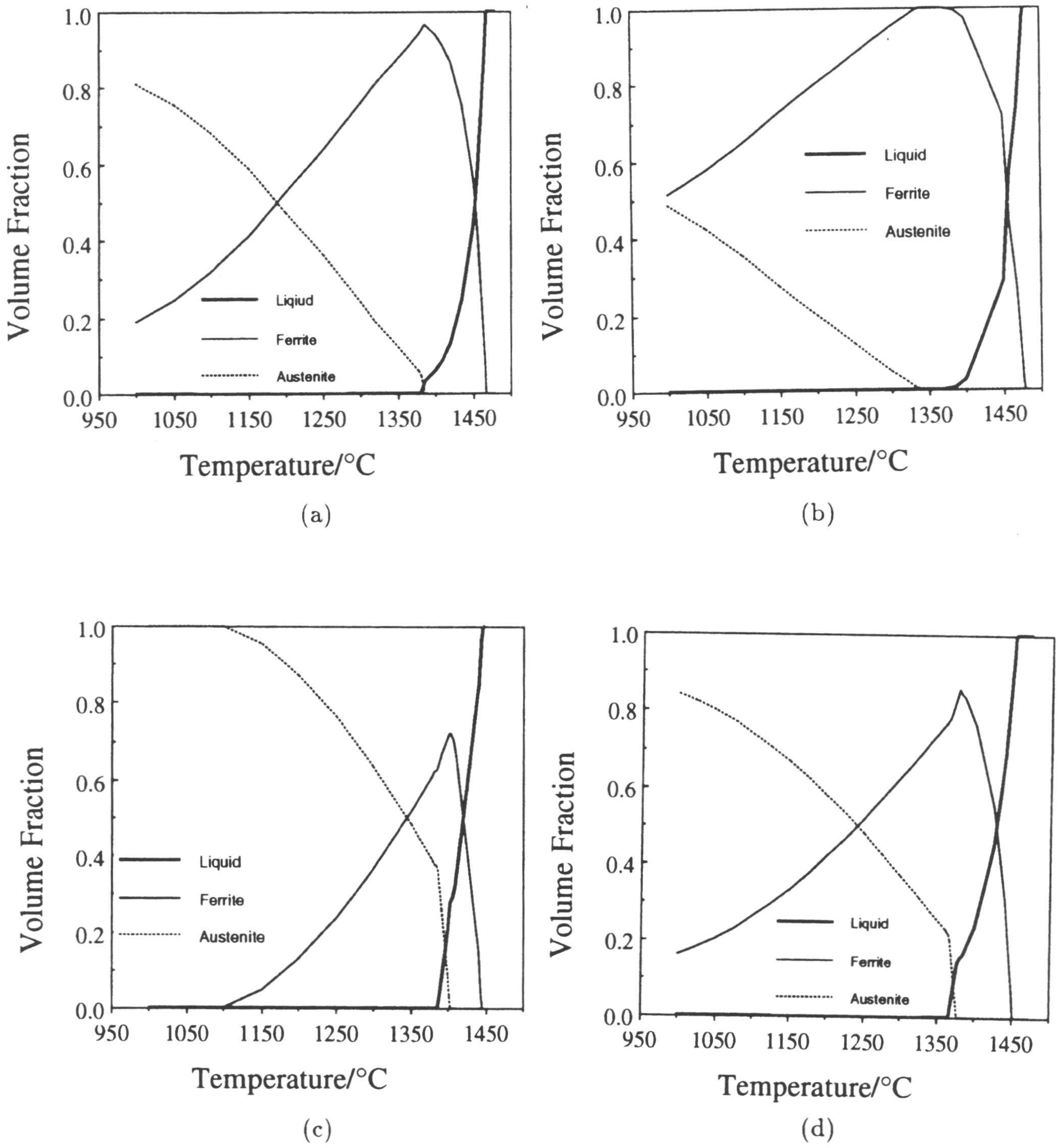

(a) (b)

(c) (d)

Figure 6.1. The calculated equilibrium phase diagrams for alloys a) typical duplex wrought metal (IC381); b) duplex composition overalloyed with Cr (IC373); c) duplex weld metal (UNS31); d) super duplex wrought metal (ZERON100); e) super duplex weld metal (A219).

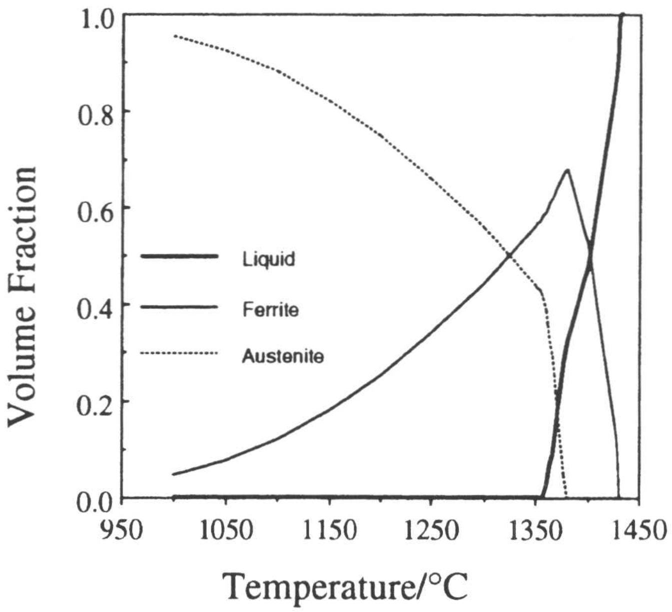

(e)

Figure 6.1. (Continued)

6.3 Equilibrium isothermal heat treatments

Equilibriation heat treatments were carried out on duplex stainless steel rolled metals IC373, IC381 and super duplex weld metal A219 (Table 5.1); the heat treatment conditions are summarised in Table 6.1. To avoid oxidation, decarburisation and the escape of nitrogen, all the specimens were sealed in silica-quartz tubes containing a partial pressure of argon (about 100 mm Hg). The minimum temperature of the heat treatments is 1100 °C to avoid the precipitation of sigma-phase, especially in alloy A219. Figure 6.2 shows the precipitation of sigma-phase at 1050 °C in super duplex weld metal A219. The maximum heat treatment temperature used was 1300 °C as the silica-quartz tube is not stable at temperatures higher than that.

Table 6.1. Heat treatments.

Temperature (°C)	1100	1150	1200	1250	1300
Time (h)	315	165	65	48	26

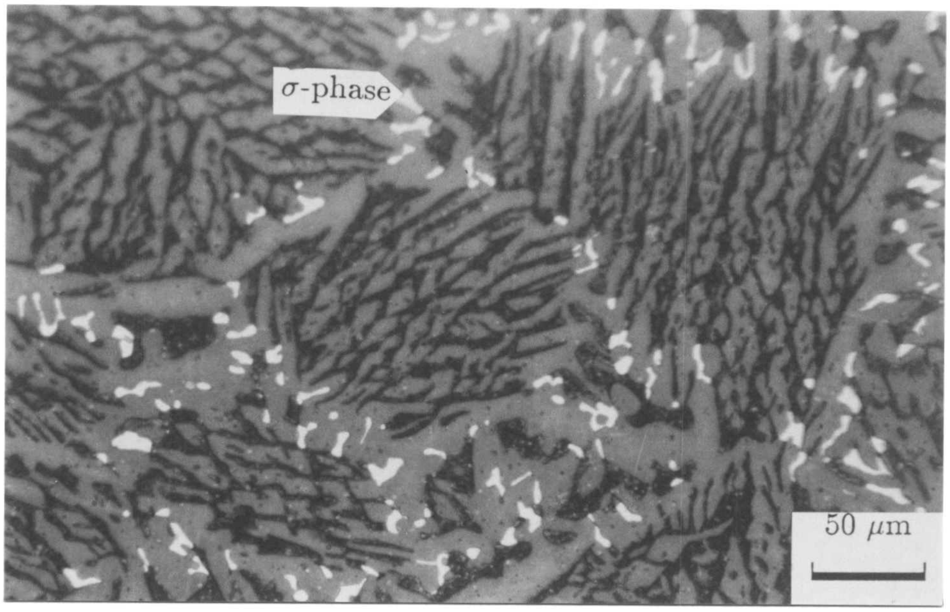

Figure 6.2. The microstructure of super duplex stainless steel alloy A219 solution treated at 1150 °C for 2.5 hours before quenching in water. Sigma-phase (bright white) has been precipitated on the grain boundaries between austenite (yellow) and ferrite (dark colour).

Figures 6.3-6.6 show the microstructures of duplex alloy IC381 after heat treated at different temperatures. The light phase is austenite and the dark one is ferrite. The fine particles inside the ferrite grains are austenite formed during quenching. The volume fraction of austenite (excluding the fine particles) was measured using both the linear point counting and image analysing techniques. As the temperature was reduced from 1300 (Figure 5.19) to 1100 °C (Figure 6.6) the measured volume fraction of austenite (excluding fine austenite which has precipitated during quenching) increased from about 0.19 to 0.65.

Duplex rolled metal IC373 has a Cr_{eq}/Ni_{eq} ratio which is much higher so that the formation of austenite is retarded to a much lower temperature compared with IC381 (Figure 6.7-6.10). Figure 6.9 shows allotriomorphic austenite at δ-ferrite grain boundaries after heat treatment at 1150 °C for 165 hours. The volume fraction of austenite (excluding the fine particles) is less than 0.05. By comparison, the specimen which was heat treated at 1100 °C, contained about 0.28 volume fraction of austenite (excluding the fine particles).

In the case of super duplex weld metal A219 (Figures 6.11 to 6.14) with a Cr_{eq}/Ni_{eq} ratio of 2.20 (Table 5.2) the solidification mode is ferritic-austenitic (chapter 5), so the volume fraction of austenite at all temperatures is much higher compared with IC373 and IC381. As the temperature was reduced from 1300 (Figure 5.21) to 1100 °C (Figure 6.14) the measured volume fraction of austenite (excluding fine austenite which has precipitated during quenching) increased from 0.53 to 0.70. The microstructure of specimen heat treated at 1100 °C (Figure 6.14) shows that δ-ferrite has decomposed to austenite plus sigma phase. This confirms that sigma phase in super duplex stainless steel weld metal A219 forms at higher temperatures compared with duplex stainless steel wrought metals IC381 and IC373. This is due to higher amount of Cr and Mo in the super grade (these two elements are strong sigma formers).

The measured volume fractions of austenite for different specimens are listed in Table 6.2. Figures 6.15-6.17 shows the variations of equilibrium (calculated and measured) volume fraction of austenite with temperature for alloys IC381, IC373 and A219 respectively. The agreement is good in all cases except for IC373 which contains a less austenite at high temperatures than is predicted. This is the only alloy which solidifies completely to ferrite. The nucleation of austenite must therefore be difficult. The situation would be worse by the fact that elevated temperature heat treatments lead to excessively coarse δ grain structures, so that the number density of haterogenous nucleation sites is drastically reduces. Consequently, the observed discrepancies at elevated temperatures are attributed to the kinetic hindrance of transformations. The fact that agreement with the phase calculations is recovered for the heat treatment at 1100 °C (fine δ grain structure, larger nucleation site) confirms this hypothesis.

Table 6.2. Equilibrium volume fraction of austenite measured using both the linear point counting and image analysis techniques.

Steel Grade	Temperature °C				
	1100	1150	1200	1250	1300
IC381	0.65±0.07	0.60±0.05	0.34±0.03	0.29±0.03	0.19±0.03
IC373	0.28±0.04	<0.05	<0.05	<0.05	<0.05
A219	0.70±0.06	0.75±0.05	0.68±0.06	0.57±0.05	0.53±0.06

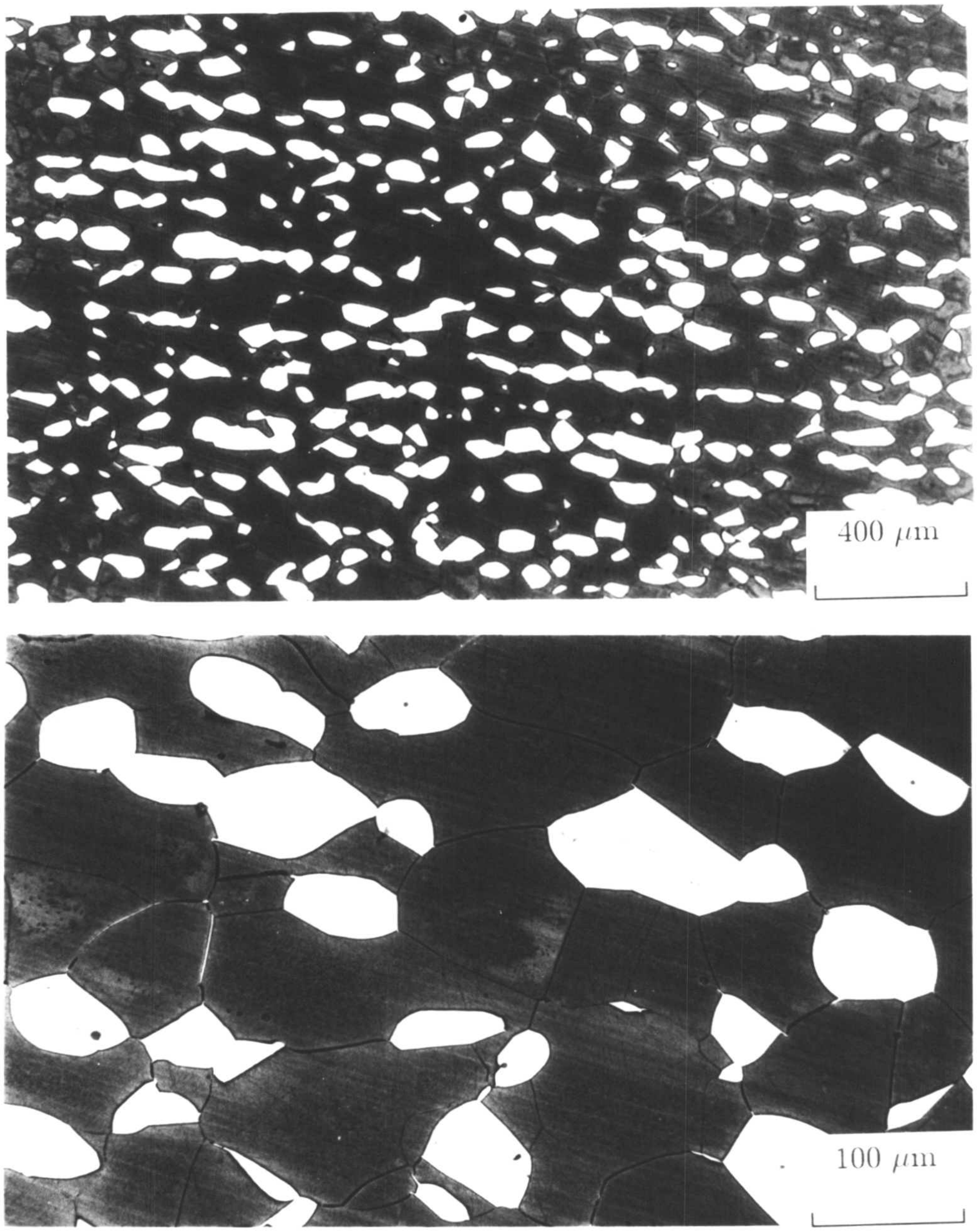

Figure 6.3. Light micrographs showing the microstructure of duplex rolled metal IC381 heat treated at 1250 °C for 48 hours and then quenched into water. The light phase is austenite and the dark one is ferrite. The fine particles inside the ferrite grains are austenite formed during quenching. The measured volume fraction of austenite (excluding the fine particles) is about 0.29.

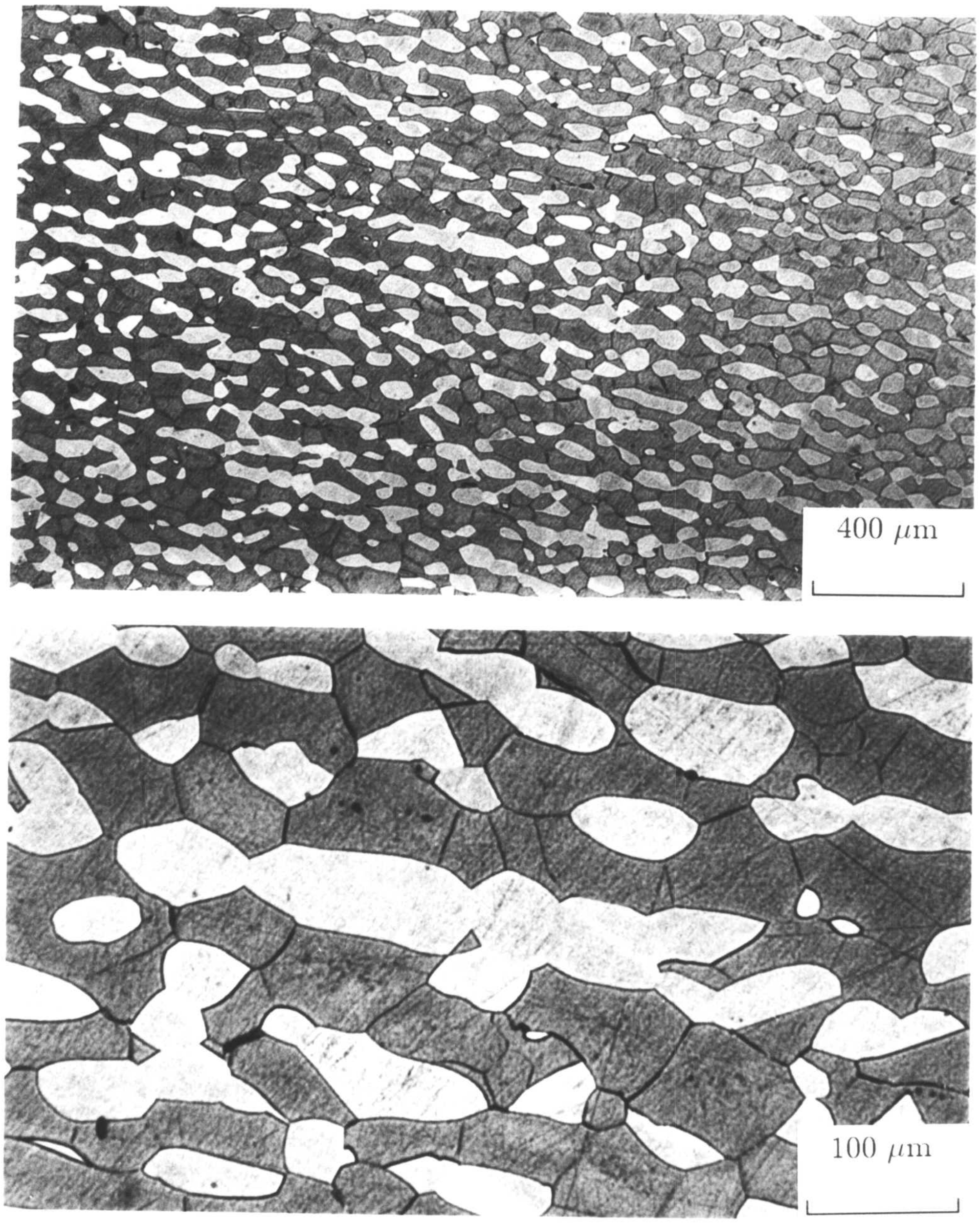

Figure 6.4. Light micrographs showing the microstructure of duplex rolled metal IC381 heat treated at 1200 °C for 65 hours and then quenched into water. The light phase is austenite and the dark one is ferrite. The fine particles inside the ferrite grains are austenite formed during quenching. The measured volume fraction of austenite (excluding the fine particles) is about 0.34.

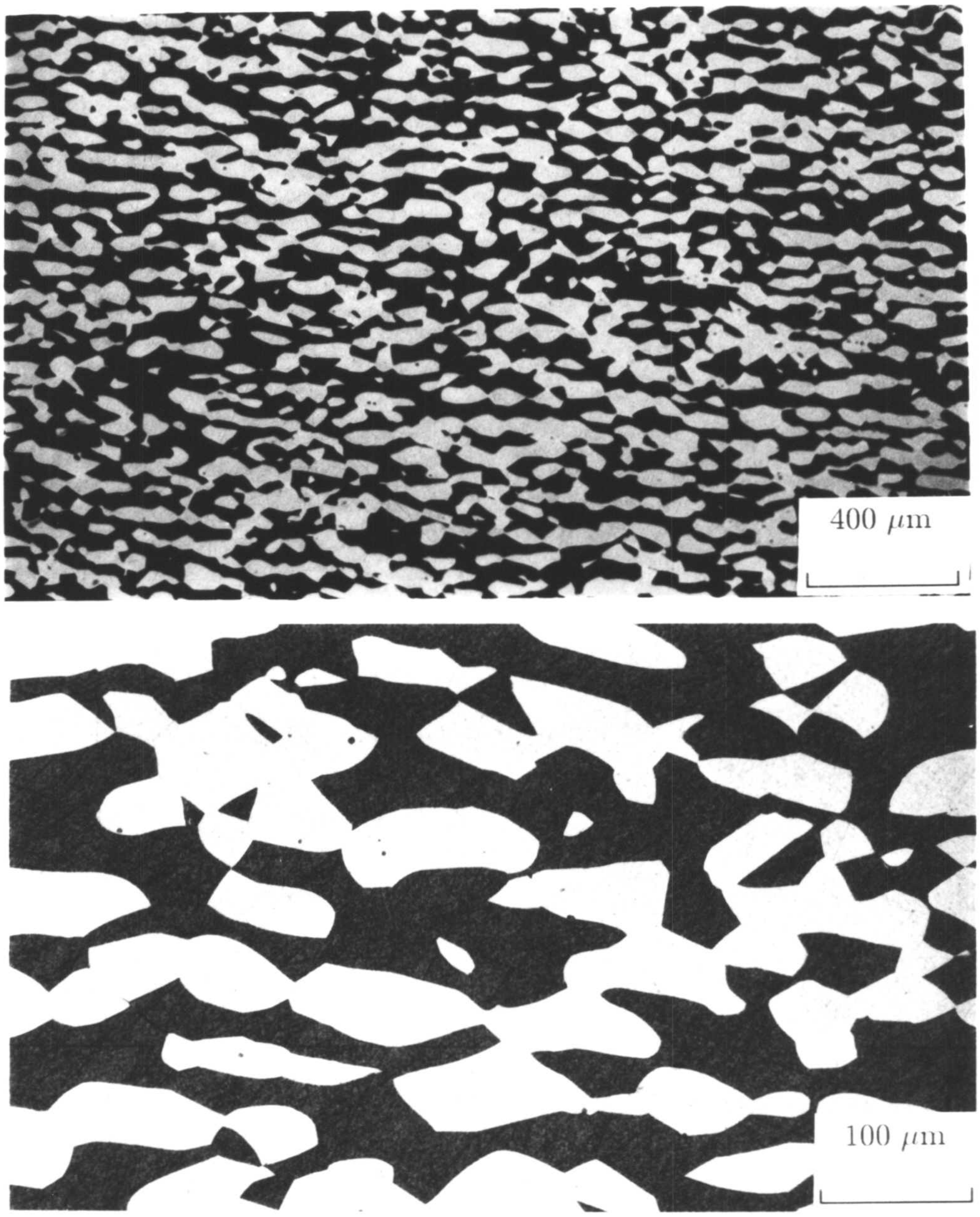

Figure 6.5. Light micrographs showing the microstructure of duplex rolled metal IC381 heat treated at 1150 °C for 165 hours and then quenched into water. The light phase is austenite and the dark one is ferrite. The fine particles inside the ferrite grains are austenite formed during quenching. The measured volume fraction of austenite (excluding the fine particles) is about 0.60.

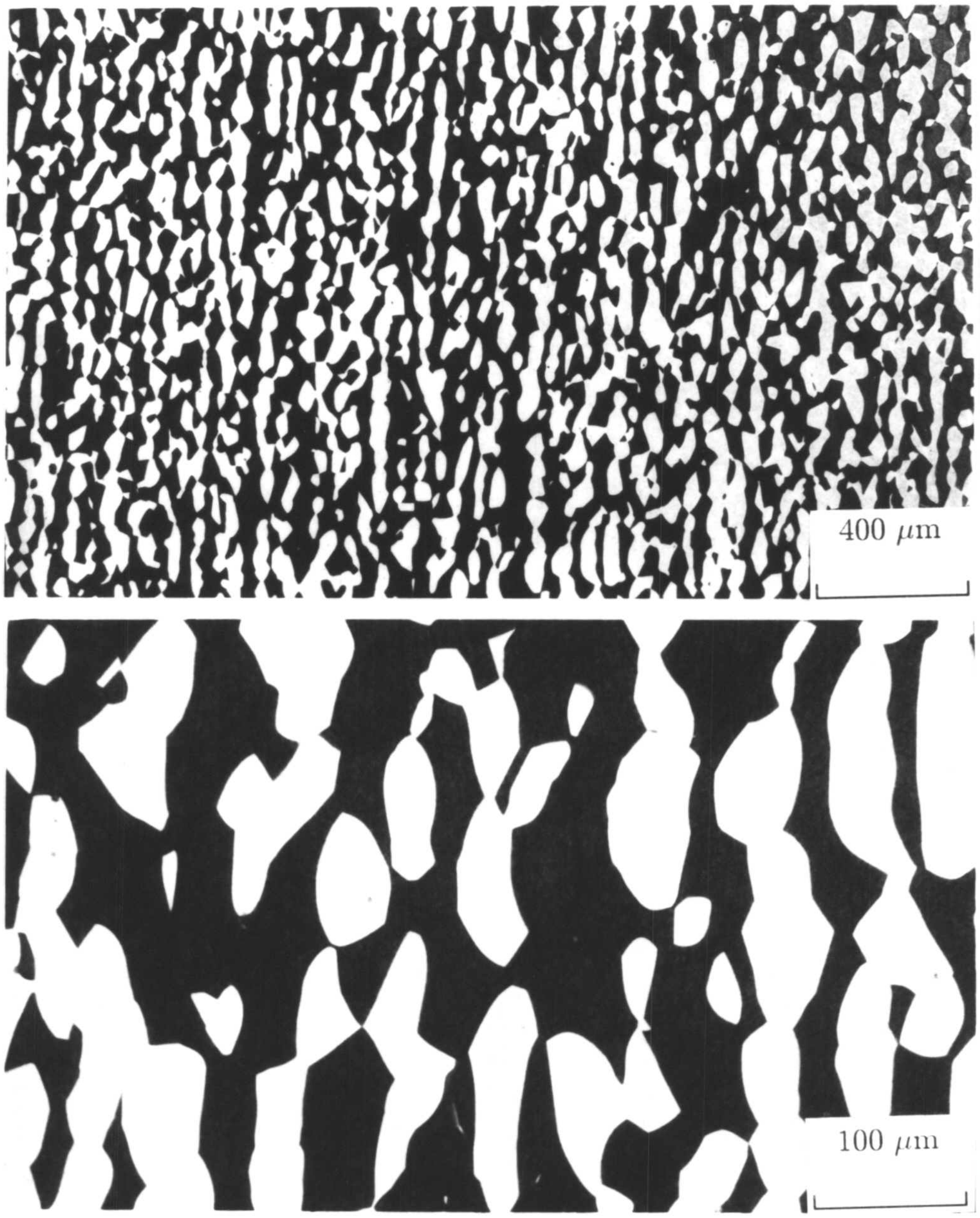

Figure 6.6. Light micrographs showing the microstructure of duplex rolled metal IC381 heat treated at 1100 °C for 315 hours and then quenched into water. The light phase is austenite and the dark one is ferrite. The fine particles inside the ferrite grains are austenite formed during quenching. The measured volume fraction of austenite (excluding the fine particles) is about 0.65.

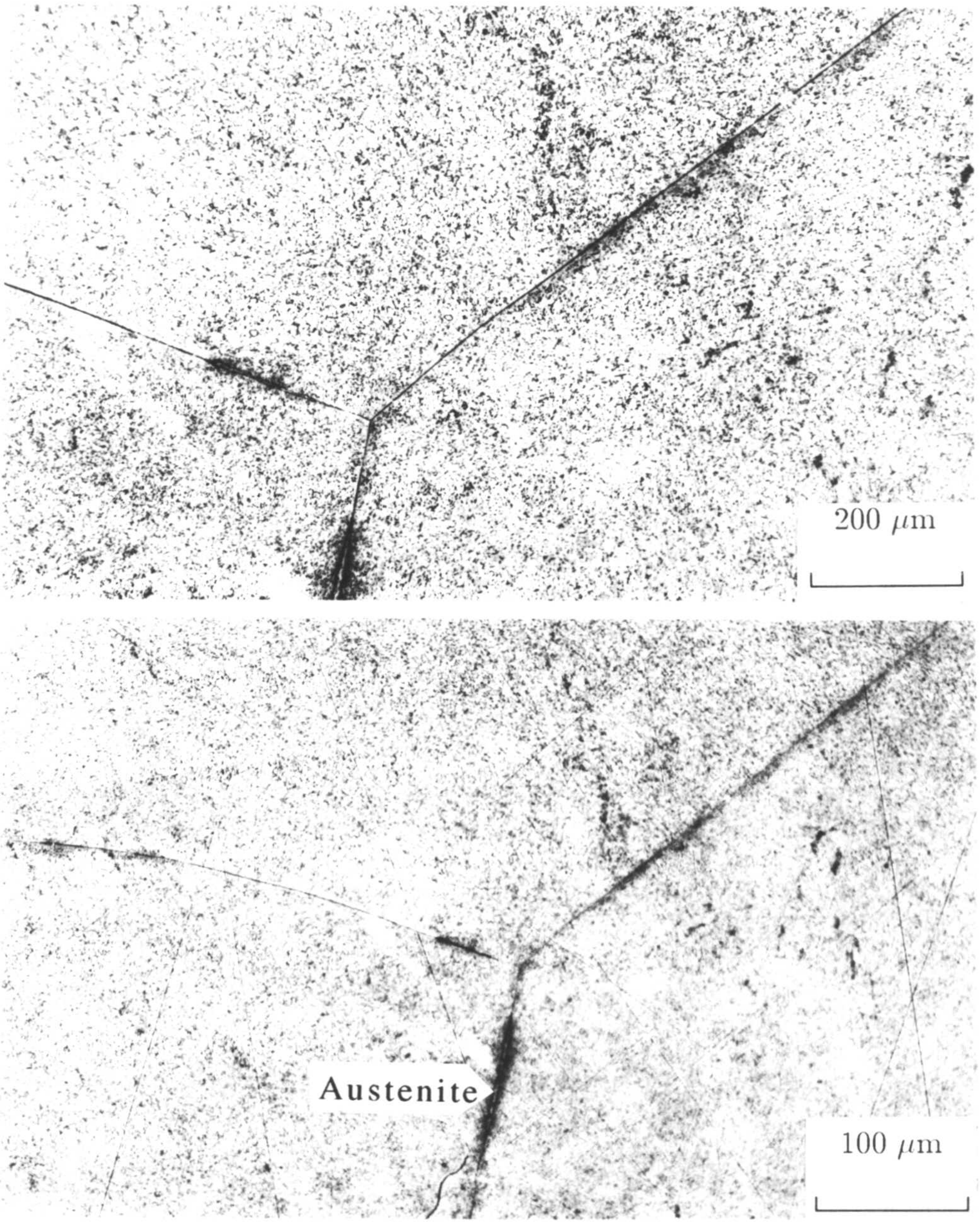

Figure 6.7. Light micrographs showing the microstructure of duplex rolled metal IC373 heat treated at 1250 °C for 48 hours and then quenched into water. This figure shows that the equilibrium microstructure at the elevated temperature consists of huge δ-ferrite grains with a small amount of austenite formed mainly at the grain boundaries. The fine particles inside the ferrite grains are austenite formed during quenching. The measured volume fraction of austenite (excluding the fine particles) is less than 0.05.

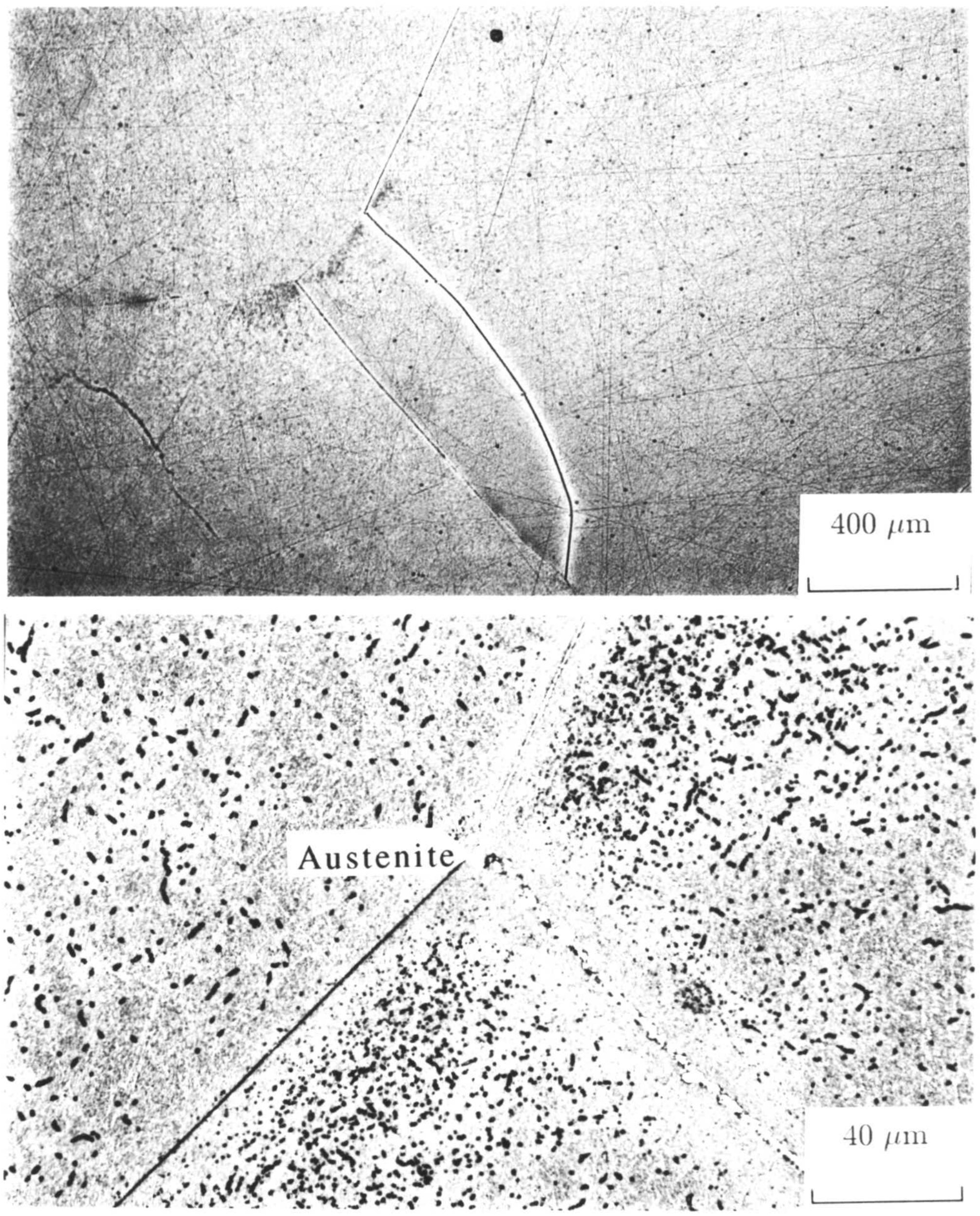

Figure 6.8. Light micrographs showing the microstructure of duplex rolled metal IC373 heat treated at 1200 °C for 65 hours and then quenched into water. This figure shows that the equilibrium microstructure at the elevated temperature consists of huge δ-ferrite grains with a small amount of austenite formed mainly at the grain boundaries. The fine particles inside the ferrite grains are austenite formed during quenching. The measured volume fraction of austenite (excluding the fine particles) is less than 0.05.

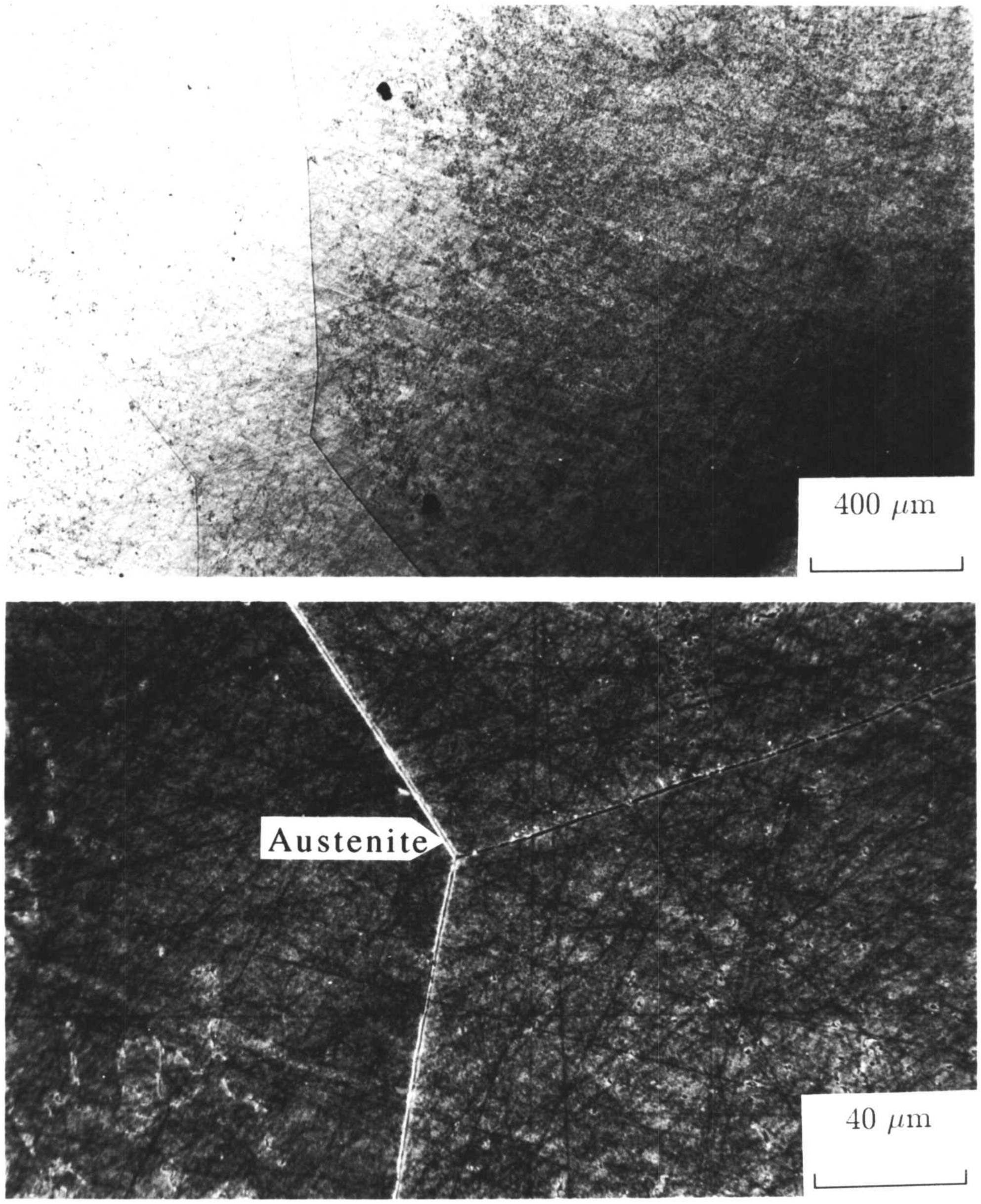

Figure 6.9. Light micrographs showing the microstructure of duplex rolled metal IC373 heat treated at 1150 °C for 165 hours and then quenched into water. This figure shows that the equilibrium microstructure at the elevated temperature consists of huge δ-ferrite grains with a small amount of austenite formed mainly at the grain boundaries. The fine particles inside the ferrite grains are austenite formed during quenching. The measured volume fraction of austenite (excluding the fine particles) is less than 0.05.

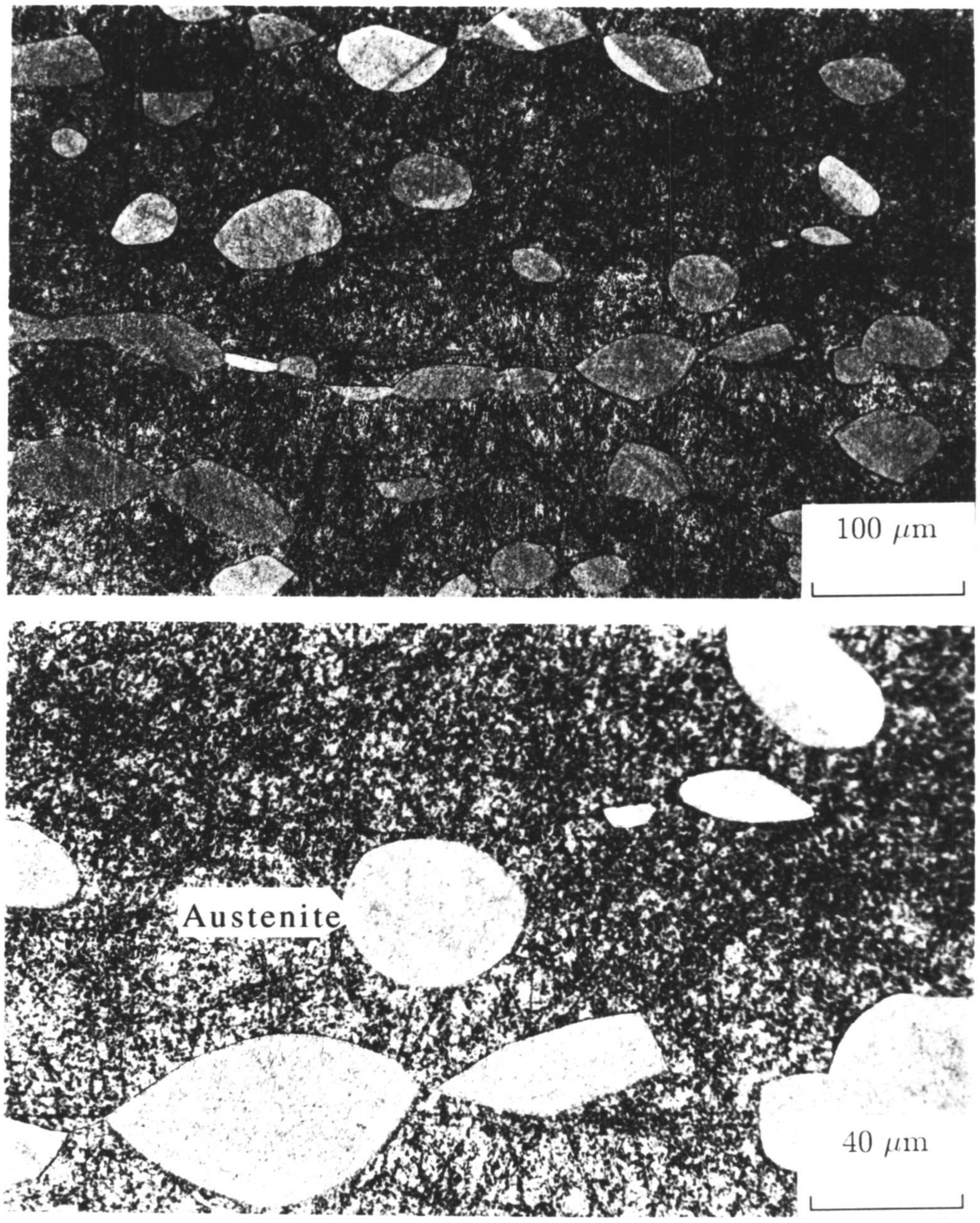

Figure 6.10. Light micrographs showing the microstructure of duplex rolled metal IC373 heat treated at 1100 °C for 315 hours and then quenched into water. The light phase is austenite and the dark one is ferrite. The fine particles inside the ferrite grains are austenite formed during quenching. The measured volume fraction of austenite (excluding the fine particles) is about 0.28.

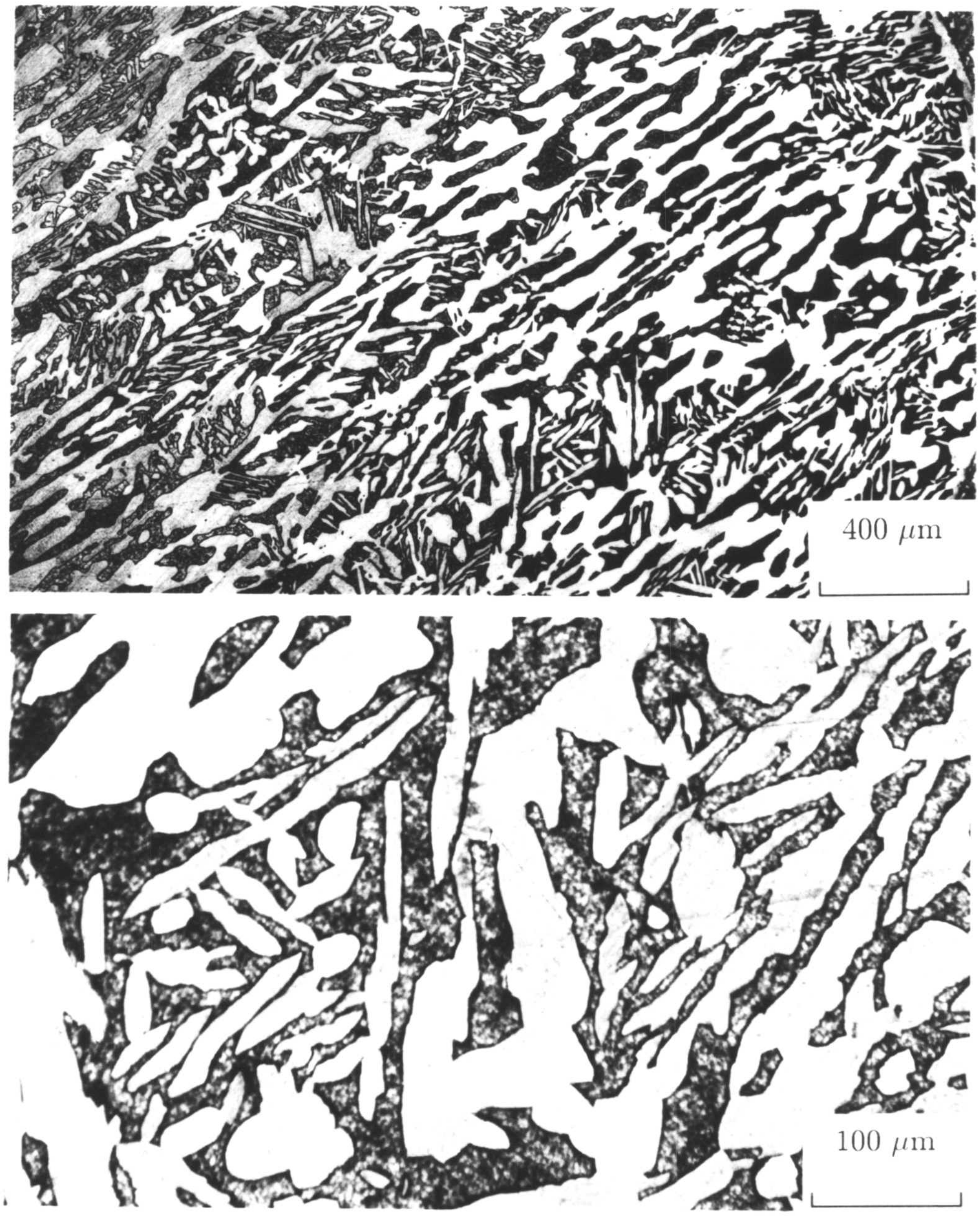

Figure 6.11. Light micrographs showing the microstructure of super duplex weld metal A219 heat treated at 1250 °C for 48 hours and then quenched into water. The light phase is austenite and the dark one is ferrite. The fine particles inside the ferrite grains are austenite formed during quenching. The measured volume fraction of austenite (excluding the fine particles) is about 0.57.

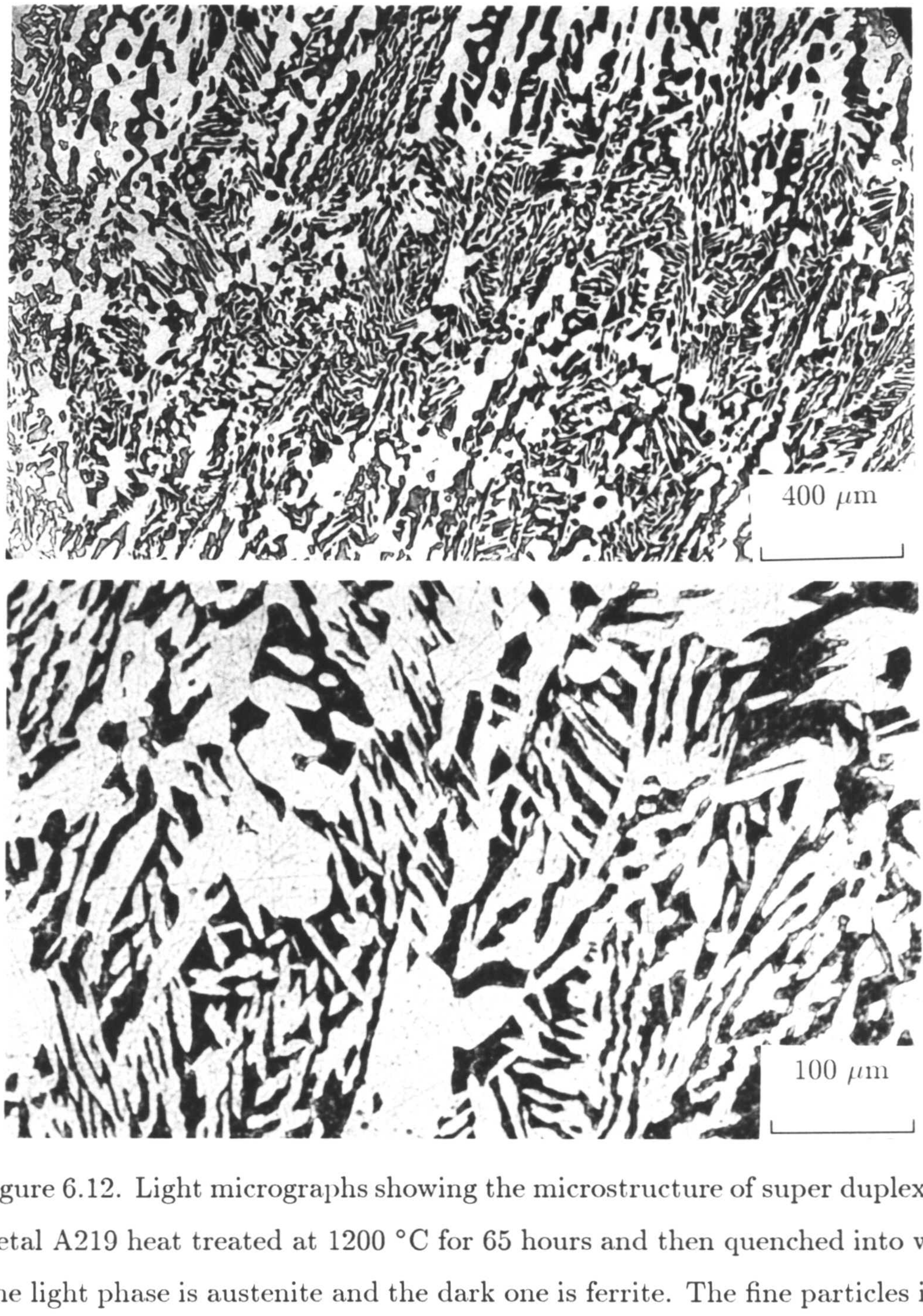

Figure 6.12. Light micrographs showing the microstructure of super duplex weld metal A219 heat treated at 1200 °C for 65 hours and then quenched into water. The light phase is austenite and the dark one is ferrite. The fine particles inside the ferrite grains are austenite formed during quenching. The measured volume fraction of austenite (excluding the fine particles) is about 0.68.

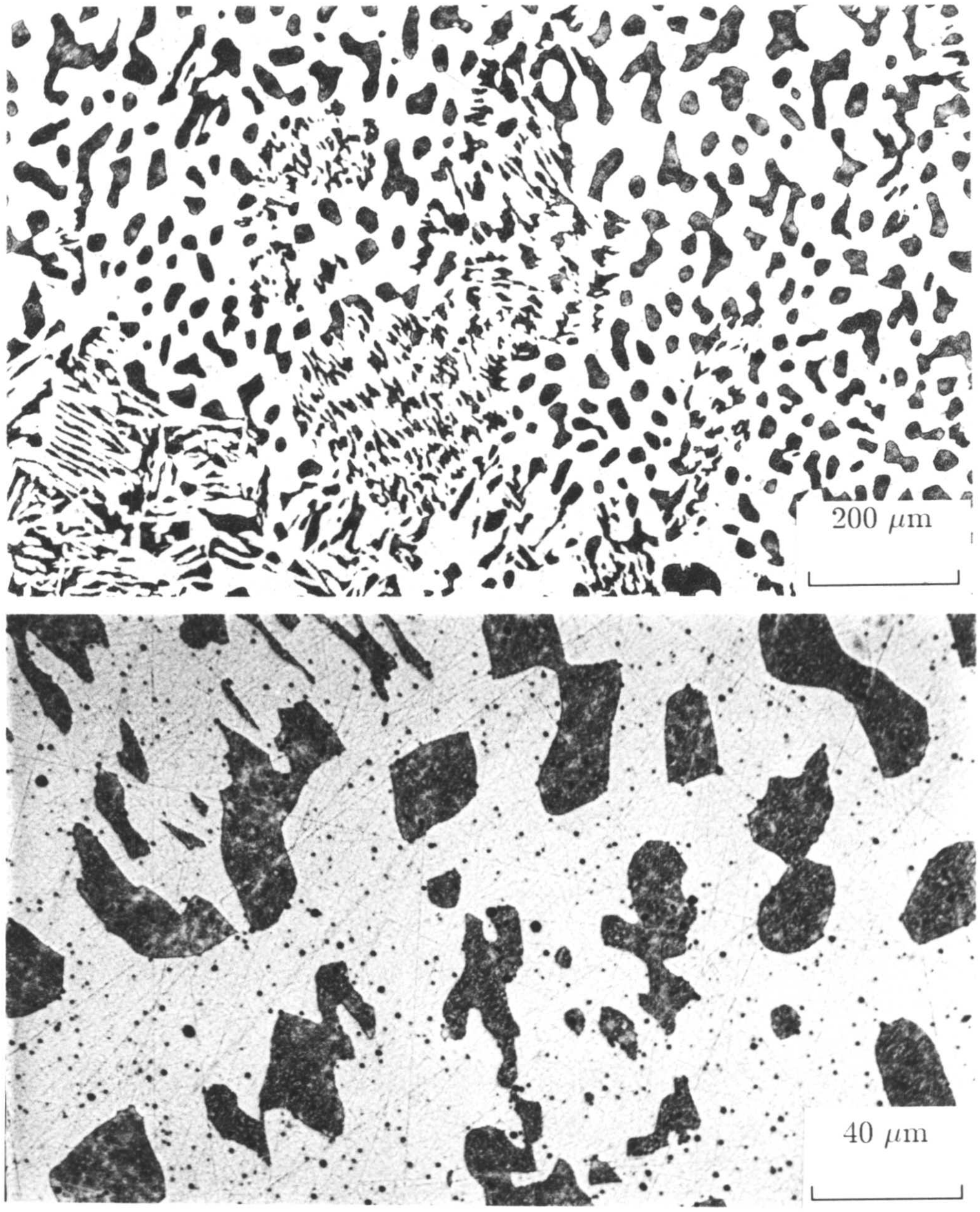

Figure 6.13. Light micrographs showing the microstructure of super duplex weld metal A219 heat treated at 1150 °C for 165 hours and then quenched into water. The light phase is austenite and the dark one is ferrite. The fine particles inside the ferrite grains are austenite formed during quenching. The measured volume fraction of austenite (excluding the fine particles) is about 0.75.

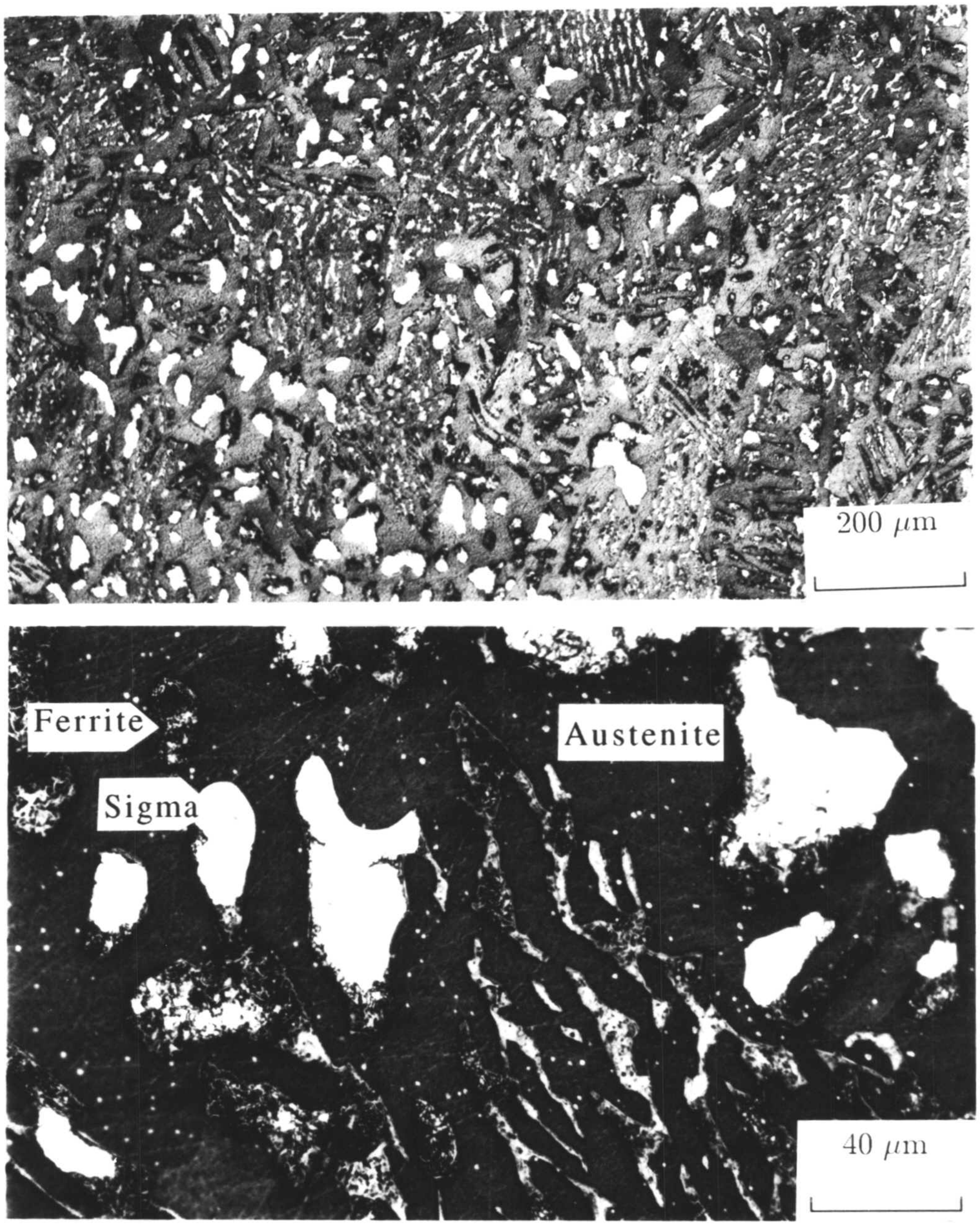

Figure 6.14. Light micrographs showing the microstructure of super duplex weld metal A219 heat treated at 1100 °C for 315 hours and then quenched into water. This figure shows that ferrite (dark phase) has decomposed to austenite (gray phase) plus sigma (bright phase). is austenite. The measured volume fraction of austenite is about 0.70.

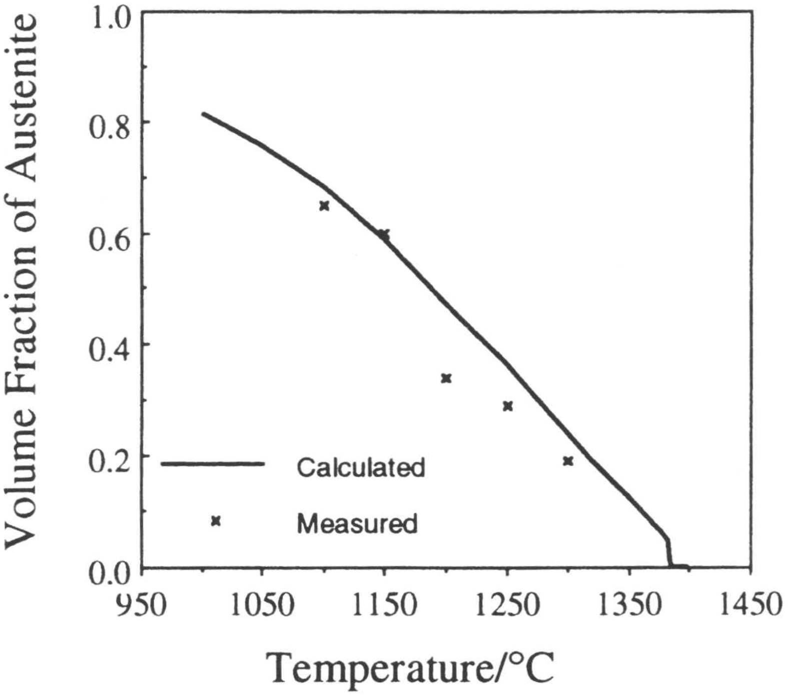

Figure 6.15. Calculated and measured equilibrium volume fractions of austenite as a function of temperature in duplex alloy IC381.

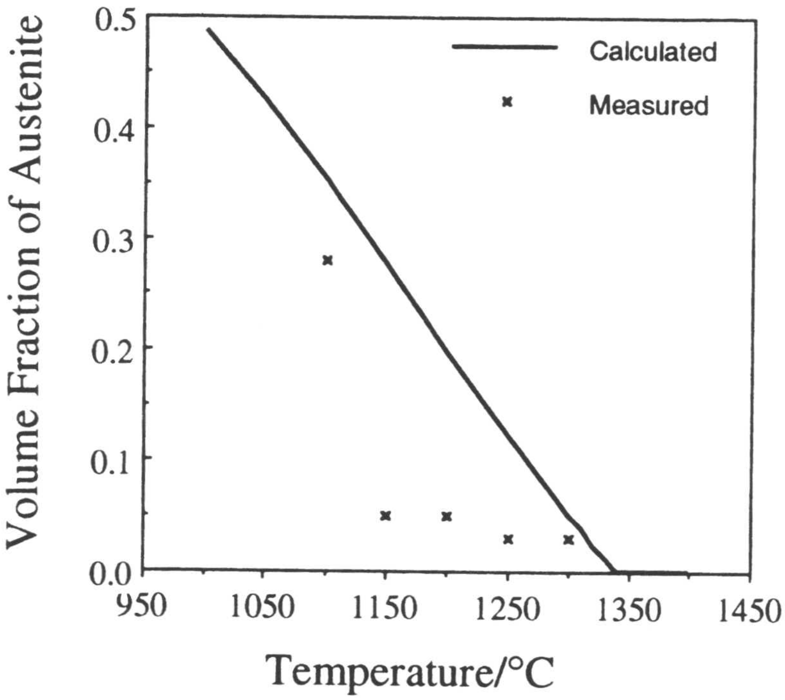

Figure 6.16. Calculated and measured equilibrium volume fractions of austenite as a function of temperature in duplex alloy IC373.

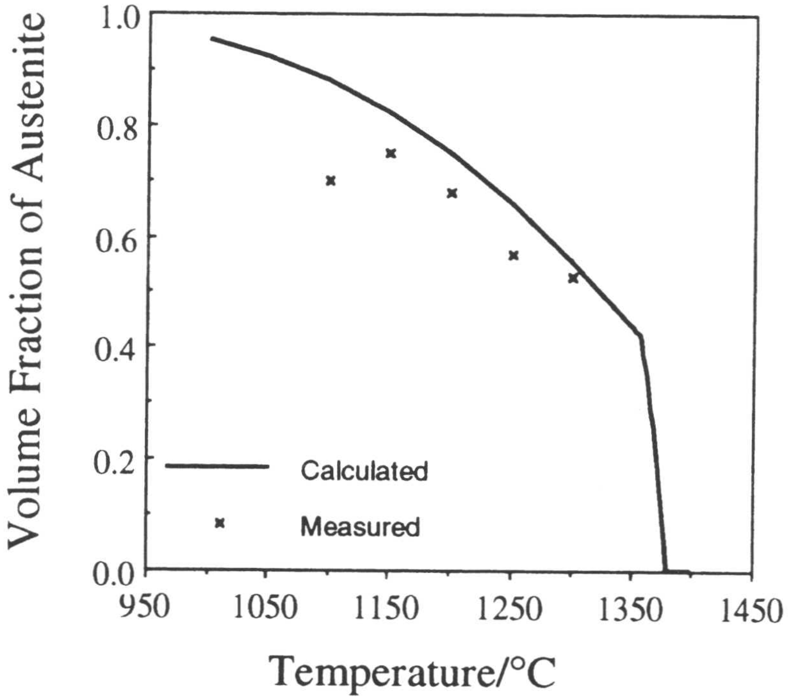

Figure 6.17. Calculated and measured equilibrium volume fractions of austenite as a function of temperature in super duplex weld metal A219.

6.4 Effect of Ferrite/Austenite Balance on Hardness

The experiments show that the hardness has a close relation with the volume fraction of δ-ferrite in duplex stainless steels. Figure 6.18 shows the measured hardness against the heat treatment temperature over the temperature range 1100-1300 °C. In this temperature range, the microstructure is ferritic-austenitic and almost free from other precipitation (except for alloy A219 heat treated at 1100 °C that microstructure consists of three phases austenite, ferrite and sigma phase). The hardness was found to increase with increasing heat treatment temperature. This is expected because of the accompanying increase in the volume fraction of δ-ferrite which is the harder of the two phases. For temperatures below 1200 °C, super duplex weld metal A219 is harder than duplex rolled metal IC381 although its volume fraction of austenite is higher. This is due to the formation of sigma phase at 1100 °C in alloy A219 (Figure 6.14). In the case of 1150 °C this can be due to precipitation of chromium nitride as the nitrogen and chromium content of A219 is larger than in IC381 (see section 6.6).

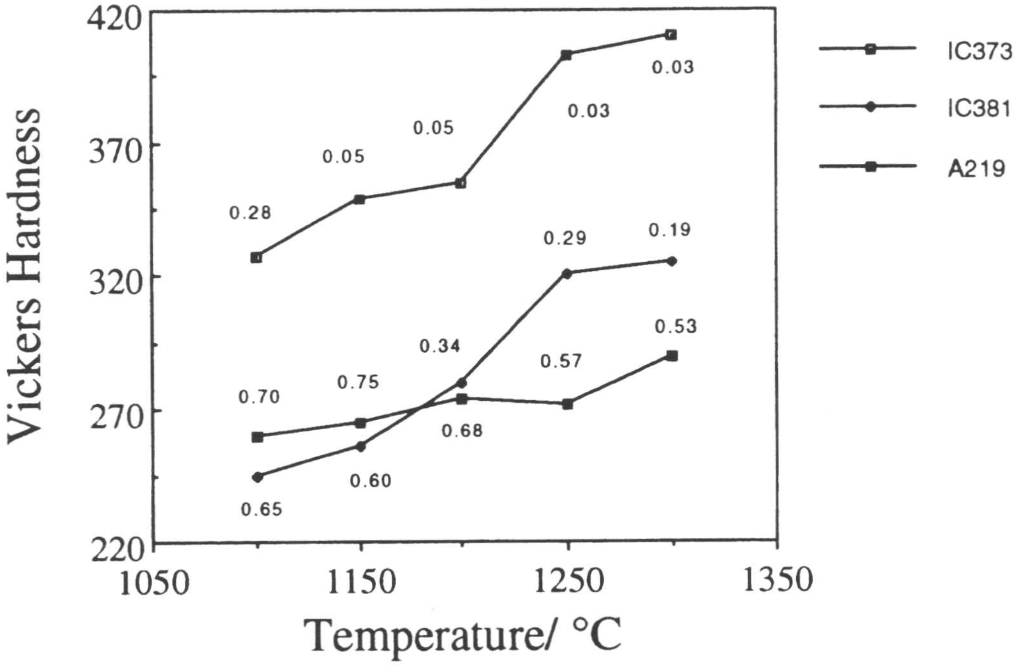

Figure 6.18. Measured hardness values as a function of the heat treatment temperatures. The measured fractions of austenite (excluding fine particles) are also included.

6.5 Equilibrium partitioning of alloying elements

The concentrations of different elements in each phase were measured using an EDX analyser on a scanning electron microscope (see section 2.10). Only the major constituents were analysed, namely Fe, Cr, Ni, Mo, Mn and Si. The concentrations of these elements were normalised to 100 wt.%. Between these elements molybdenum has a much larger atomic mass compared with the others. Since the microanalytic measurements are carried out assuming that all the elements absorb X-rays to a similar degree, the molybdenum data are likely to be flawed, the extent of the error depending on the thickness of the particle along the electron beam direction (a parameter which is very difficult to determine). The chemical composition of each phase was analysed twenty times in each heat treated specimen (Tables 6.3 to 6.6), the error bars show the standard deviation. Figures 6.19 to 6.24 show the calculated and measured partitioning of different alloying elements in duplex rolled metal IC381 and super duplex weld metal A219 as a function of temperature. As the temperature increases the equilibrium concentration of chromium in ferrite decreases while its nickel content increases (Figures 6.19 and 6.20). The equilibrium nickel content of austenite also increases with temperature (Figures 6.20 and 6.23). There is broad agreement between calculations and measurements, except for molybdenum where the discrepancies are large.

Table 6.3. TEM EDX microanalysis of δ-ferrite in duplex rolled metal IC381 heat treated at different temperatures (all concentrations in wt.%).

Temperature °C	Fe	Cr	Ni	Mo	Mn	Si
1300	64.30±0.47	24.30±0.47	5.47±0.09	3.37±0.19	1.97±0.05	0.47 ±0.02
1250	65.00±0.82	24.67±0.47	4.97±0.17	3.30±0.14	1.80±0.22	0.43 ±0.02
1200	64.67±0.47	24.67±0.47	5.00±0.14	3.47±0.12	1.87±0.25	0.47 ±0.05
1150	64.00±0.62	26.00±0.35	4.60±0.27	3.71±0.23	1.43±0.21	0.49 ±0.02
1100	63.67±0.47	25.67±0.47	4.47±0.17	3.87±0.12	1.83±0.05	0.46 ±0.04

Table 6.4. TEM EDX microanalysis of austenite in duplex rolled metal IC381 heat treated at different temperatures (all concentrations in wt.%).

Temperature °C	Fe	Cr	Ni	Mo	Mn	Si
1300	64.67±0.47	23.20±0.47	7.00±0.22	2.90±0.73	2.13±0.05	0.45 ±0.07
1250	65.67±0.47	22.67±0.47	7.00±0.22	2.27±0.12	2.13±0.26	0.40 ±0.04
1200	66.00±0.87	22.00±0.57	7.23±0.19	2.37±0.05	2.10±0.08	0.41 ±0.03
1150	66.10±0.43	22.10±0.63	7.31±0.23	2.33±0.13	1.70±0.16	0.33 ±0.05
1100	65.00±0.61	22.00±0.72	7.20±0.33	2.60±0.67	2.40±0.15	0.46 ±0.06

Table 6.5. TEM EDX microanalysis of δ-ferrite in super duplex weld metal A219 heat treated at different temperatures (all concentrations in wt.%).

Temperature °C	Fe	Cr	Ni	Mo	Mn	Si
1300	58.00±0.97	28.75±0.43	8.27±0.25	4.15±0.17	0.63±0.07	0.48 ±0.06
1250	57.33±0.47	29.33±0.47	7.73±0.15	4.43±0.41	0.67±0.13	0.56 ±0.04
1200	58.00±0.50	29.00±0.50	7.17±0.26	4.73±0.29	0.66±0.06	0.55 ±0.06
1150	57.00±0.50	30.10±0.63	6.95±0.25	4.45±0.55	0.99±0.01	0.43 ±0.07
1100	57.00±0.50	30.00±0.20	6.80±0.20	4.85±0.05	0.77±0.11	0.62 ±0.02

Table 6.6. TEM EDX microanalysis of austenite in super duplex weld metal A219 heat treated at different temperatures (all concentrations in wt.%).

Temperature °C	Fe	Cr	Ni	Mo	Mn	Si
1300	59.00±0.50	26.50±0.50	10.25±0.43	2.60±0.25	0.68±0.13	0.45 ±0.10
1250	58.50±0.50	27.00±0.50	10.00±0.50	3.20±0.40	0.76±0.06	0.48 ±0.09
1200	59.00±0.50	27.00±0.82	9.90±0.14	2.35±0.55	0.85±0.19	0.39 ±0.17
1150	58.00±0.82	27.33±0.47	9.87±0.12	3.00±0.08	1.5±0.64	0.40 ±0.08
1100	59.00±0.50	26.00±0.50	11.00±0.50	3.05±0.25	0.70±0.11	0.47 ±0.05

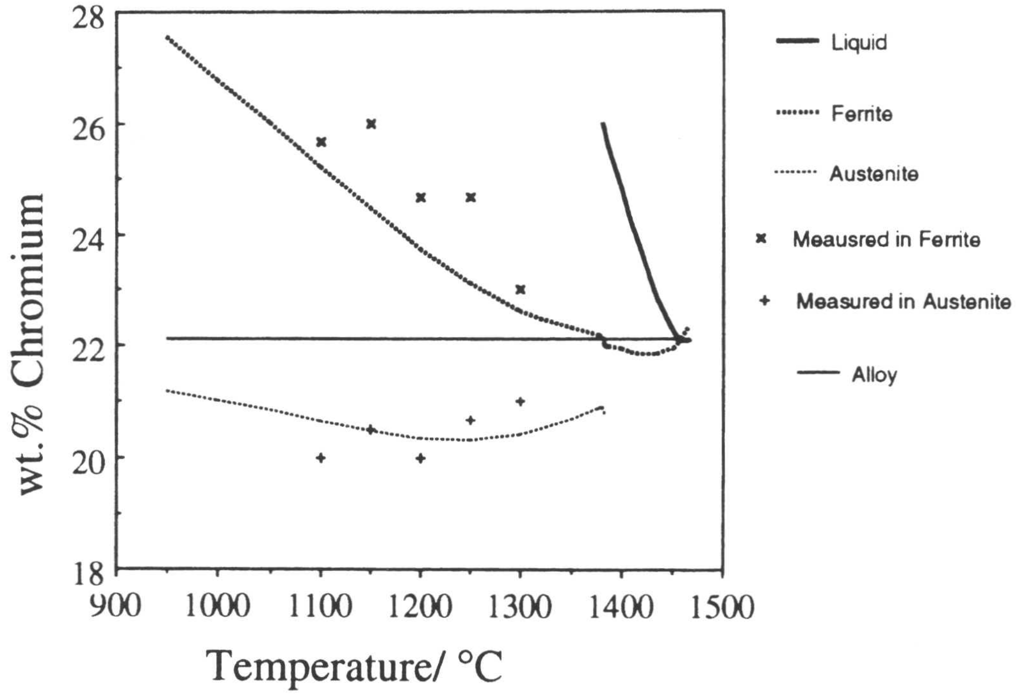

Figure 6.19. The calculated and measured partitioning of chromium in duplex rolled metal IC381 as a function of temperature.

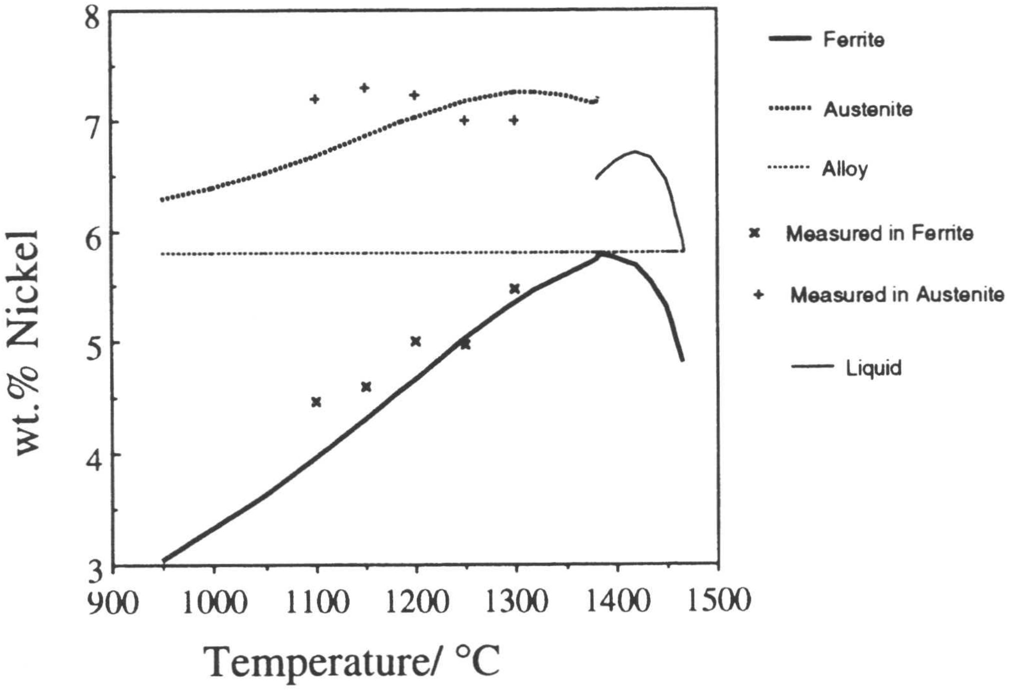

Figure 6.20. The calculated and measured partitioning of nickel in duplex rolled metal IC381 as a function of temperature.

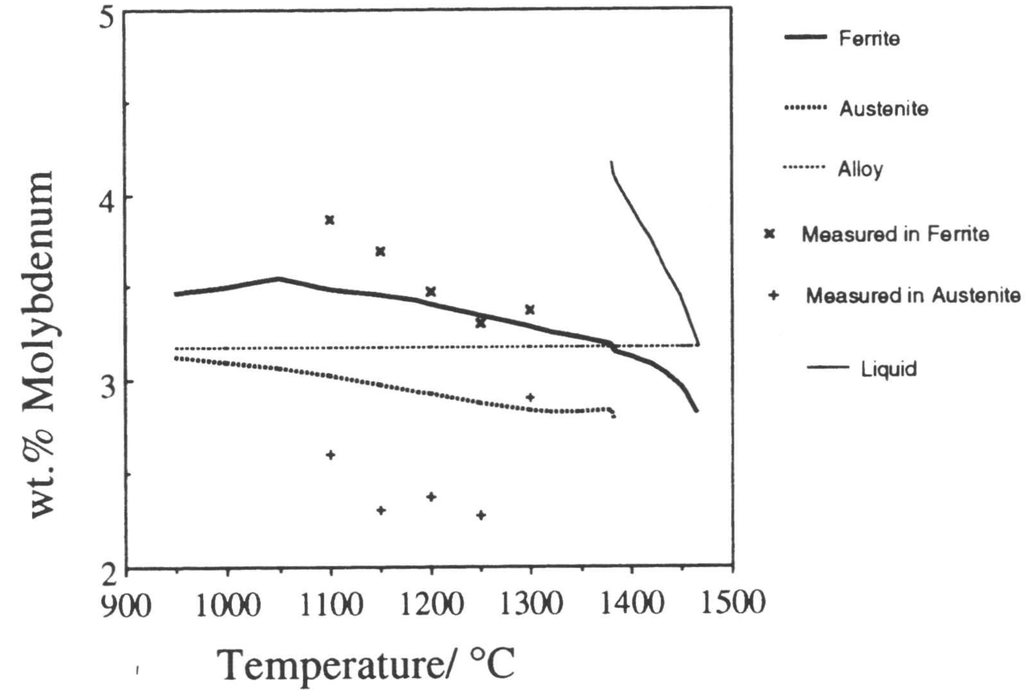

Figure 6.21. The calculated and measured partitioning of molybdenum in duplex rolled metal IC381 as a function of temperature.

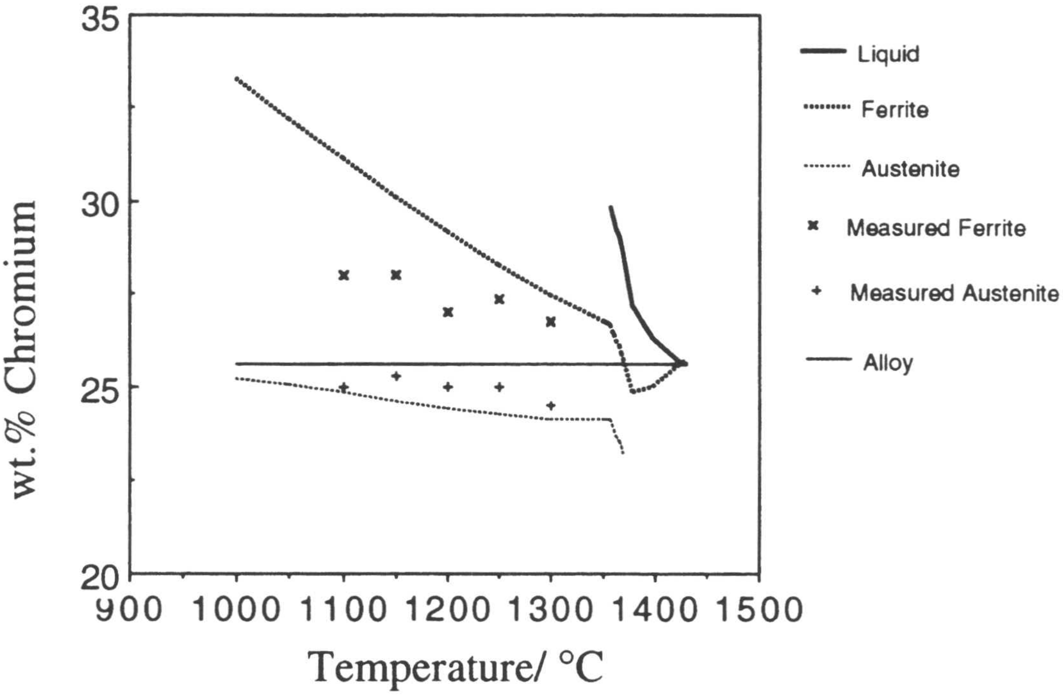

Figure 6.22. The calculated and measured partitioning of chromium in super duplex weld metal A219 as a function of temperature.

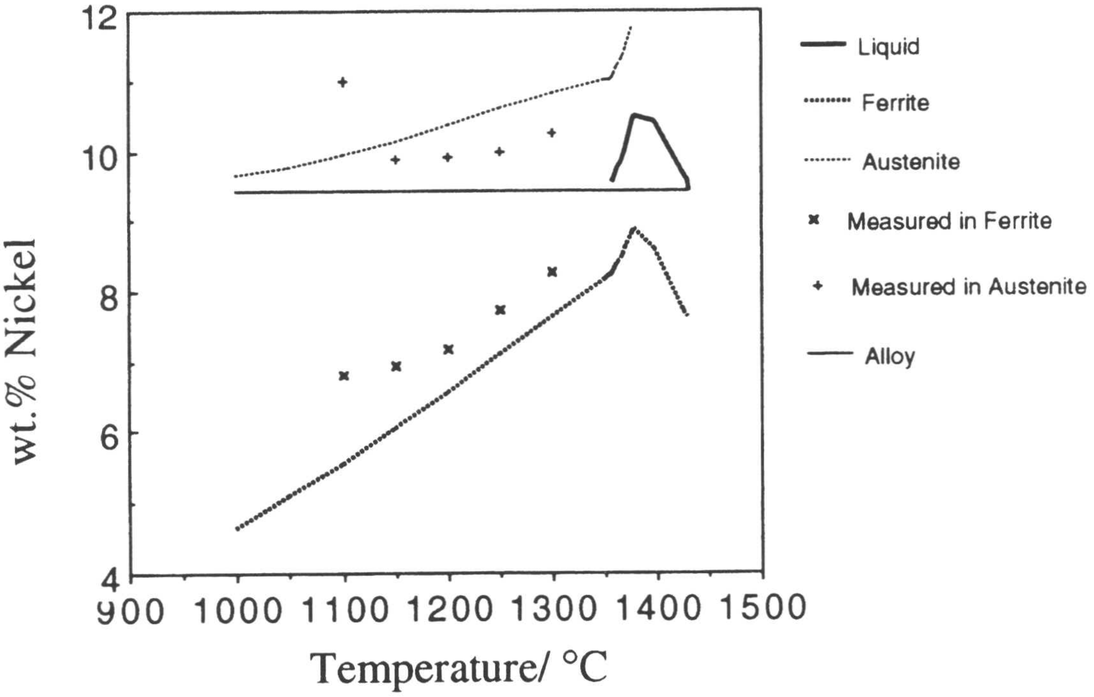

Figure 6.23. The calculated and measured partitioning of nickel in super duplex weld metal A219 as a function of temperature.

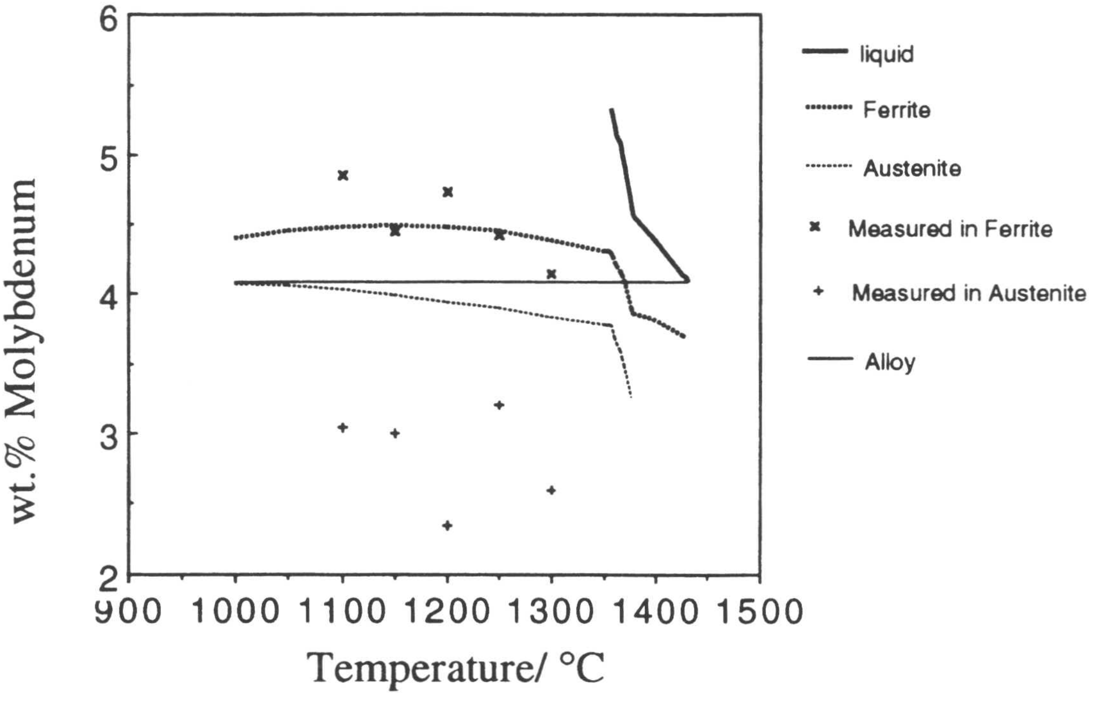

Figure 6.24. The calculated and measured partitioning of molybdenum in super duplex weld metal A219 as a function of temperature.

6.6 Precipitation of Cr_2N

With increased use of N as an alloying element in duplex and super duplex stainless steels, the tendency for the precipitation of chromium nitrides of type Cr_2N in the temperature range 700-900 °C has been enhanced (Hochmann *et al.*, 1974). The precipitate can even form during quenching from solution treatment temperatures. Nilsson and Liu (1988) have observed Cr_2N of 200-500 Å diameter at δ/δ boundaries after quenching in water from 1150 °C in some super duplex steels. Roscoe *et al.*, (1985) have shown that precipitation of Cr_2N is more likely when solutionising is performed at higher temperatures, for instance 1300 °C. However, the effect of Cr_2N on the mechanical and corrosion properties has not been separated from that of sigma, since Cr_2N and sigma often coexist.

In this study, chromium nitride was found to precipitate intragranularly inside the δ-ferrite grains during quenching from solution temperatures higher than 1100 °C in super duplex weld metal A219. Their precipitation was not observed in duplex rolled metals IC381 and IC373. This is due to the fact that the nitrogen content of A219 is more than twice that of IC381 and IC373. Specimens of alloy A219 heat treated at 1150 °C were found to be harder than specimens of alloy IC381 even though the ferrite volume fraction of IC381 is higher (Figure 6.18). This may be due to the precipitation of chromium nitride in alloy A219. Figure 6.25 shows the very fine precipitations of chromium nitride particles inside δ-ferrite grain which have formed during quenching from 1300 °C in A219. Figure 6.26 shows the dark field image of the same particles and Figure 6.27 shows the diffraction pattern of the matrix confirming that matrix has a b.c.c. crystal structure and chromium nitride precipitation do occur in ferrite. Figure 6.28 shows TEM micrographs of carbon replica extract from same sample. The electron diffraction pattern shown in Figure 6.29 confirms that particles have a structure which is trigonal, consistent with that reported by Eriksson (1934). The EDX microanalysis of the carbon replica samples shows that the particles are very rich in chromium (Table 6.7). These results confirm that the particles are likely to be chromium nitrides.

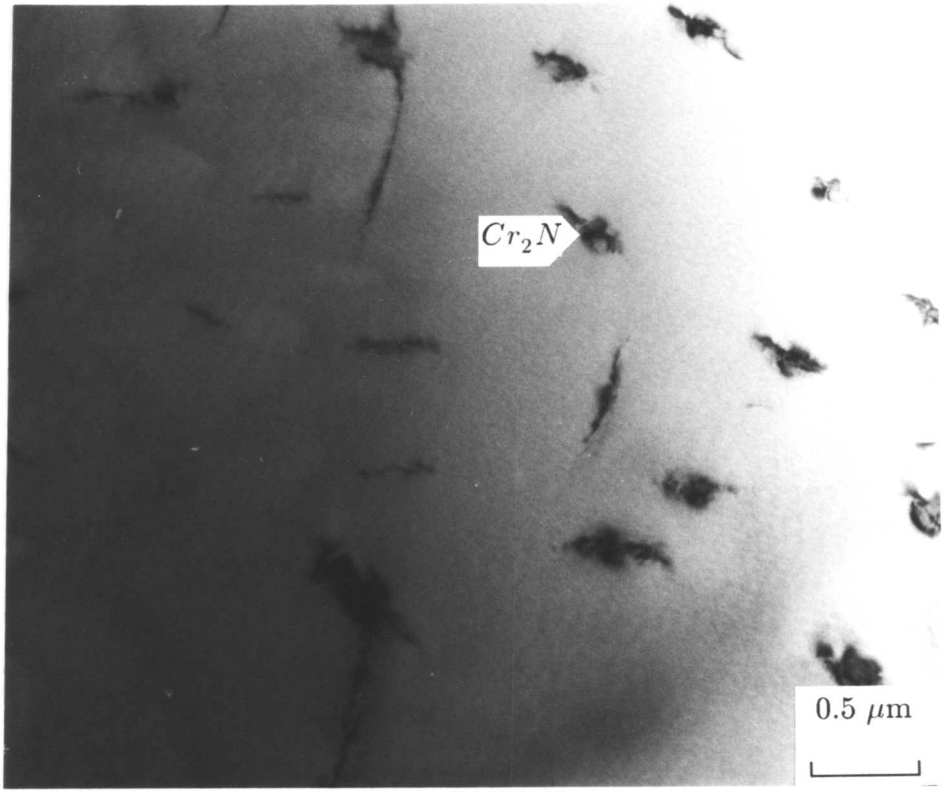

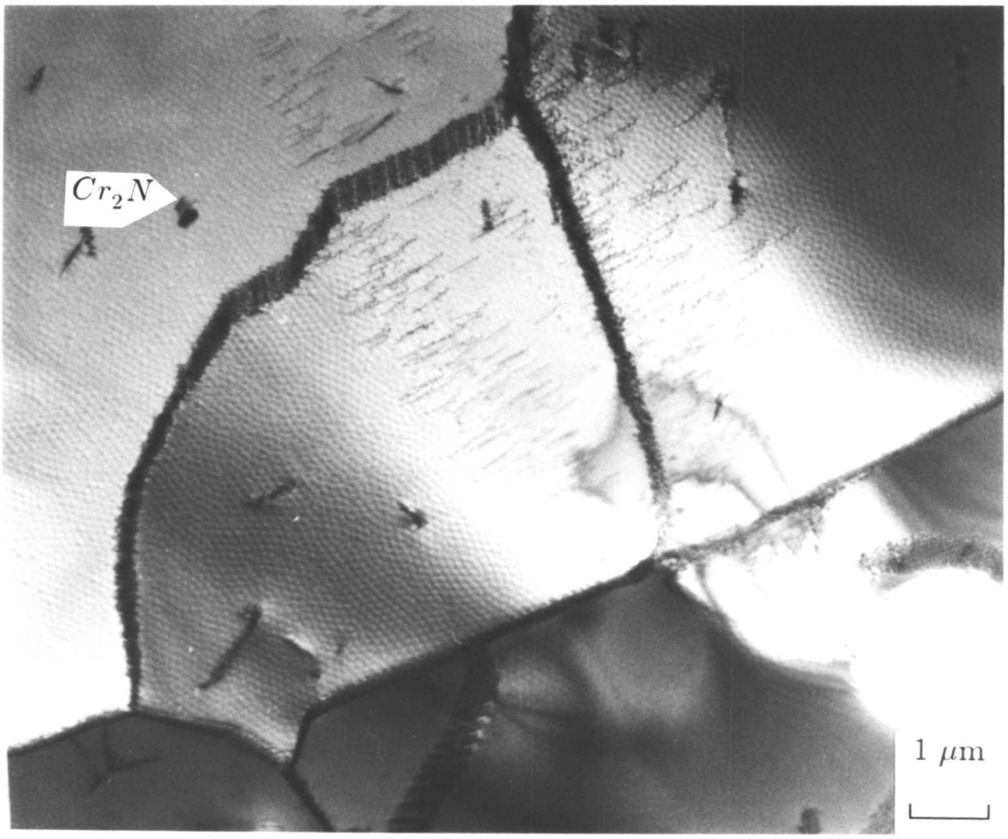

Figure 6.25. Bright field TEM micrographs from thin foils showing the intragranular precipitation of Cr_2N in δ-ferrite formed in A219 during quenching from 1300 °C.

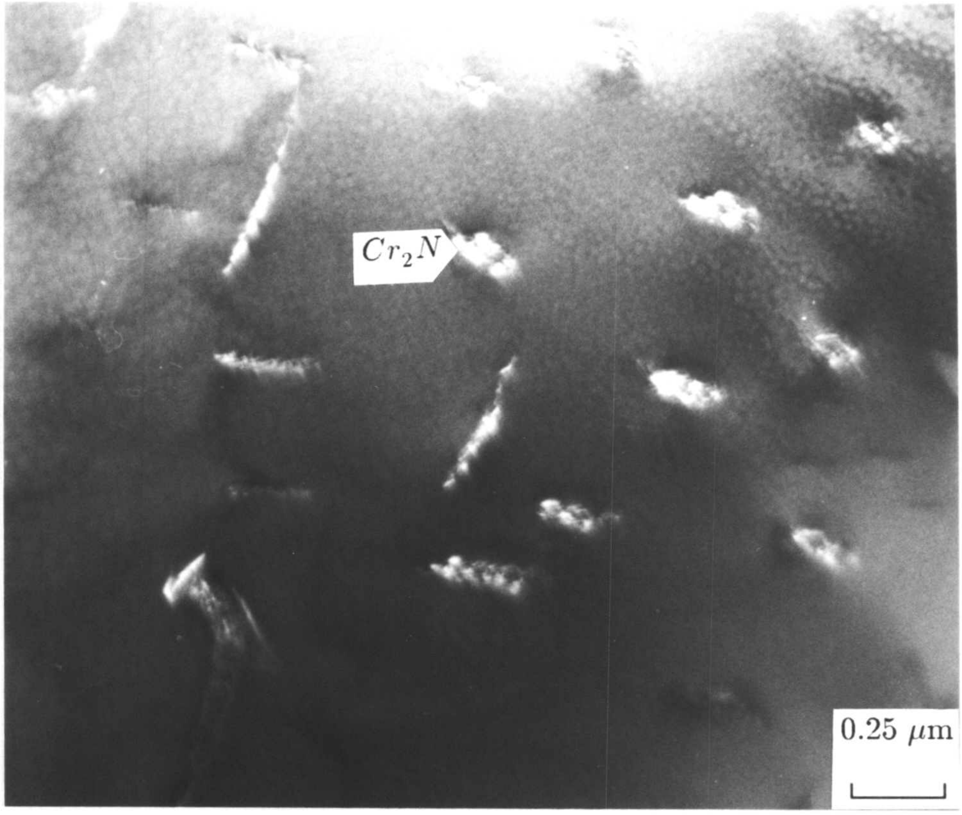

Figure 6.26. Dark field TEM micrographs from thin foils showing the intragranular precipitation of Cr_2N in δ-ferrite formed in A219 during quenching from 1300 °C.

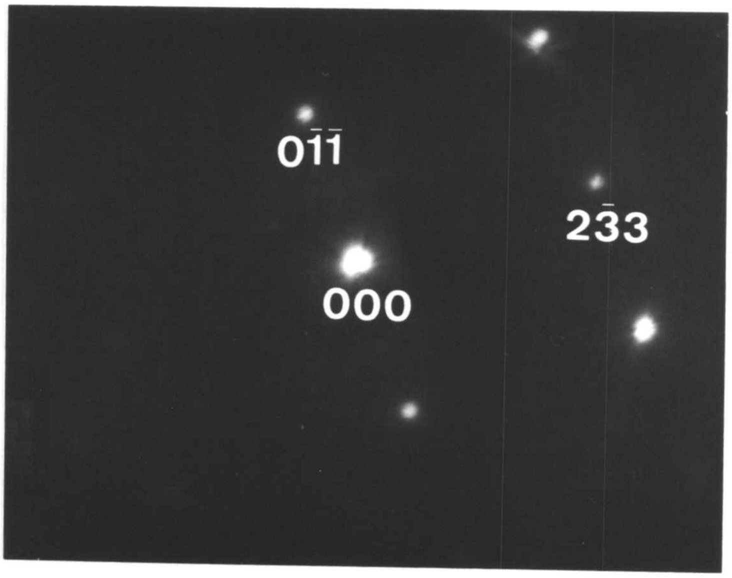

Figure 6.27. SADP of the matrix of Figure 6.25. The zone direction of the diffraction pattern is $[\overline{31}1]$.

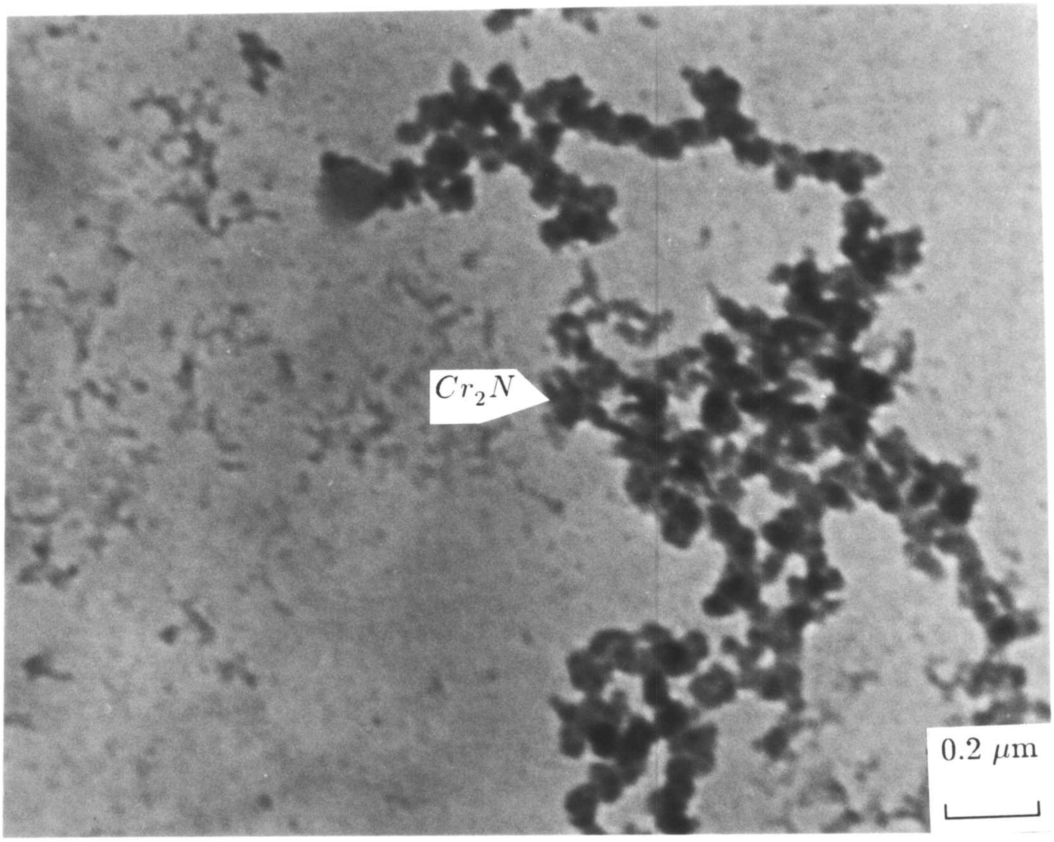

Figure 6.28. Bright field TEM micrographs from carbon replica extracted from A219 sample quenched from 1300 °C showing the Cr_2N particles formed during quenching.

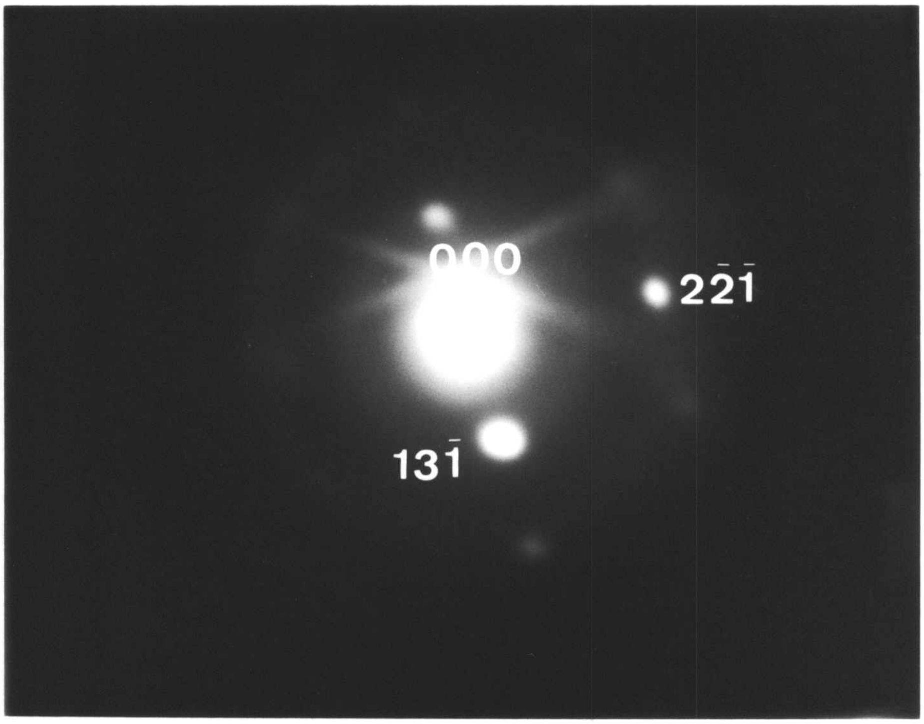

Figure 6.29. SADP of the Cr_2N particles. The zone direction of the diffraction pattern is [518].

Table 6.7. TEM EDX microanalysis of chromium nitride particles formed during quenching from 1300 °C in A219 (all concentrations in wt.%).

Fe	Cr	Ni	Mo	Mn	Si
7.25±0.43	84.57±0.61	0.51±0.09	0.12±0.03	2.72±0.05	-

6.7 Modelling of T_δ

Computer programs have been used to estimate the ferritisation temperature (the temperature where the microstructure is wholly ferritic, T_δ) and volume fractions of austenite. The aim was to provide a simple way of estimating these values. MTDATA therefore provided the raw data which were fitted using regression analysis. These computer programs are presented in appendices A, B and C respectively.

The first program calculates the Ni_{eq} and Cr_{eq} using the Pickering equation (see section 3.4). It then employs regression analysis using values of T_δ calculated by the MTDATA package as actual values, in order to determine an empirical formula for T_δ as a function of Ni_{eq} and Cr_{eq}. In some cases, the calculation of T_δ by MTDATA required the liquid phase to be suppressed. These calculations have produced the following empirical equation where T_δ in degree °C.

$$T_\delta = 1201 + 30.59 \times Ni_{eq} - 3.62 \times Cr_{eq} \qquad (6.1)$$

Figure 6.30 shows calculated and actual T_δ against Ni_{eq}/Cr_{eq} for the steels presented in Table 2.1.

The second computer program is written to calculate the coefficients of the elements in Cr_{eq} and Ni_{eq}, in order to design a new equation for super duplex stainless steels. These calculations have produced the following empirical equation where all the concentrations are in wt.%.

$$Cr_{eq} = Cr + 2Si + 4Mo + 5V + 5.5Al + 0.75Nb + 1.5Ti + 0.75W$$

$$Ni_{eq} = Ni + Co + 0.5Mn + 0.3Cu + 15C + 11N$$

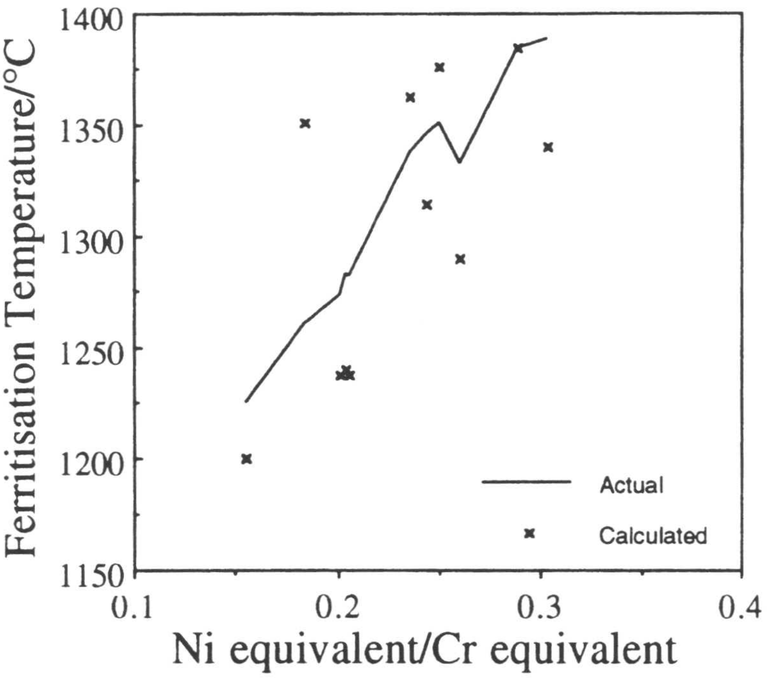

Figure 6.30. Calculated and actual T_δ of different types of duplex stainless steels listed in Table 2.1.

The third computer program is designed to predict the volume fraction of austenite using two dimensional regression analysis on input values of austenite fraction (calculated by MTDATA) against undercooling below T_δ. The following empirical formula is the result of these calculations where T and T_δ are in degree °C and V_γ is the volume fraction of austenite (T_δ can be calculated from equation 6.1).

$$\ln(V_\gamma + 0.0194) = 1.393\ln(T_\delta - T + 1) - 3.945 \tag{6.2}$$

Where T is less than T_δ. It is important to know that the application of equation 6.2 to predict the equilibrium volume fraction of austenite is limited over the temperature range where the microstructure is duplex (i.e. where sigma phase and other precipitates are unstable). This means for the steels that we studied in this chapter this equation can be used only where $1100<T<T_\delta$. Secondly, this equation gives the equilibrium volume fraction of austenite at the

desired temperature. But since austenite always forms during quenching in order to obtain the desired balance between austenite and ferrite at room temperature, a heat treatment should be designed which produces lower fractions of austenite than that required. Figure 6.31 shows the variation of calculated volume fraction of austenite (predicted by equation 6.2) and actual values (calculated by MTDATA) with temperature for super duplex weld metal A201.

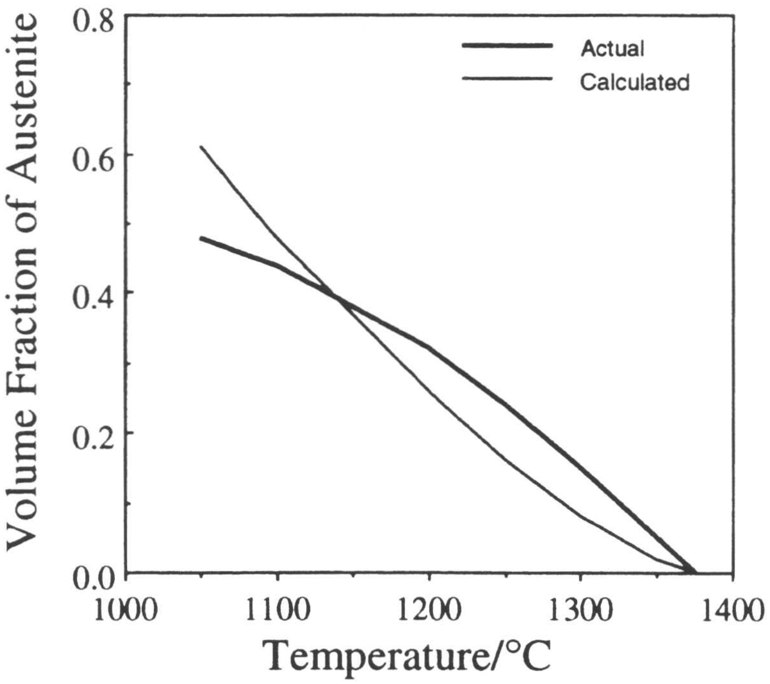

Figure 6.31. The variation of volume fraction of austenite (predicted and actual) with temperature for super duplex stainless steel weld metal A201 (Table 2.1).

6.8 Conclusions

1. Both the thermodynamic calculations and experimental measurements show that within the temperature range 1100-1300 °C, ferrite and austenite are the only phases which are present in duplex and super duplex stainless steels studied (except in super duplex A219 that sigma phase was found to form at 1100 °C).
2. The agreement between thermodynamic calculations and experimental volume fractions of austenite for samples which underwent prolonged isothermal heat treatments is good in all cases where the nucleation of austenite is rela-

tively easy.

3. As the temperature decreases the volume fraction of austenite in duplex and super duplex increases, causing the hardness to decrease.

4. Sigma phase does form at higher temperatures in super duplex stainless steel compared with the duplex grades. This is the effect of the higher Cr and Mo content (which are the strong sigma-phase formers) in the super duplex grades.

5. Chromium nitride was found to form during quenching from elevated solution temperature in super grade A219 (which has higher nitrogen content). The precipitation of these particles increases the hardness.

Chapter 7

PRECIPITATION IN SUPER DUPLEX STAINLESS STEELS

7.1 Introduction

Duplex stainless steels have better mechanical and corrosion properties compared with austenitic and/or ferritic stainless steels, because they combine the favourable properties of ferrite (δ) and austenite (γ), which are present in approximately equal amounts. However, a variety of undesired phases and precipitates may also appear if the steel is improperly treated at elevated temperatures. The presence of these precipitates can spoil the mechanical and corrosion properties. This chapter deals with an experimental characterisation of these undesired phases.

7.2 Previous Work

Josefsson *et al.* (1991) have reviewed the work which has been done by many researchers on phase transformation in duplex stainless steels, as summarised in Table 7.1. Solomon *et al.* (1979) have studied the phase transformations for the duplex alloy U50 and have proposed a TTT diagram which is presented in Figure 7.1.

Table 7.1. Precipitates and phases which have been observed in duplex stainless steels (Josefsson *et al.*, 1991).

Type of precipitate	Nominal chemical formula	Temperature range (°C)	Lattice parameter (Å)	Reference
δ	-	-	a=2.86-2.88	-
γ	-	-	a=3.58-3.62	-
σ	$Fe-Cr-Mo$	600-1000	a=8.79, c=4.54	Hall and Algie, 1966
Cr_2N	Cr_2N	-900	a=4.795, c=4.469	Eriksson, 1934
χ	$Fe_{36}Cr_{12}Mo_{10}$	700-850	a=8.92	Kasper, 1954
R	$Fe-Cr-Mo$	550-650	a=10.903, c=19.342	Rideout *et al.*, 1951
π	$Fe_7Mo_{13}N_4$	550-600	a=6.47	Evans and Jack, 1957
M_7C_3	M_7C_3	950-1050	a=4.52, b=6.99 c=12.11	Rouault *et al.*, 1970
$M_{23}C_6$	$M_{23}C_6$	600-950	a=10.56-10.65	Bowman *et al.*, 1972

7.2.1 Secondary austenite

Secondary austenite is the austenite produced by transformation from ferrite. The ferrite to austenite transformation can happen over a wide temperature range and via different mechanisms depending on the transformation temperature.

7.2.1.1 Transformation temperatures greater than 650 °C

At temperatures above 650 °C austenite will form as Widmanstätten precipitates in various morphologies (Southwick and Honeycombe, 1980). Because of the high temperature, diffusion accompanies transformation and the austenite has a higher content of Ni than the ferrite matrix from which it grows.

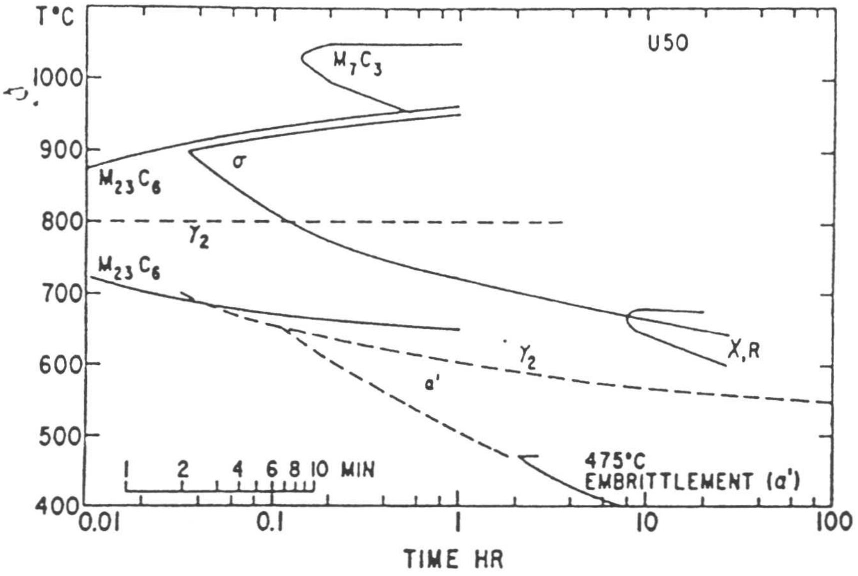

Figure 7.1. TTT diagram of a duplex stainless steel alloy U50 after Solomon *et al.*, 1979.

7.2.1.2 Transformation temperature in the range 700-900 °C

In this temperature range the transformation of δ-ferrite to austenite tends to occur by a eutectoid reaction

$$\delta_{\text{ferrite}} \rightarrow \sigma + \gamma_{\text{austenite}} \qquad (7.1)$$

because the δ-ferrite becomes destabilised by the precipitation of σ which reduces the Cr and Mo concentrations in ferrite. The δ-ferrite grains therefore change into intimate mixtures of austenite and σ.

7.2.1.3 Transformation temperatures less than 650 °C

At temperatures less than 650 °C the mobility of substitutional elements such as Cr, Ni and Mo is very small. Ferrite will transform to austenite via a mechanism that shows great similarities with martensite formation. The precipitation of austenite is isothermal and there is no difference in the composition of austenite and ferrite matrix with respect to the substitutional solutes. Southwick *et al.* (1980) have shown that the γ/δ orientation relationship is of the Nishiyama-Wasserman type. This form of austenite precipitates inside the ferrite grains independently of the precipitation of other phases and has been called γ_2 in some literature (Southwick and Honeycombe, 1980).

7.2.2 Sigma phase

Sigma phase is an intermetallic compound with a body centred tetragonal (b.c.t.) crystal structure, occurring mostly in the Fe-Cr and Fe-Cr-Mo systems. In Fe-Cr alloys containing more than 22 wt.% Cr, sigma phase has a composition centred on a Cr content of about 45 wt.%, and can appear during prolonged heat treatment at temperatures above 550 °C (Castro and de Candenet, 1968). In Fe-Cr-Mo systems the temperature range of stability is extended as Mo stabilises sigma. Maehara *et al.* (1983) have shown that Cr, Mo and Si increase both the precipitation rate and volume fraction of sigma in a large number of duplex steels. Ni on the other hand reduces the equilibrium volume fraction of sigma. However, it accelerates precipitation kinetics by reducing the δ-ferrite fraction, and increasing the partitioning of σ-promoting elements to ferrite.

Strutt and Lorimer (1984) have investigated the structure property relationships of ZERON 100 which is a super duplex stainless steel of nominal composition 25 Cr, 7.5 Ni, 3.5 Mo and 0.25 N wt.%. Their measured C-curve for 5 vol.% sigma is shown in Figure 7.2. They found that the nucleation of sigma-phase occurs on ferrite/austenite boundaries, presumably due to the good crystallographic match of the {111} plane of sigma and the {111} plane of austenite.

Preferential growth of sigma-phase into ferrite occurs because the ferrite is Cr-rich. The ferrite near the sigma naturally becomes depleted in Cr and Mo, and hence sometimes tends to partially transform to austenite.

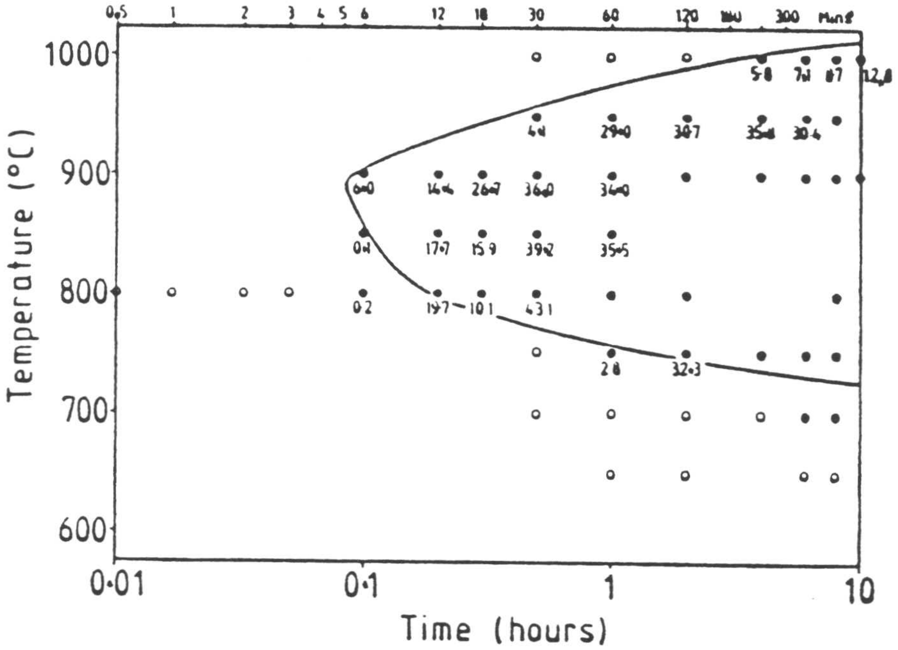

Figure 7.2. The measured C-curve for 5 vol.% sigma-phase formation in forged ZERON100 based on quantitative metallographic data (Strutt and Lorimer, 1986).

As sigma phase is hard and brittle, its presence in welds can cause embrittlement and its absorption of chromium can sensitise the alloy to corrosion (Hevbsleb and Schwabb, 1984).

7.2.3 Cr_2N

See chapter six.

7.2.4 Chi phase

Chi phase is another intermetallic compound which can precipitate in duplex and super duplex steels which precipitates in the temperature range 700-900 °C (Thorvaldsson *et al.*, 1985). As it is brittle it has an adverse effect on toughness, but owing its much lower volume fraction, it is much less important than sigma phase.

7.2.5 R phase

R phase is a Mo-rich compound which appears to be detrimental to toughness. Nilsson *et al.* (1991) have investigated its precipitation in a Fe-22Cr-8Ni-3Mo wt.% weld metal. It precipitates in temperature interval 550-650 °C and has an approximate composition of Fe-25Cr-6Ni-34Mo-4Si wt.%. These data must obviously depend on alloy chemistry as well, although the details are not known.

7.2.6 Carbides

Carbides of type M_7C_3 precipitate in the temperature range 950-1050 °C and $M_{23}C_6$ below about 950 °C. Thorvaldsson *et al.* (1985) have observed precipitation of both types of carbide at δ/δ, γ/γ and δ/γ boundaries. However, due to the low carbon content of duplex and super duplex steels carbides play a less important role compared with other types of stainless steels with higher carbon contents.

7.2.7 π-nitride

π-nitride is a detrimental intermetallic compound that may precipitate intragranularly in duplex and super duplex stainless steels (Thorvaldsson *et al.*, 1991). It can easily be confused with sigma phase with a chemistry of approximately Fe-35Cr-3Ni-34Mo wt.% (ideally $Fe_7Mo_{13}N_4$).

7.2.8 Low temperature ageing

Iron–chromium ferritic solid solutions have a tendency to show the clustering of atoms, rather than a random distribution. The clustering manifests at low temperatures since at elevated temperatures, entropy effects tend to randomise the solution. There are severe embrittling effects which occur as a consequence during prolonged low temperature ageing, at temperatures in the vicinity of 430-470 °C. A chromium rich α' "phase" precipitates on a very fine scale, probably by a mechanism involving spinodal decomposition. These effects are not explored in the present work, but could be quite important if duplex and super duplex alloys are used in the appropriate service conditions (Strangwood and Druce, 1990).

7.3 Thermodynamic calculations

The purpose here was to investigate the carbide and sigma phases using the MTDATA package for super duplex weld metal A219 (Table 5.1). Figure 7.3 shows the calculated phase diagram of the alloy. In addition to δ-ferrite and austenite, sigma phase and $M_{23}C_6$ also precipitate. Note that other carbides (M_7C_3 and M_2C) were also included in the analysis but do not form in the equilibrium state.

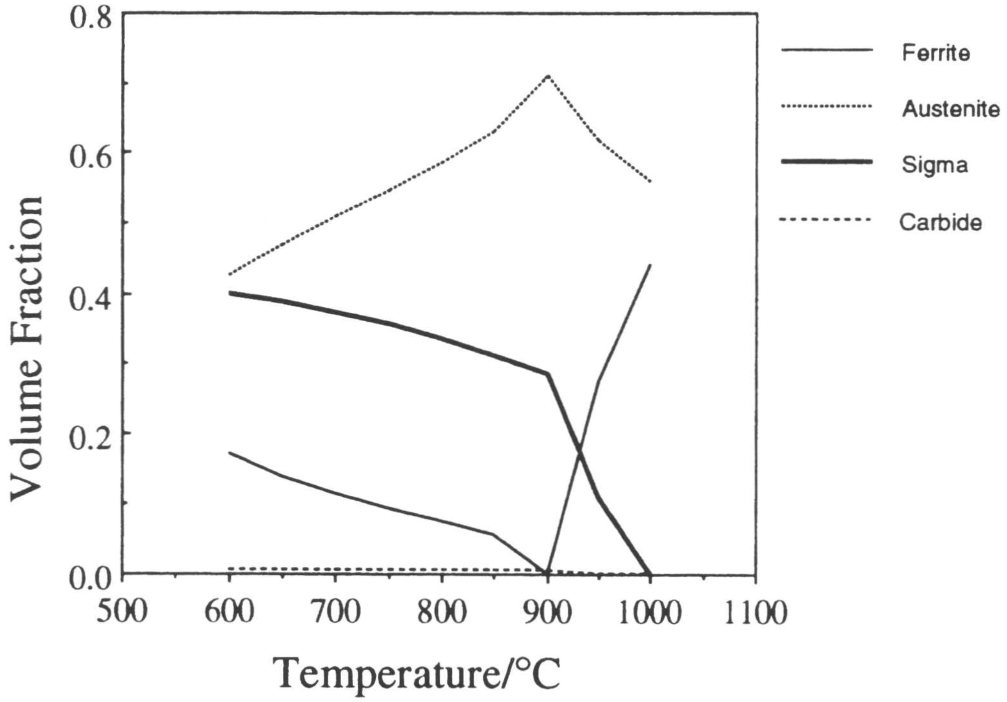

Figure 7.3. The equilibrium phase fractions for super duplex weld metal A219.

7.3.1 Discussion

The above calculations are in good agreement with literature data which indicate the only important precipitation in duplex and super duplex stainless steels in temperature range 600-1000 °C is sigma-phase and $M_{23}C_6$, although the maximum volume fraction of the latter phase is only about 0.006, negligible when compared with sigma phase. This is because new duplex and super duplex alloys contain little carbon (less than 0.03 wt.%). Further calculations therefore neglect any phases other than δ, γ and σ.

7.3.2 Calculations assuming only δ, γ and σ exist

Thermodynamic calculations have been done for duplex and super duplex alloys IC381, IC373, UNS31, ZERON100 and A219 (Table 5.1) in the temperature range of 600-1000 °C. the results are presented in Figure 7.4. Figure 7.4a shows the equilibrium precipitation of sigma-phase in an ordinary duplex stainless steel IC381. The sigma-phase begins to precipitate at 865 °C and its volume fraction increases as the temperature drops. At about 680 °C its equilibrium volume fraction reaches a maximum of about 0.18. At temperatures below 680 °C the austenite should transform to ferrite.

Figure 7.4b shows that the σ_s temperature is much higher for alloy IC373 which has been overalloyed with Cr compared with TIC381. The sigma-phase volume fraction is also much higher (its maximum is about 0.32 at 680 °C). In the duplex weld metal UNS31 as Mo and Cr are lower in concentration compared with IC381 σ_s is lowered to 820 °C with correspondingly smaller volume fraction. Super duplex alloy ZERON100 (Figure 7.4d) contains a larger Cr and Mo content compared with TIC381 leading to a higher σ_s temperature and volume fraction. The interesting result is that the calculated phase diagram for super duplex weld metal A219, shows the highest σ_s temperature (about 990 °C). However, due to its higher Ni content the volume fraction of σ-phase is smaller than in ZERON100. With large Ni concentrations (UNS31 and A219) ferrite does not form at low temperatures at all until σ precipitation is completed. Consequently there is no δ-ferrite phase available to decompose to austenite plus sigma. Hence, the calculated fraction of sigma-phase is in such alloys always rather small.

7.3.3 Partitioning

Sigma-phase is a brittle phase rich in chromium, and in the alloys such as A219, exists in equilibrium with austenite for temperatures below 990 °C. Figures 7.5 to 7.7 show the expected equilibrium partitioning of Cr, Mo and Ni respectively between austenite and sigma over temperature range of 600-990 °C. It is interesting that the Cr concentration in sigma-phase is about twice that in austenite with the partitioning becoming more pronounced at lower temperatures.

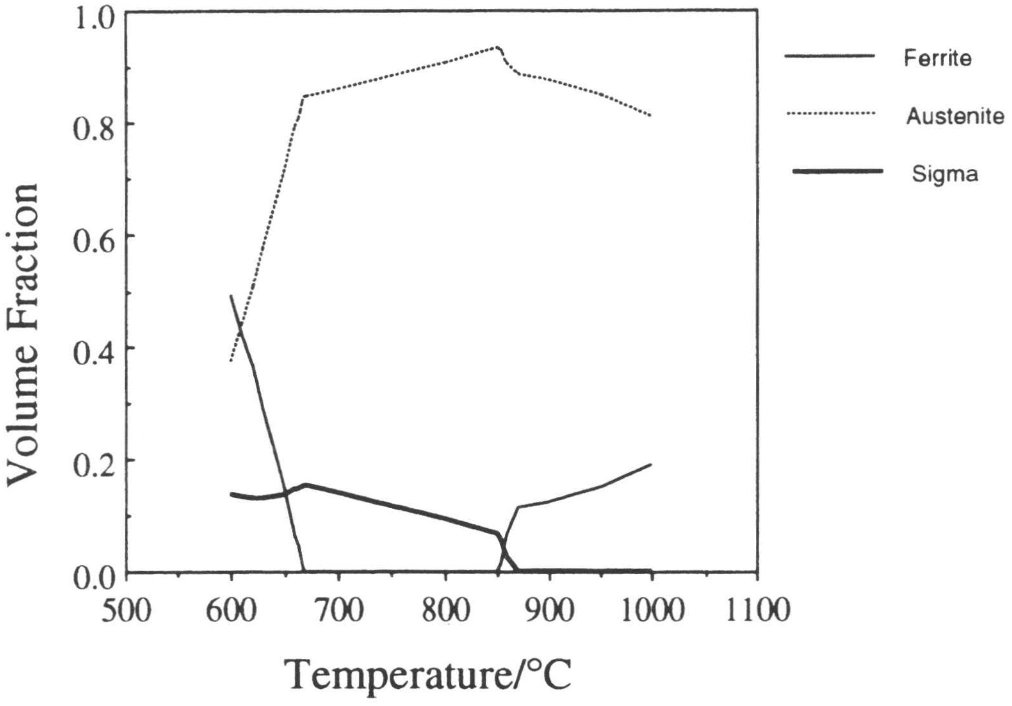

(a)

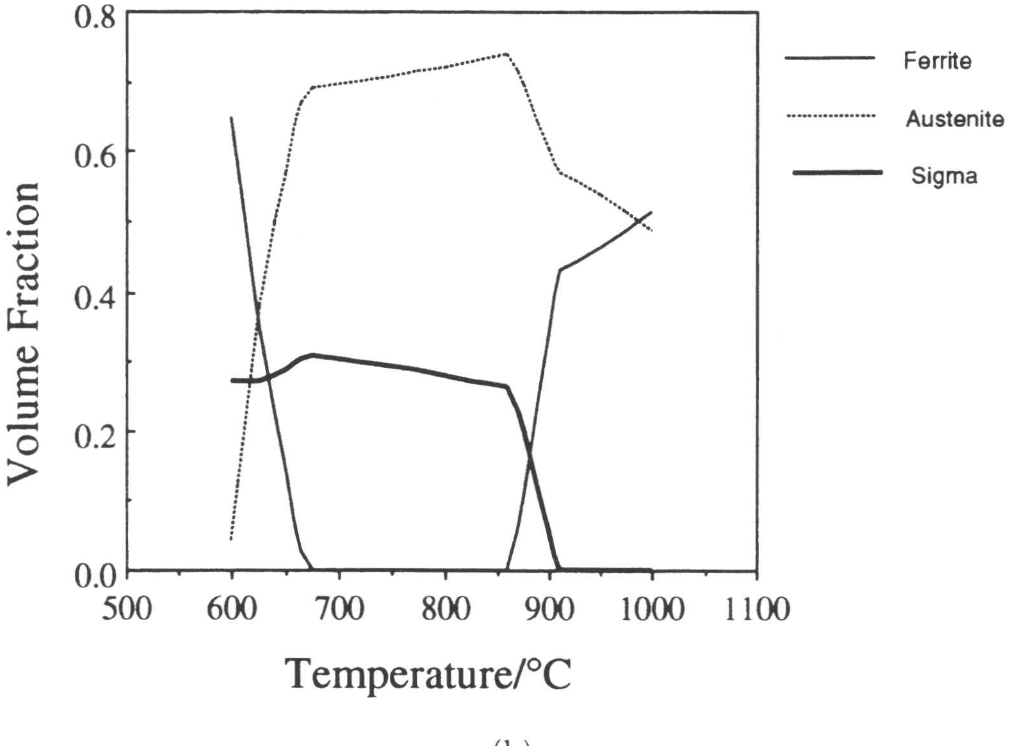

(b)

Figure 7.4. The calculated equilibrium phase fractions. a) duplex stainless steel IC381; b) overalloyed with Cr, IC373; c) duplex weld metal UNS31; d) super duplex stainless steel ZERON100; e) super duplex weld metal A219.

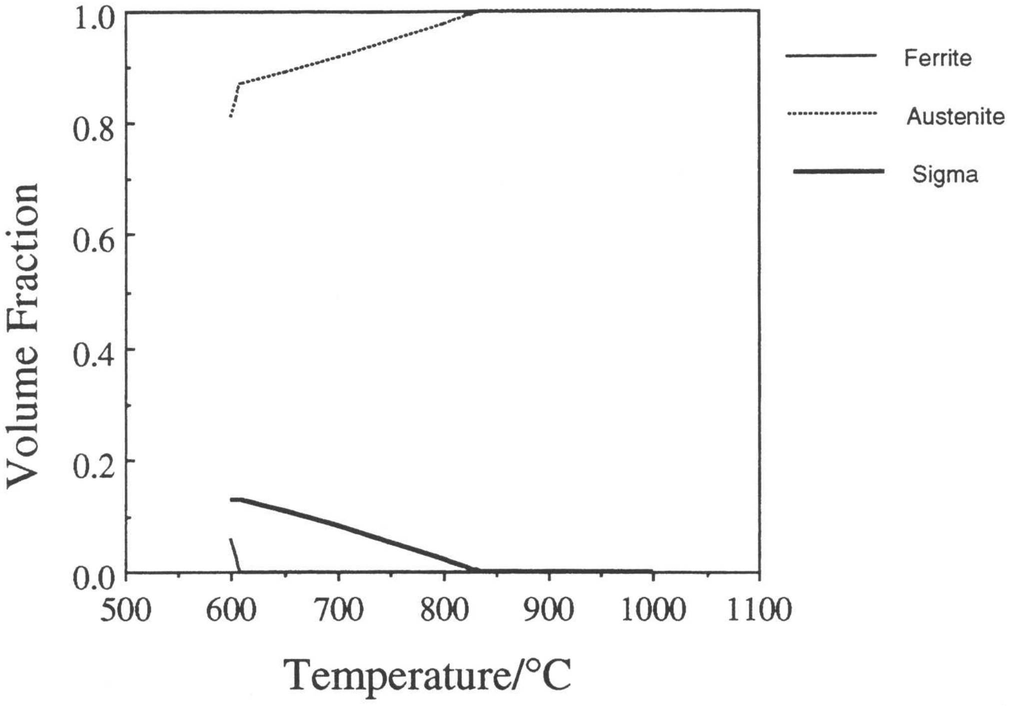

(c)

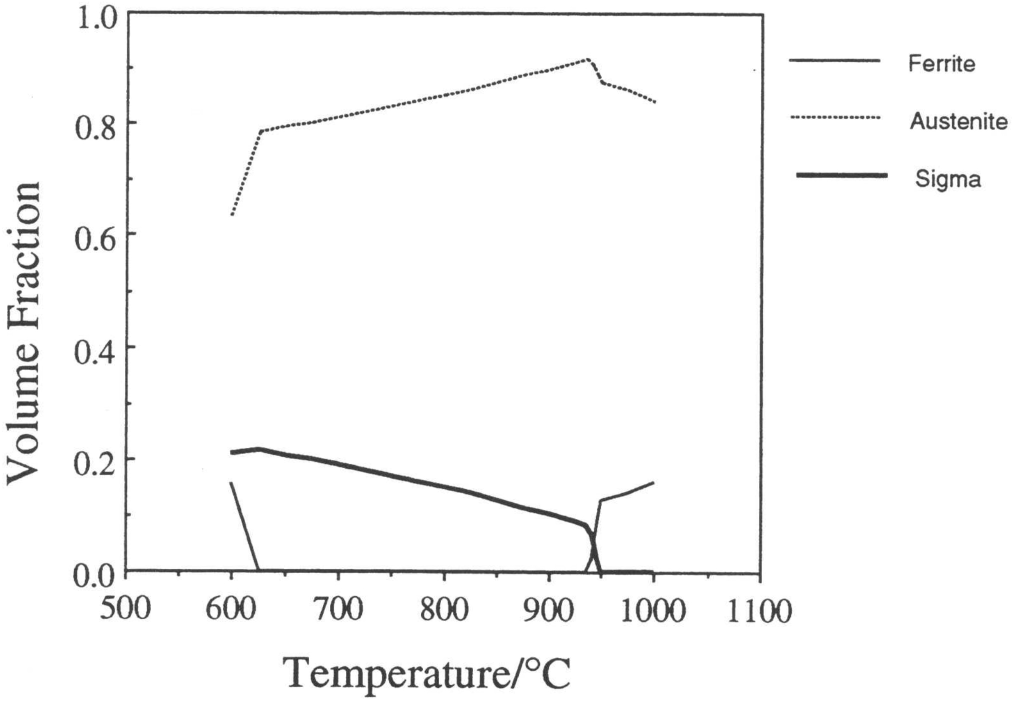

(d)

Figure 7.4. (Continued)

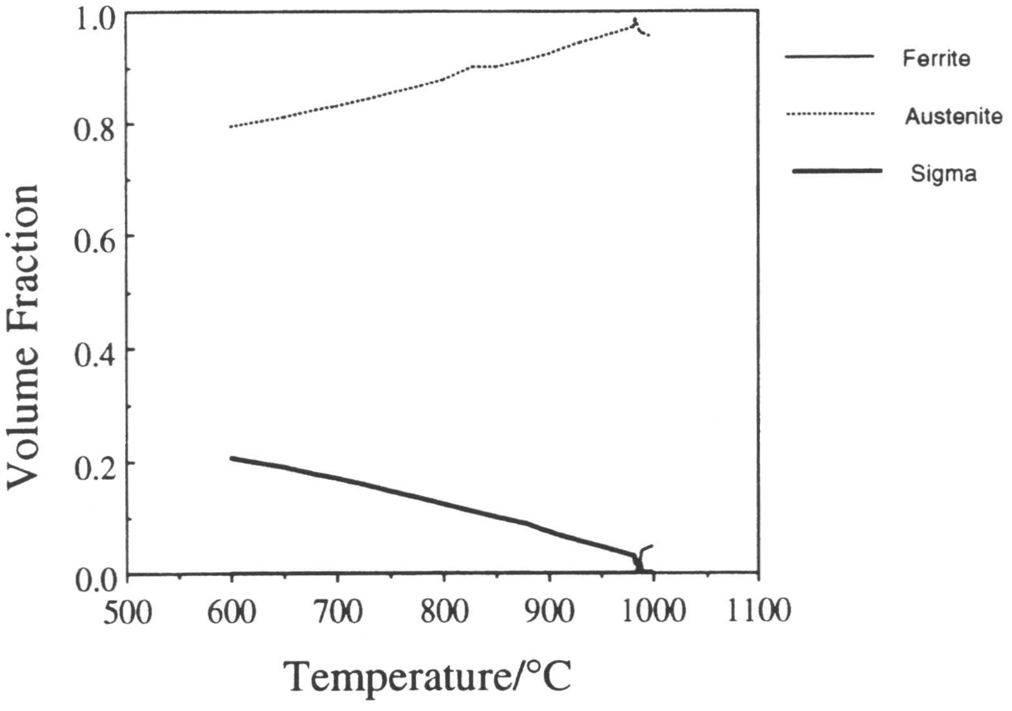

(e)

Figure 7.4. (Continued)

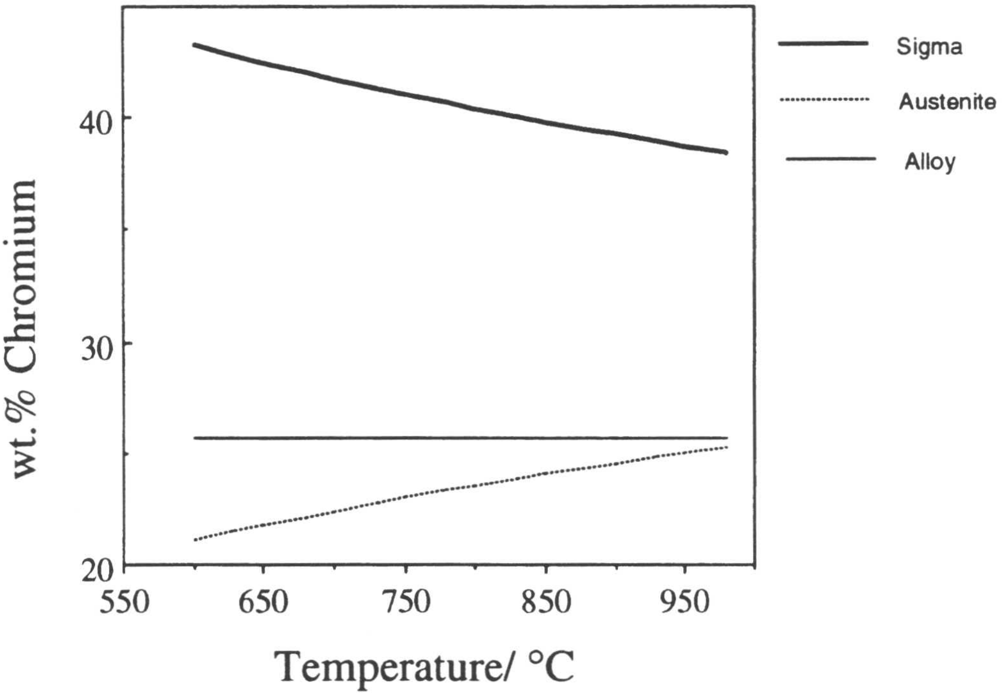

Figure 7.5. The calculated equilibrium partitioning of chromium between sigma phase and austenite in super duplex weld metal A219.

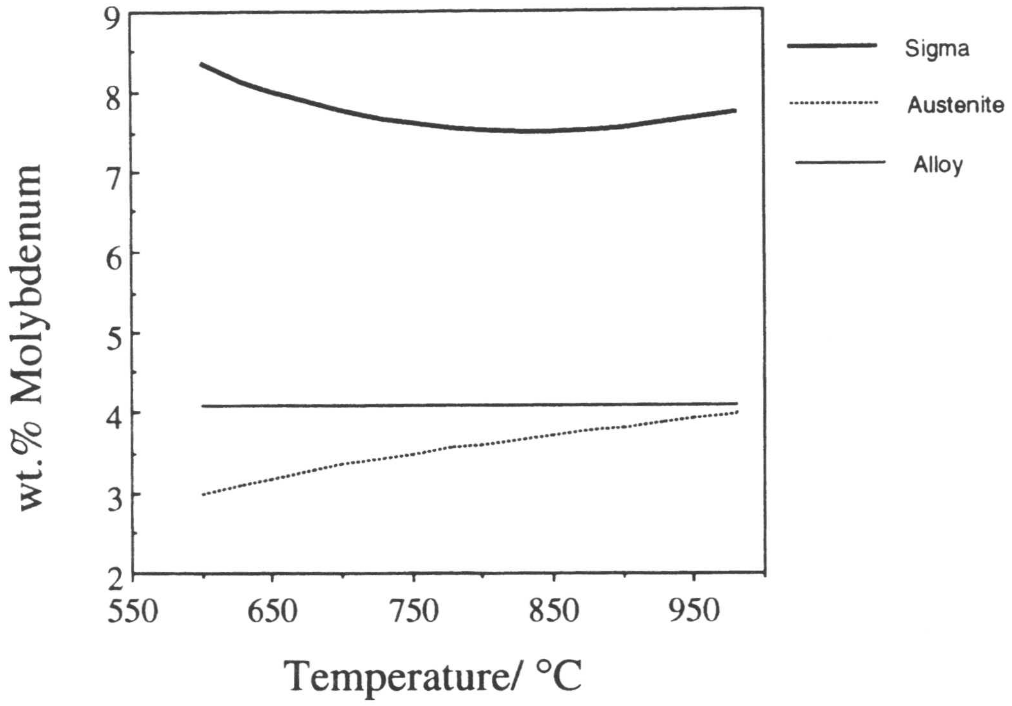

Figure 7.6. The calculated equilibrium partitioning of molybdenum between sigma phase and austenite in super duplex weld metal A219.

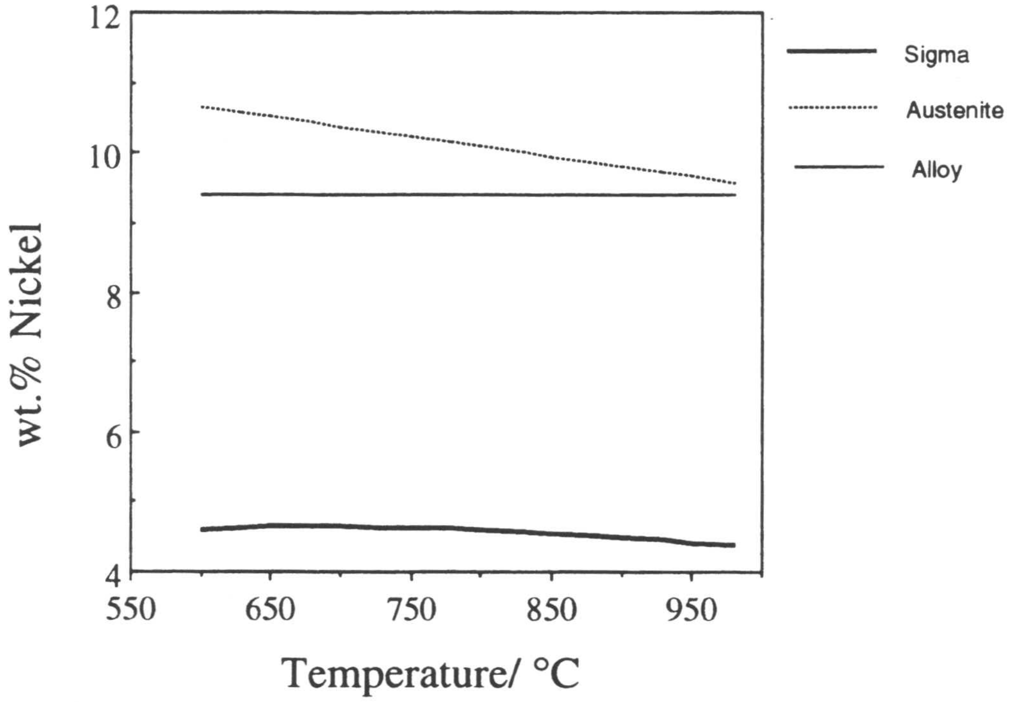

Figure 7.7. The calculated equilibrium partitioning of nickel between sigma phase and austenite in super duplex weld metal A219.

7.3.4 The equilibrium sigma-start temperature

The previous work has shown that most of the elements which are ferrite formers (for example Cr and Mo), also promote sigma-phase formation and widen the temperature range where sigma phase is stable. The calculations show that as the Cr_{eq} increases, so does the equilibrium σ_s temperature (Figure 7.8).

There is a strong effect of Mo on the precipitation of sigma-phase (Figure 7.9), the correlation of the σ_s temperature against Mo content being better than against the Cr_{eq}. These results lead to the conclusion that although the Cr_{eq} of the alloy is important in determining the precipitation of sigma phase (specially on the volume fraction of the phase), but the most important factor on this precipitation is the Mo content of the alloy (specially on the temperature range where the sigma-phase is thermodynamically stable).

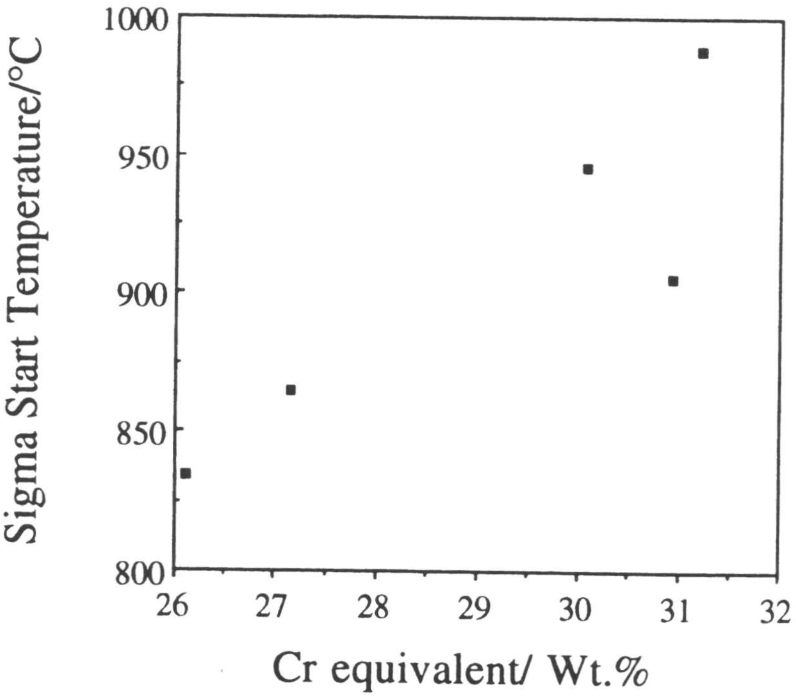

Figure 7.8. The calculated equilibrium sigma start temperature against Cr_{eq} of the different duplex and super duplex stainless steel alloys as listed in Table 5.1. The chromium equivalents are calculated according to Hammar and Svensson (1979).

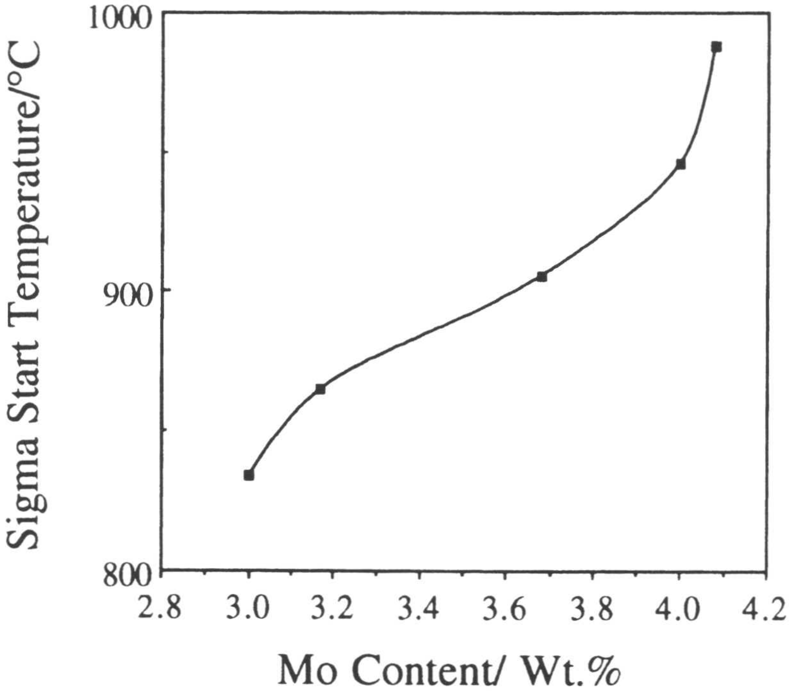

Figure 7.9. The calculated equilibrium sigma start temperature against Mo content of the different duplex and super duplex stainless steel alloys as listed in Table 5.1.

7.4 Isothermal aging Heat Treatments

To construct the TTT diagrams for sigma phase precipitation in super duplex stainless steel alloy A219, specimens were isothermally heat treated in the range 600-1100 °C. To prevent oxidation and decarburisation, they were sealed in silica tubes under partial pressure of argon (about 100 mm Hg). An electric furnace with an even temperature distribution was used for the heat treatments with an accuracy of ±5 °C. After an appropriate time interval, the specimens in their capsules were dropped into and broken under water. Sigma phase formation causes a sharp increase in the hardness (Table 7.2).

The Vickers hardness number (VHN) of the as-received material is 293. Figure 7.10 shows the hardness of specimens aged for 2 hours at different temperatures. The hardness peaks at about 850 °C, indicating that the amount of sigma phase formed at this temperature is a maximum compared with other ageing temperatures. Up to 30 vol% of σ- phase was observed in specimens aged at 900 and 800 °C.

Table 7.2. Vickers hardness for aged specimens of super duplex stainless steel weld metal A219 (see Table 5.1 for chemical compositions and Table 2.2 for welding conditions).

Temp°C	1 min	5 min	10 min	.5 hr	1 hr	2 hr	4 hr	8 hr	16 hr
1100	291	293	287	292	287	283	285	285	282
1000	298	301	318	320	360	360	366	366	382
900	278	314	341	345	398	411	433	415	389
800	294	306	323	332	400	397	385	418	384
700	292	291	291	294	296	342	356	362	392
600	288	291	286	295	294	293	309	314	305

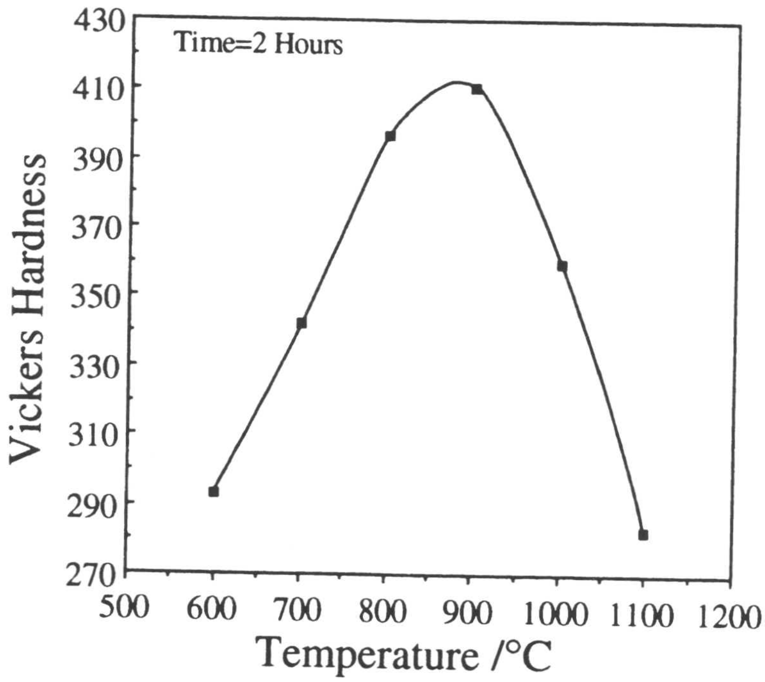

Figure 7.10. Vickers hardness of specimens of weld metal A219 (see Table 5.1 for composition and Table 2.2 for welding conditions) aged for two hours at each temperatures.

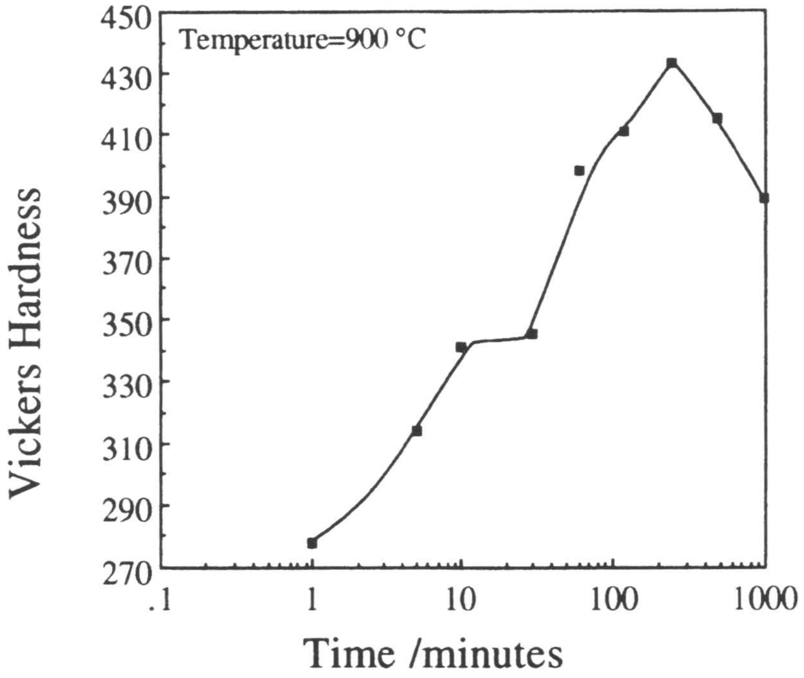

Figure 7.11. Hardness of weld metal A219 (see Table 5.1 for composition and Table 2.2 for welding conditions) aged at 900 °C for different times.

Figure 7.11 shows the hardness of specimens aged at 900 °C, as a function of ageing time. The hardness peaks at 433 VHN after four hours of aging. Metallography indicates that the fraction of sigma almost does not increase beyond an ageing time of four hours, but the precipitates coarsen with continued ageing. However, the drop of hardness probably was more to do with the fact that almost all of ferrite transformed into softer austenite.

7.5 Microstructural Observations

Optical, SEM, TEM electron diffraction and EDX analysis were used to characterise the aged specimens. Sigma phase was not found for the specimens aged at or below 600 °C and above 1050 °C. The different phases were identified by their electron diffraction patterns and also by EDX analysis on SEM or TEM. The volume fraction of sigma phase was measured both by point counting and image analysis techniques. Figure 7.12 is an optical micrograph showing the microstructure of super duplex stainless steel alloy A219 aged at 600 °C for 16 hours. The phases in this specimen were identified by TEM EDX microanalysis (Table 7.3) and TEM SADP. From this information it was found out that the light etching phase is austenite and the dark one is ferrite. Although the specimen has been aged at this temperature for a long time but there is still no sign of sigma phase precipitation.

The sigma phase volume fraction was found to be more than 0.01 in the specimens aged at 700 °C whenever the ageing time was more than 10 minutes. Figure 7.13 shows the microstructure of the alloy aged at 700 °C for 10 minutes. The fraction of sigma is estimated to be less than 0.01. Very fine particles of sigma phase precipitated on δ/γ grain boundaries. At 800 °C sigma phase was found to form more rapidly (Figure 7.14). With increasing ageing time, sigma phase was observed to grow inside the δ-ferrite grains (Figure 7.15). Figures 7.16 to 7.18 show the microstructures of specimens aged at 900 °C for 1, 5 and 10 minutes respectively. As sigma phase grows inside ferrite the surrounding area becomes depleted of Cr and Mo, and hence unstable with respect to austenite formation. These new austenite particles have a very fine Widmanstätten morphology (Figure 7.17). Table 7.4 shows the TEM EDX results for specimen aged at 900 °C for 5 minutes. As the ageing time increases, so does the sigma fraction until almost all ferrite decomposes to sigma plus austenite (Figure 7.20). Figure 7.19 shows that the decomposition of ferrite is slower at 1000 °C compared with at 900 °C. However after a long aging time (16 hours) again all ferrite transformed to sigma plus austenite at this temperature (Figure 7.20).

Table 7.3. TEM EDX microanalysis of the ferrite and austenite phases in super duplex weld metal A219 aged at 600 °C for 16 hours (all concentrations are in wt.%).

Phase	Fe	Cr	Ni	Mo	Mn	Si
Ferrite	57.7±0.3	28.5±0.7	7.9±0.6	4.9±0.3	0.4±0.1	0.5±0.1
Austenite	58.4±0.5	24.9±0.2	10.1±0.2	3.2±0.1	0.4±0.1	1.0±0.1

For short ageing times, sigma phase was observed to precipitate mostly at the austenite/ferrite grain boundaries and then grow into the ferrite grains. As the fraction of sigma phase increased (to values greater than $\simeq 0.2$) at the

---

and the remainder is austenite.

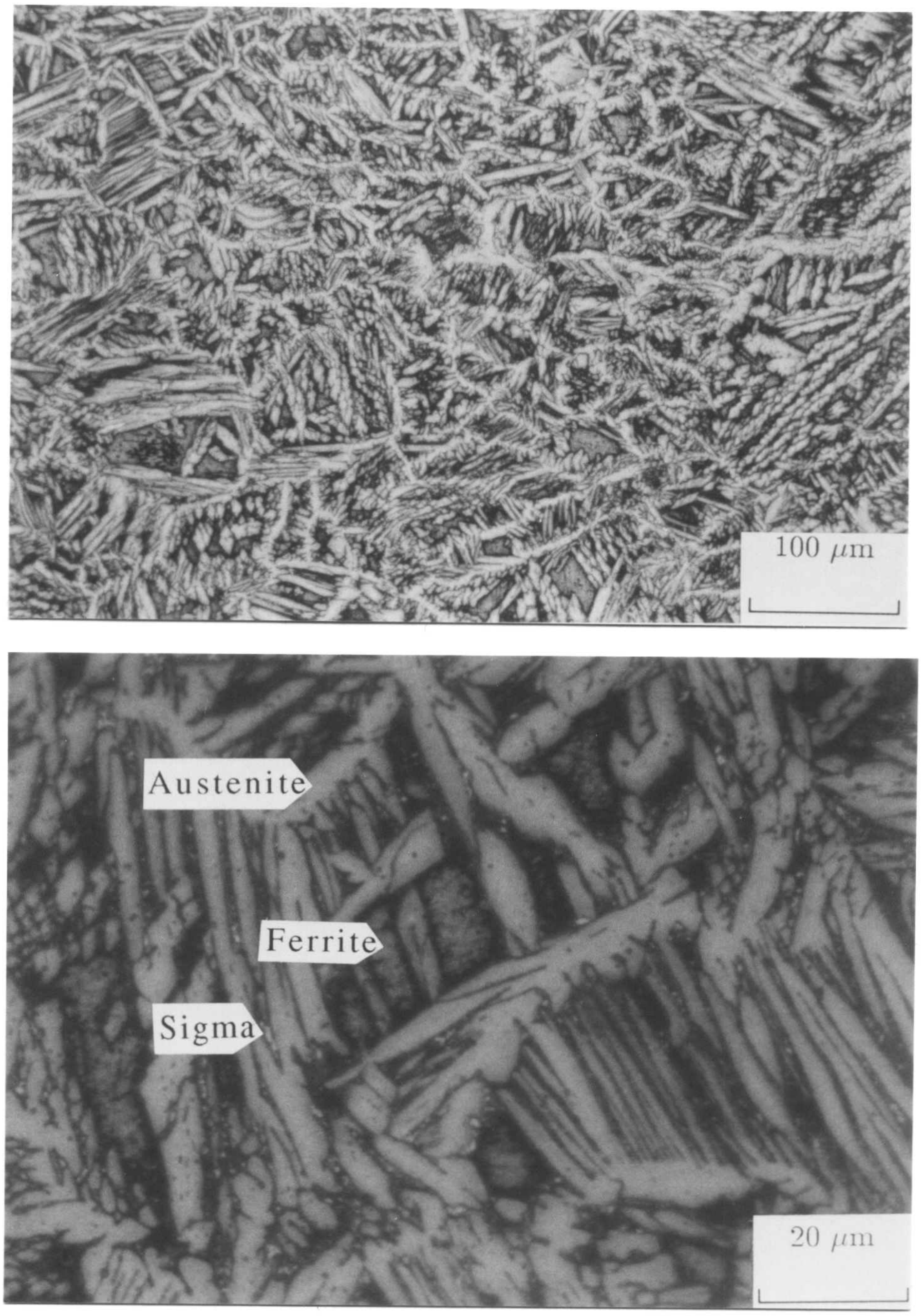

Figure 7.13. The microstructure of super duplex stainless steel A219 aged at 700 °C for 10 minutes. Note the bright fine sigma precipitations mostly at austenite/ferrite grain boundaries. The sigma fraction is probably less than 0.01.

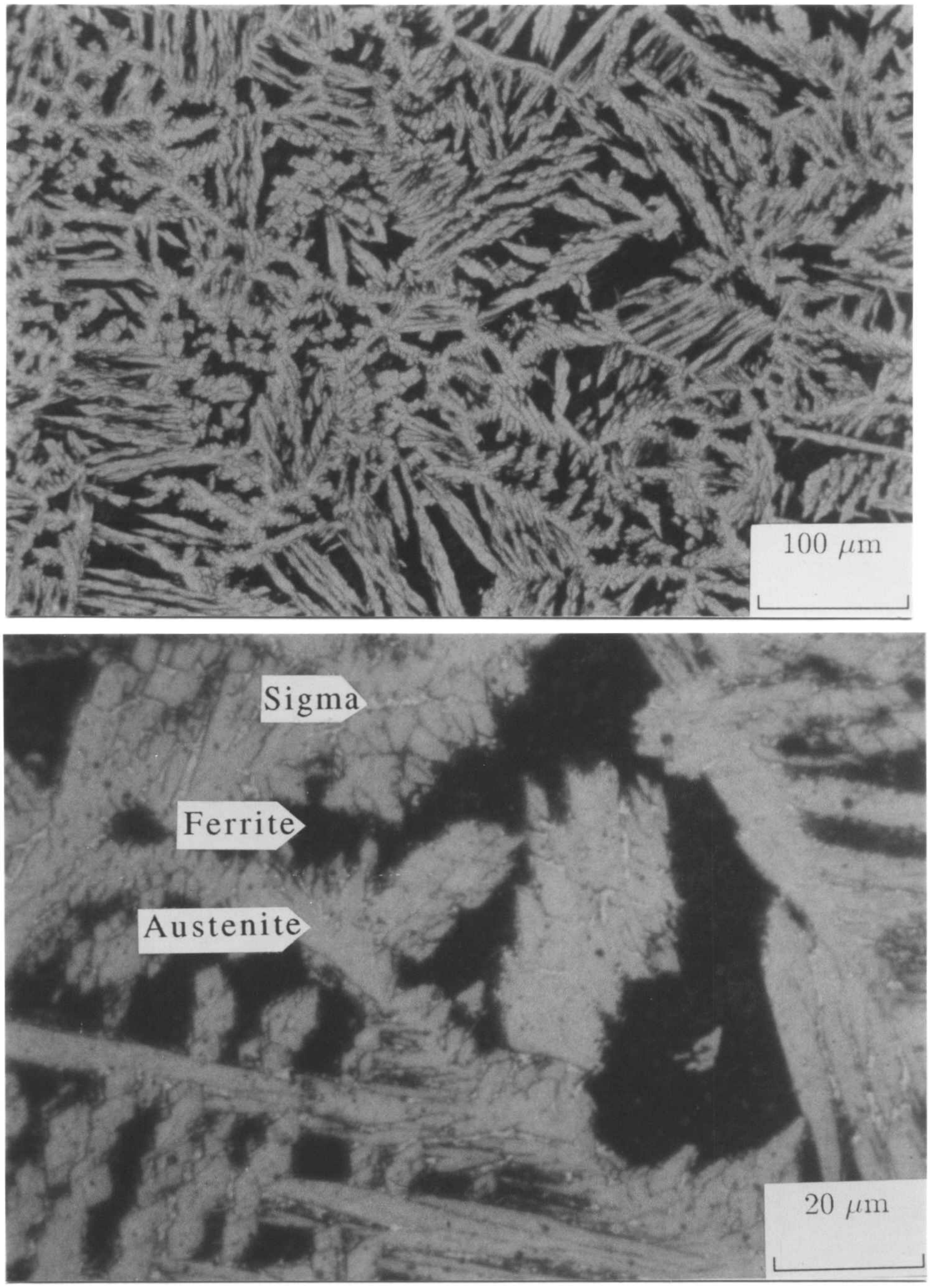

Figure 7.14. The microstructure of super duplex stainless steel A219 aged at 800 °C for 1 minute. Note the bright fine sigma precipitations mostly at austenite/ferrite grain boundaries. The sigma fraction is probably less than 0.01.

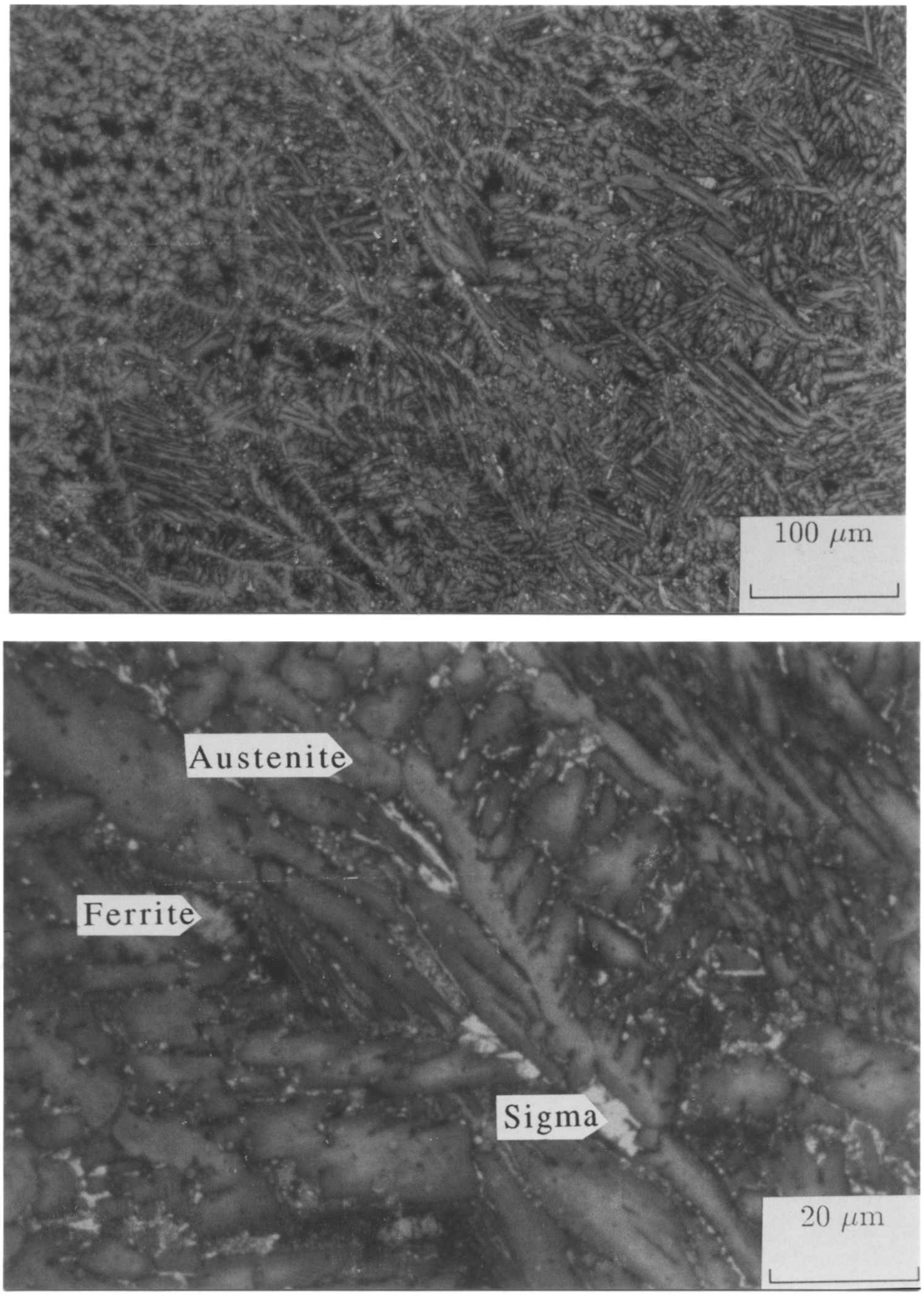

Figure 7.15. The microstructure of super duplex stainless steel A219 aged at 800 °C for 10 minutes. Note the growth of sigma phase inside ferrite grains. The sigma fraction is about 0.08.

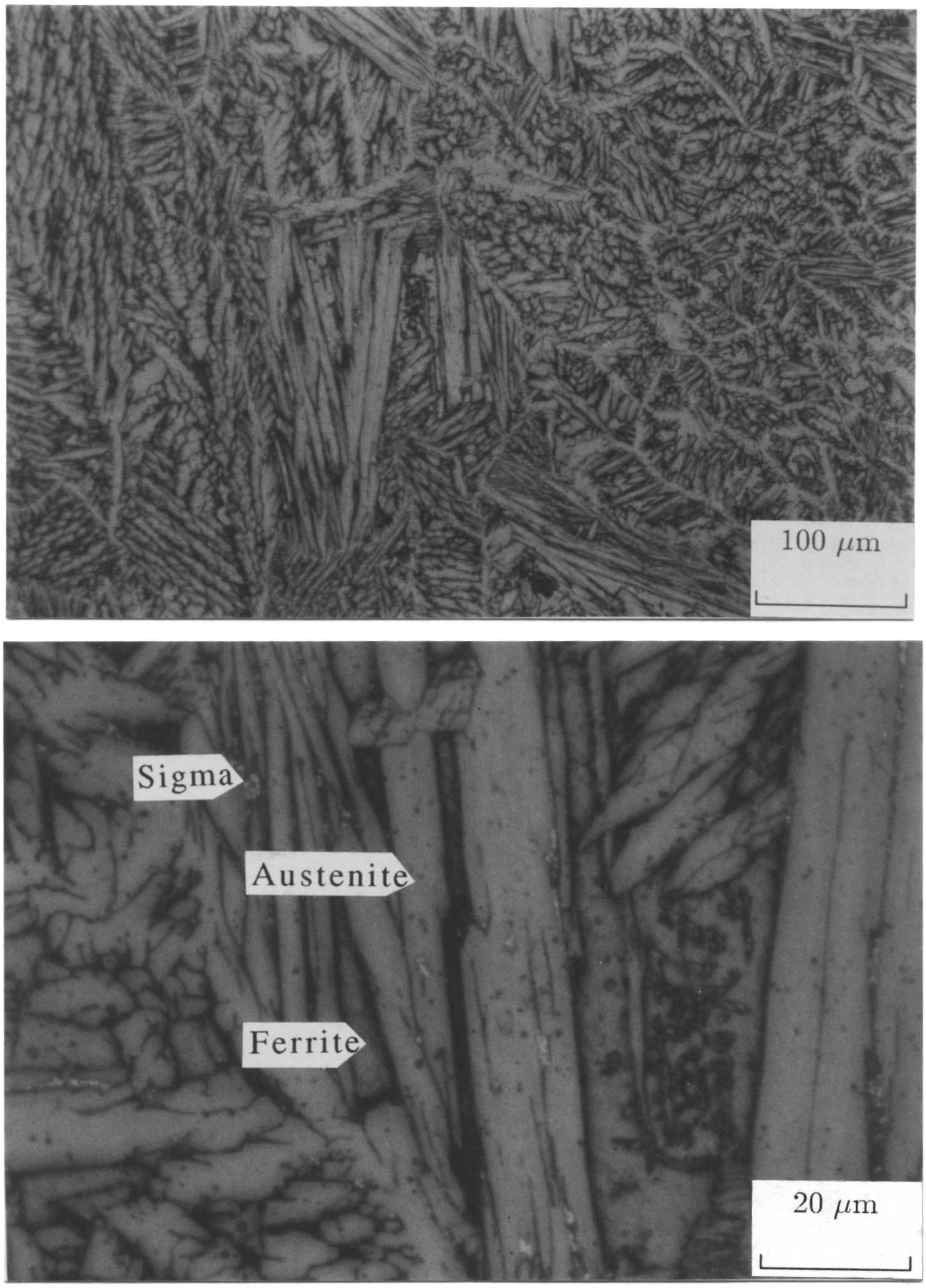

Figure 7.16. The microstructure of super duplex stainless steel A219 aged at 900 °C for 1 minute. The bright phase which has precipitated mainly in grain boundaries is sigma with fraction probably less than 0.01.

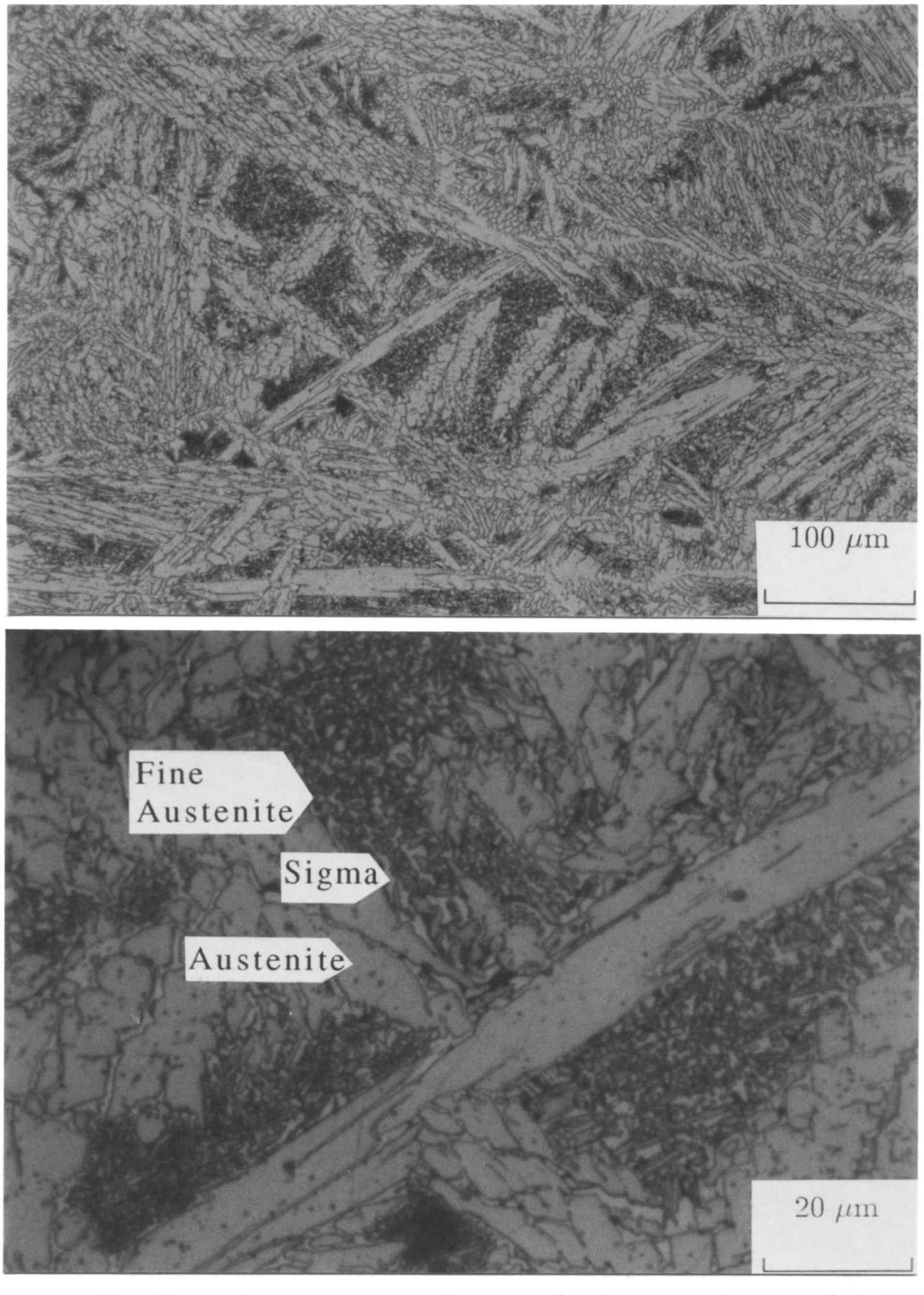

Figure 7.17. The microstructure of super duplex stainless steel A219 aged at 900 °C for 5 minutes. Ferrite grains have decomposed to sigma and austenite. The new austenite has a very fine Widmanstätten morphology. The measured volume fraction of sigma is about 0.07.

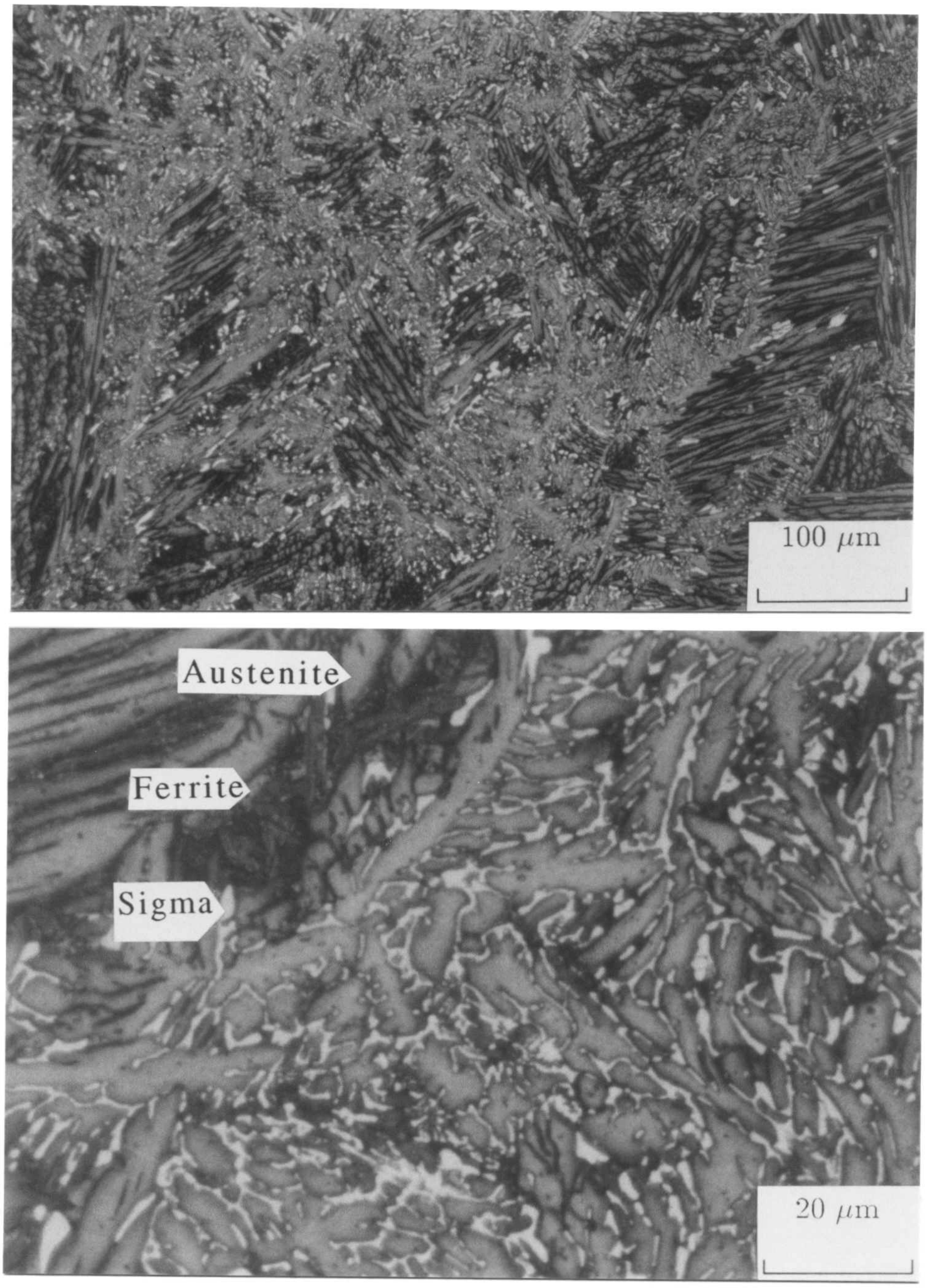

Figure 7.18. The microstructure of super duplex stainless steel A219 aged at 900 °C for 10 minutes. The measured volume fraction of sigma is about 0.21.

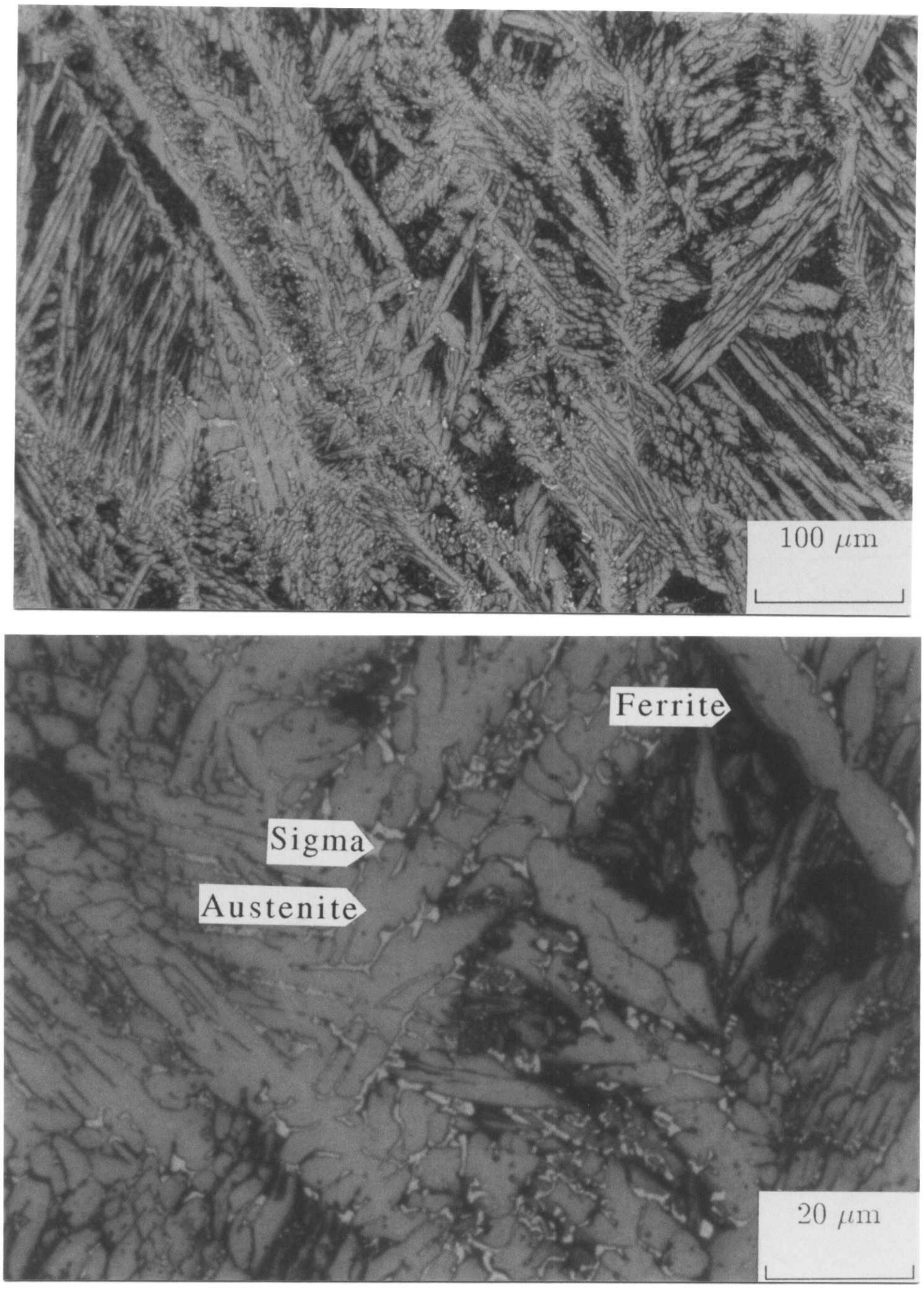

Figure 7.19. The microstructure of super duplex stainless steel A219 aged at 1000 °C for 5 minutes. The measured volume fraction of sigma is about 0.03.

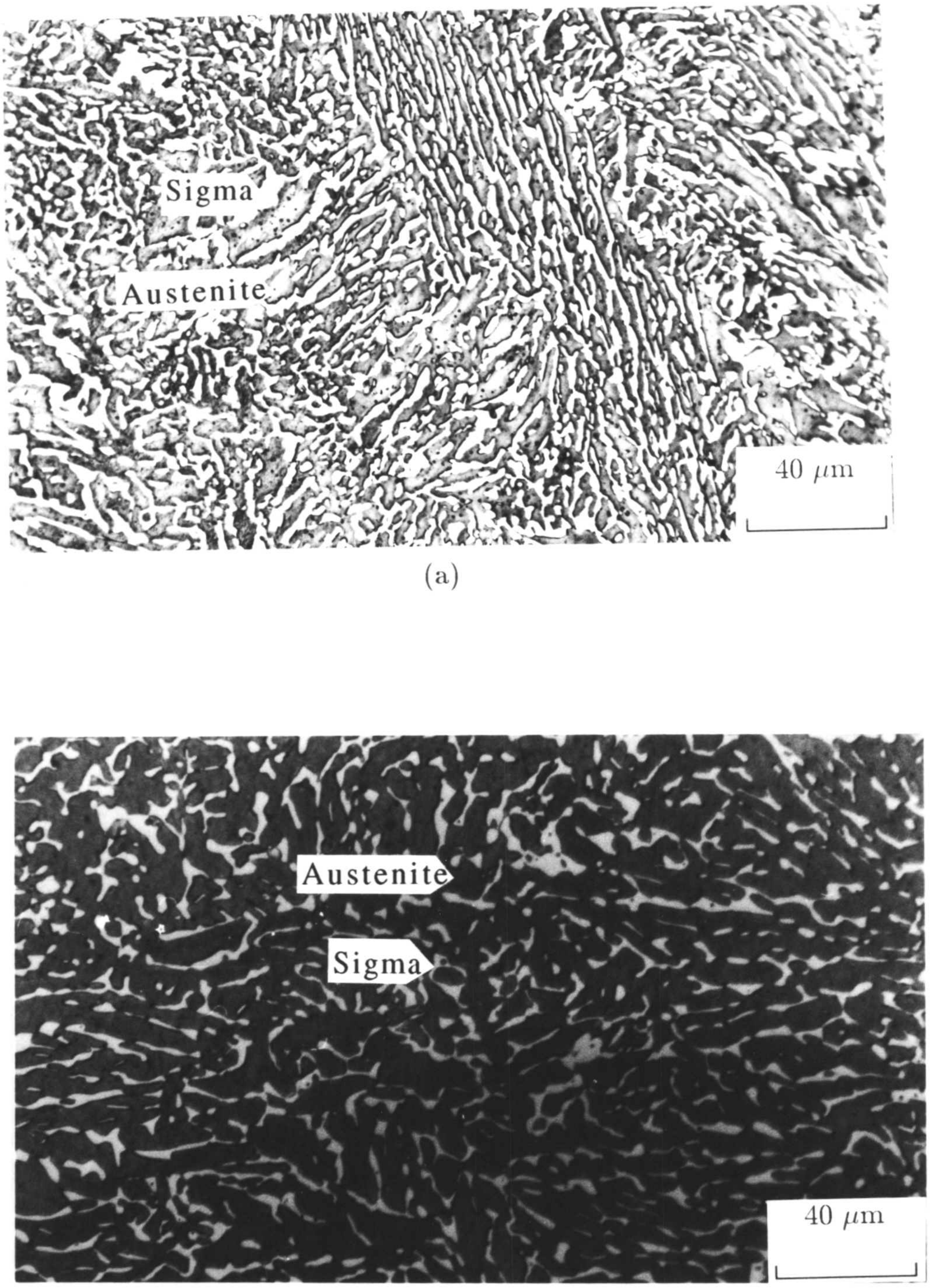

(a)

(b)

Figure 7.20. The microstructure of super duplex stainless steel A219 aged for 16 hours a) at 900 °C with about 0.30 volume fraction of sigma b) at 1000 °C with about 0.31 volume fraction of sigma. Sigma phase has become the prominent second phase and there is almost no sign of ferrite.

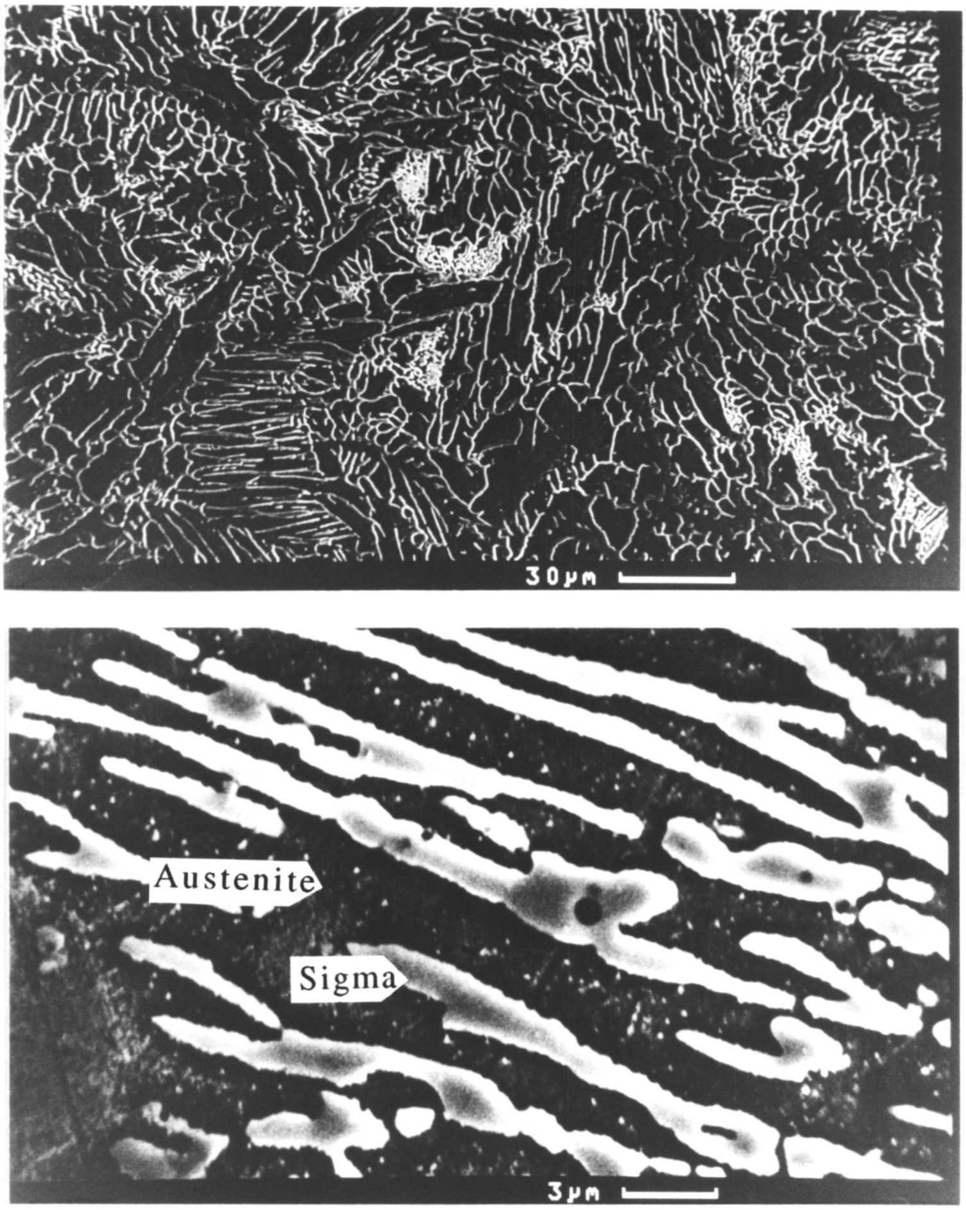

Figure 7.21. SEM micrographs showing the microstructure of super duplex stainless steel A219 aged at 900 °C for four hours. The bright phase is sigma and the dark one is austenite. Note that the sigma phase has almost formed a network.

TEM confirmed that in specimens aged for short time periods in temperature range 700-1050 °C sigma phase precipitated mostly at austenite/ferrite grain boundaries and grew into the ferrite grains. Figure 7.22 shows the microstructure of specimen aged at 900 °C for 5 minutes and Figures 7.23 to 7.25 show the SADP of different phases found in this specimen. In the samples aged for a long time, large volume fractions of sigma phase were found. Correspondingly, the volume fraction of δ-ferrite phase which was about 0.35 in the original weld microstructure, had become very low hardly detectable. It seems that all of the ferrite transformed into sigma plus austenite. Figures 7.26 to 7.31 show the microstructures of the specimens aged for 16 hours.

7.6 Measurement of Sigma Phase Volume Fraction

The volume fractions of sigma phase in different aged specimens were measured both by point counting and image analysis. Light micrographs were used to do these measurements. Table 7.5 shows the results of these measurements.

Table 7.5. Measured volume fraction of sigma phase for different aged specimens of super duplex stainless steel weld metal A219.

Temp°C	1 min	5 min	10 min	.5 hr	1 hr	2 hr	4 hr	8 hr	16 hr
1100	-	-	-	-	-	-	-	-	-
1000	-	0.03	0.04	0.06	0.29	0.22	0.21	0.20	0.25
900	-	0.07	0.21	0.28	0.38	0.36	0.38	0.35	0.30
800	-	0.01	0.08	0.31	0.35	0.32	0.33	0.31	0.31
700	-	-	-	0.01	0.04	0.33	0.35	0.34	0.31
600	-	-	-	-	-	-	-	-	-

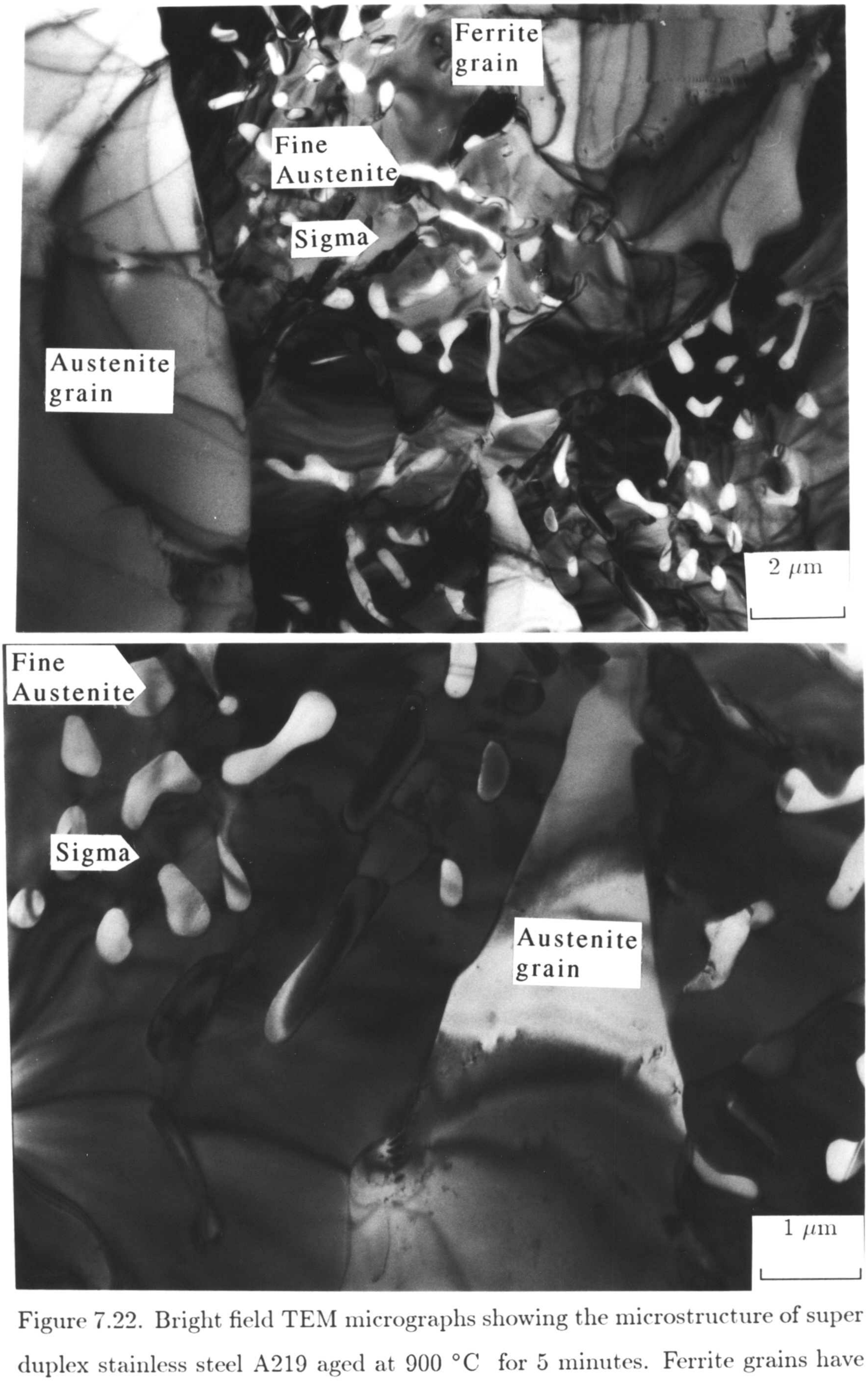

Figure 7.22. Bright field TEM micrographs showing the microstructure of super duplex stainless steel A219 aged at 900 °C for 5 minutes. Ferrite grains have decomposed to sigma plus austenite.

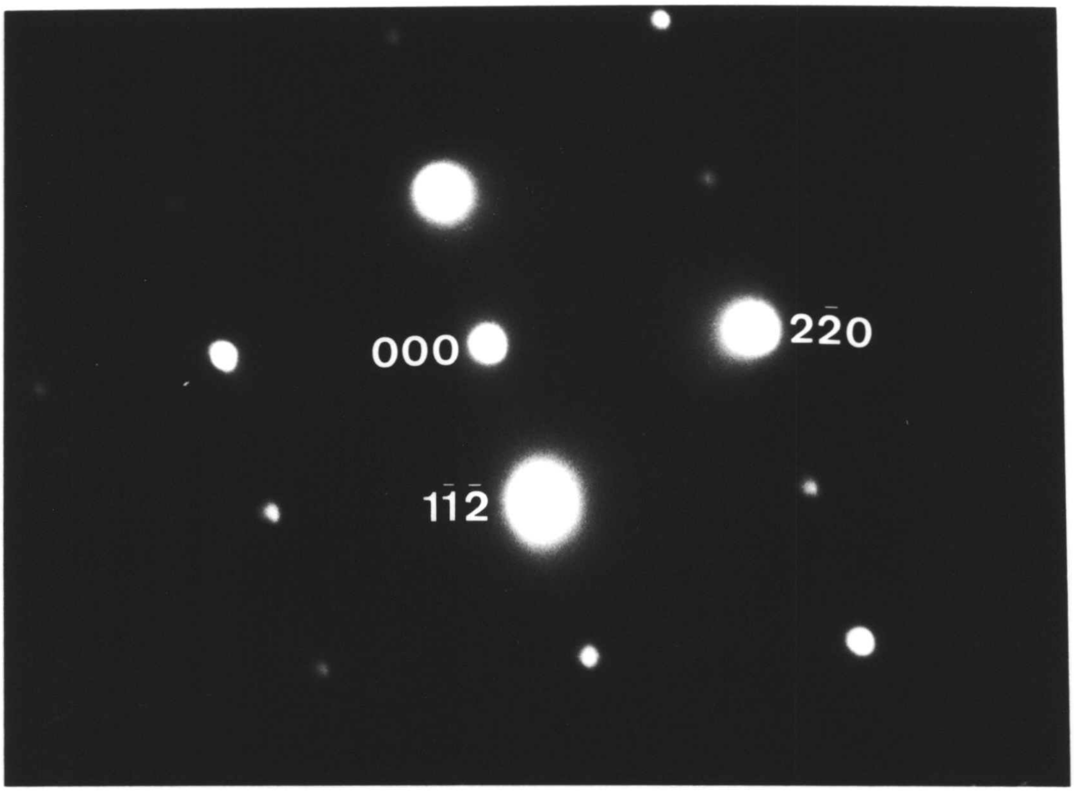

Figure 7.23. Diffraction pattern of the dark phase in figure 7.22 (sigma phase) confirms that it has a b.c.t. crystal structure. The zone axis is [110].

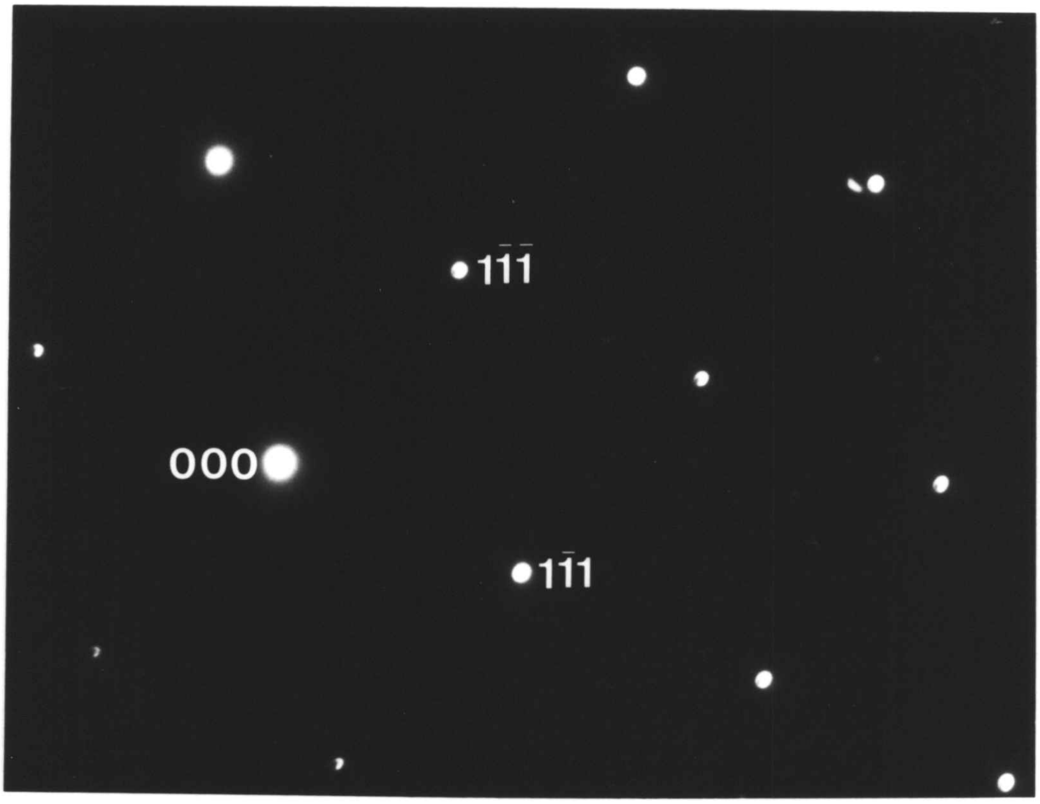

Figure 7.24. Diffraction pattern of the small light particles in figure 7.22 (austenite) confirms that they have a f.c.c. crystal structure. The zone axis is [110].

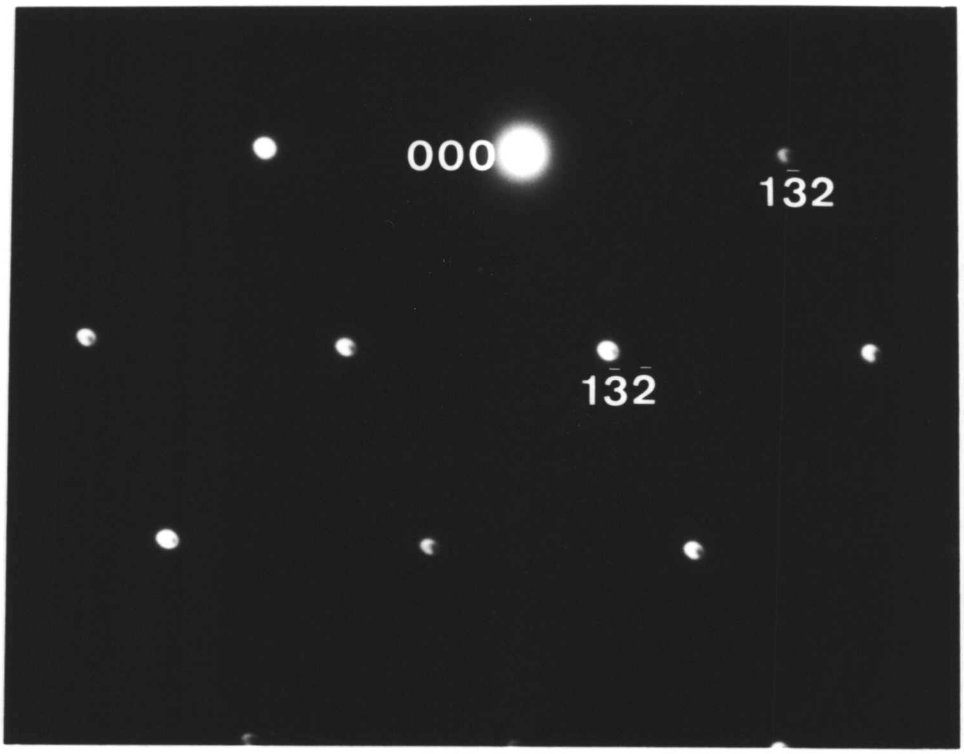

Figure 7.25. Diffraction pattern of the grain point out in figure 7.22 (ferrite) confirms that it has an b.c.c. crystal structure. The zone direction is [310].

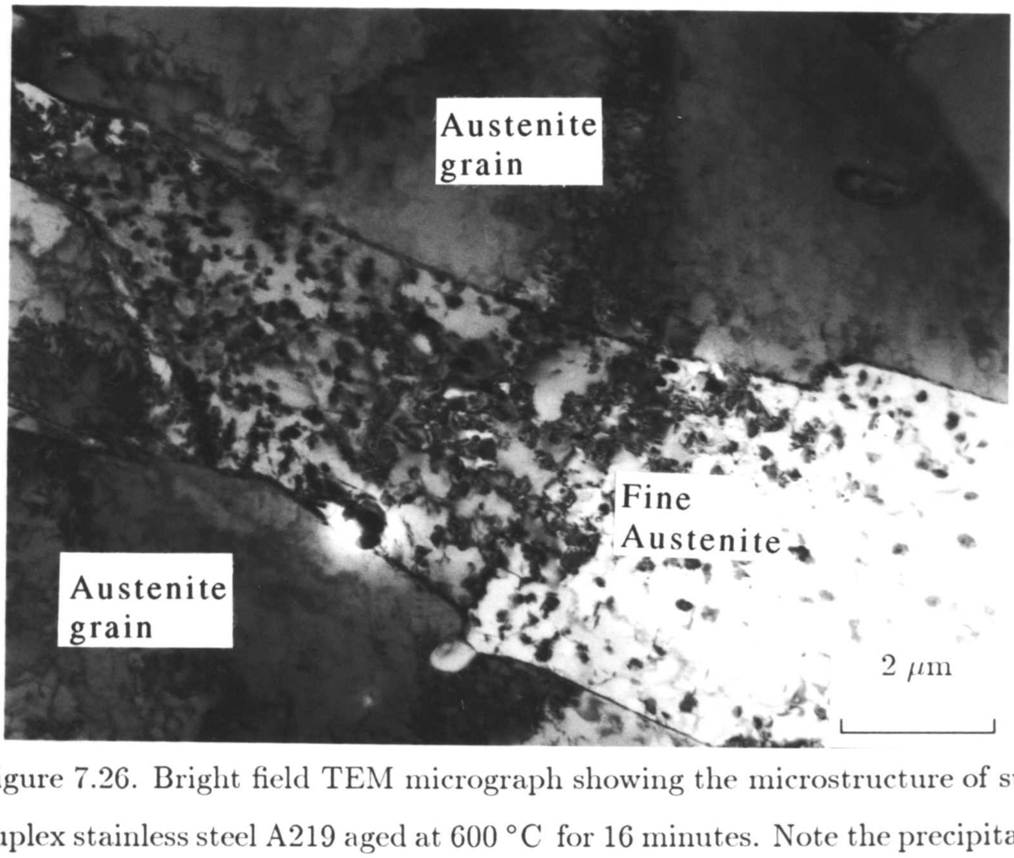

Figure 7.26. Bright field TEM micrograph showing the microstructure of super duplex stainless steel A219 aged at 600 °C for 16 minutes. Note the precipitation of fine austenite particles inside δ-ferrite grain. Microstructure consists of ferrite and austenite and there is no sign of sigma.

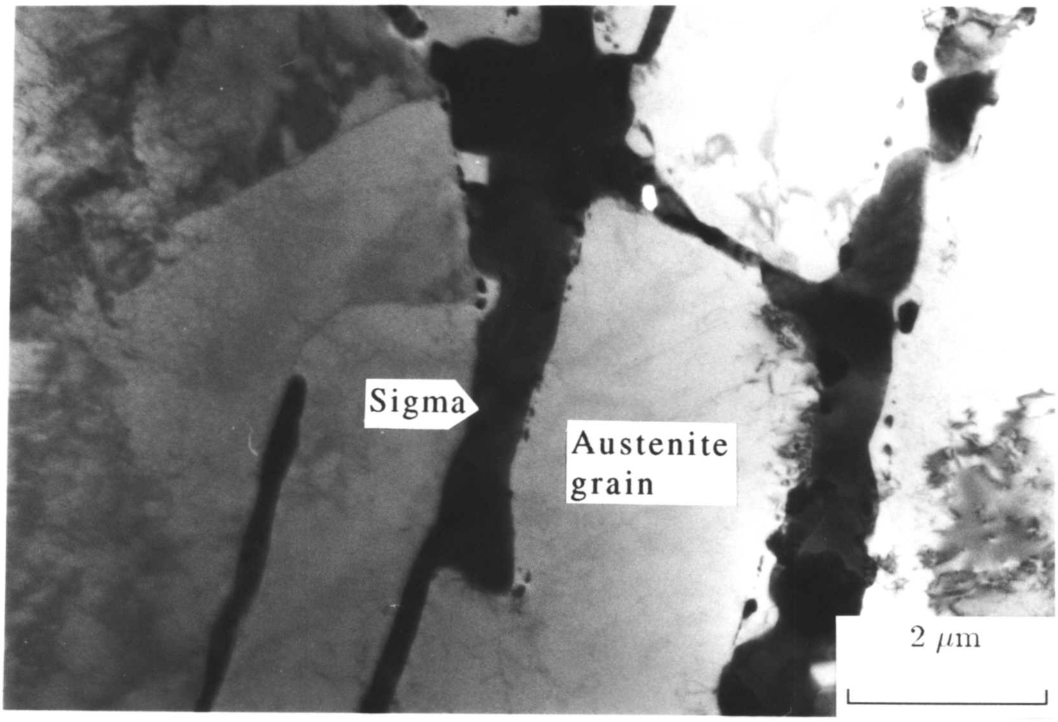

Figure 7.27. Bright field TEM micrograph showing the microstructure of super duplex stainless steel A219 aged at 700 °C for 16 hours. Sigma phase has made a network and there is no sign of ferrite as it has completely decompose to sigma plus austenite. Tables 7.6 and 7.7 show the TEM EDX data of the two phases.

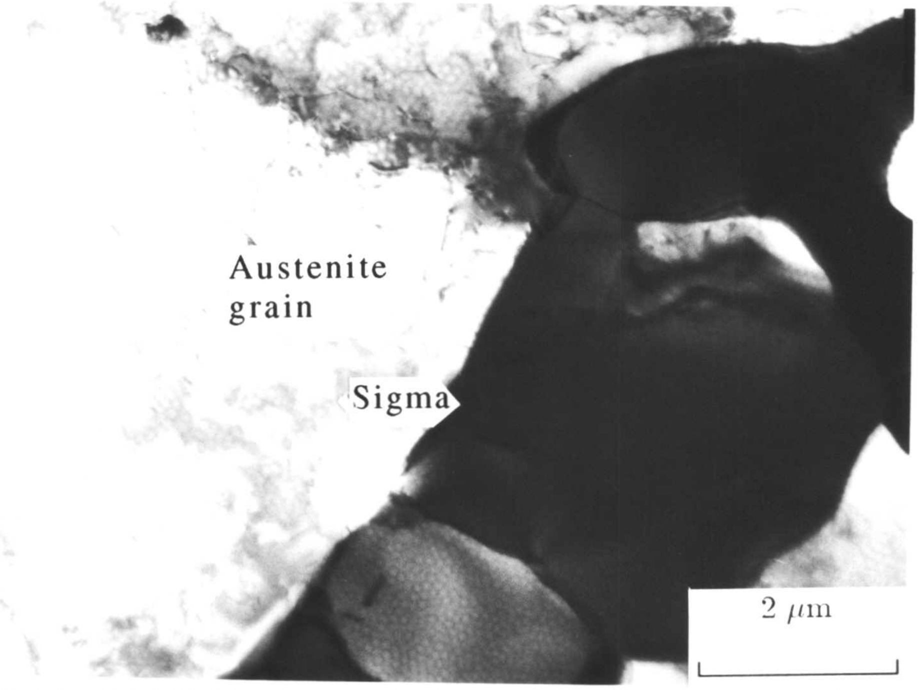

Figure 7.28. Bright field TEM micrograph showing the microstructure of super duplex stainless steel A219 aged at 800 °C for 16 hours. Sigma phase has made a network and there is no sign of ferrite as it has completely decompose to sigma plus austenite. Tables 7.6 and 7.7 show the TEM EDX data of the two phases.

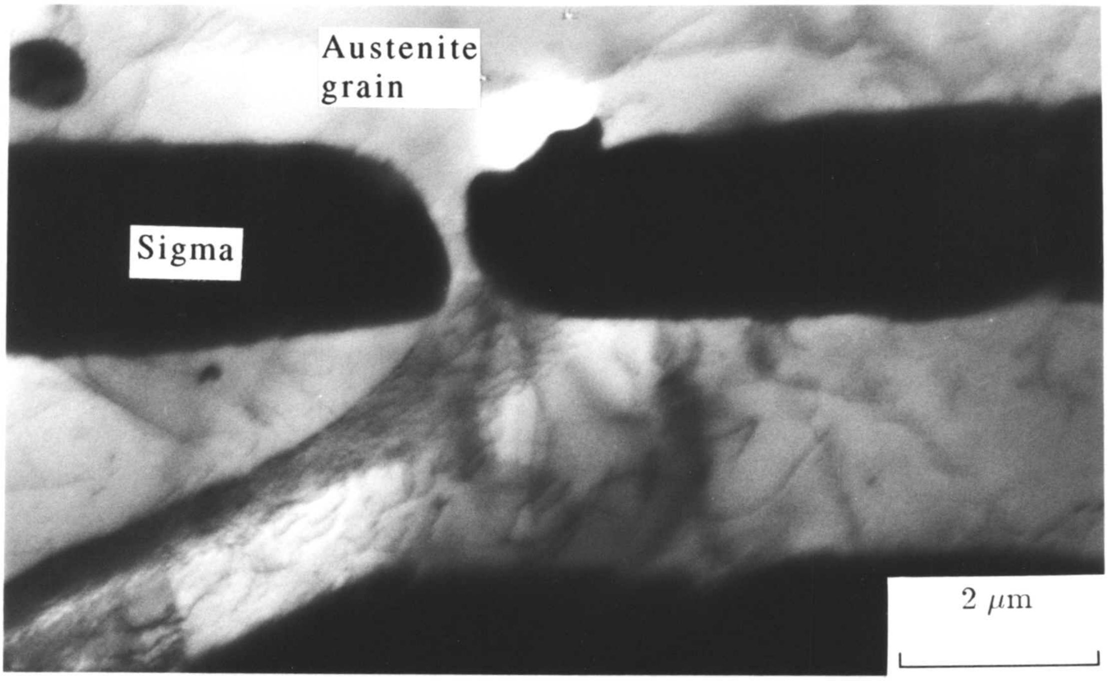

Figure 7.29. Bright field TEM micrograph showing the microstructure of super duplex stainless steel A219 aged at 900 °C for 16 hours. Sigma phase has made a network and there is no sign of ferrite as it has completely decomposed to sigma plus austenite. Tables 7.6 and 7.7 show the TEM EDX data of the two phases.

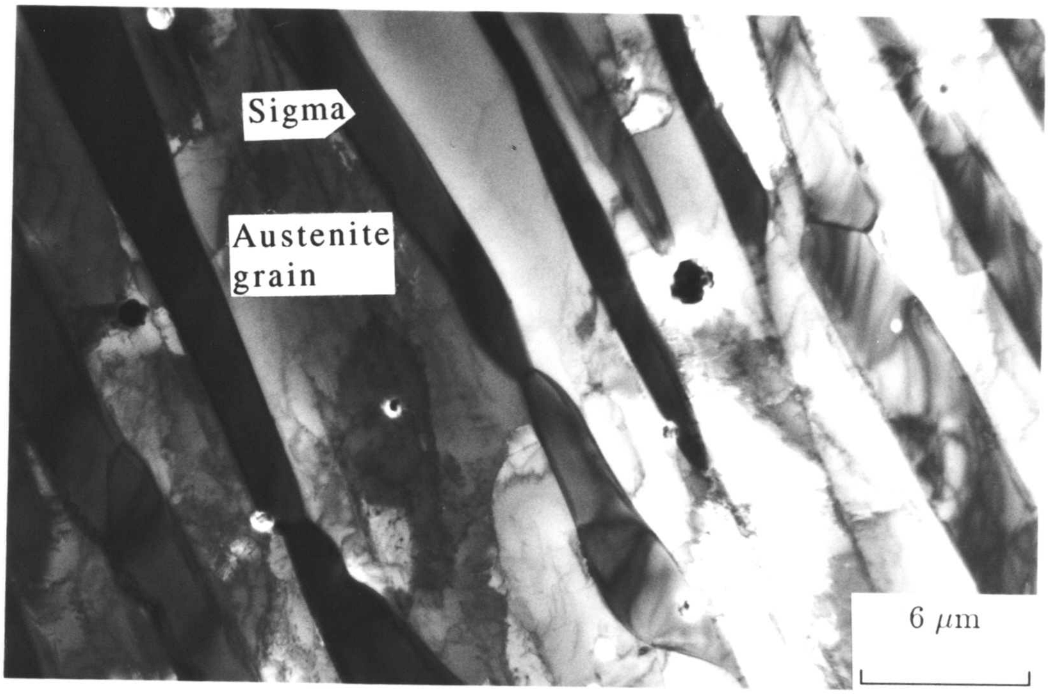

Figure 7.30. Bright field TEM micrograph showing the microstructure of super duplex stainless steel A219 aged at 1000 °C for 16 hours. Sigma phase has made a network and there is no sign of ferrite as it has completely decomposed to sigma plus austenite. Tables 7.6 and 7.7 show the TEM EDX data of the two phases.

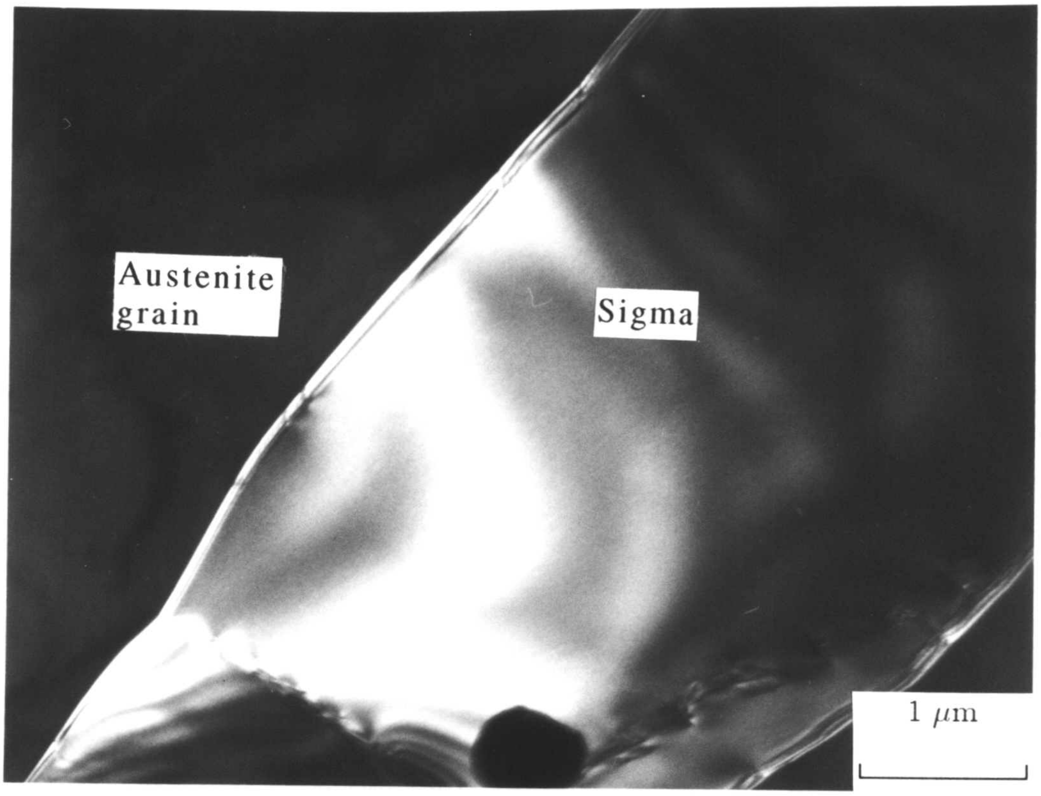

Figure 7.31. Dark field TEM micrograph showing the microstructure of super duplex stainless steel A219 aged at 1000 °C for 16 hours.

Figure 7.32 is a time-temperature-transformation (TTT) diagram for sigma phase formation in super duplex alloy A219 based on the measured volume fraction in the aged specimens. The C-curves for 1 and 5 volume % sigma phase formation is presented in that figure. Note that compared with conventional duplex stainless steels (Figure 7.1) the temperature range where sigma phase precipitates has been widened. Sigma was found to be stable even at the specimens aged at 1050 °C.

7.7 Relation between Volume Fraction of Sigma Phase and Hardness

In the temperature range 700-1050 °C both the hardness of the specimens and volume fraction of sigma phase were found to increase with ageing time. Figure 7.33 shows the variations of hardness and sigma phase volume fraction with temperature for specimens aged for two hours. A very good correlation can be seen between the amount of sigma phase formed and the hardness of the specimens. It was found that a hardness of 320 VHN corresponds to the presence of 0.05 volume fraction of sigma phase. The maximum sigma phase volume fraction of 0.38 was measured in the specimen aged at 900 °C for four hours. The measured hardness of this specimen was maximum (433 HV).

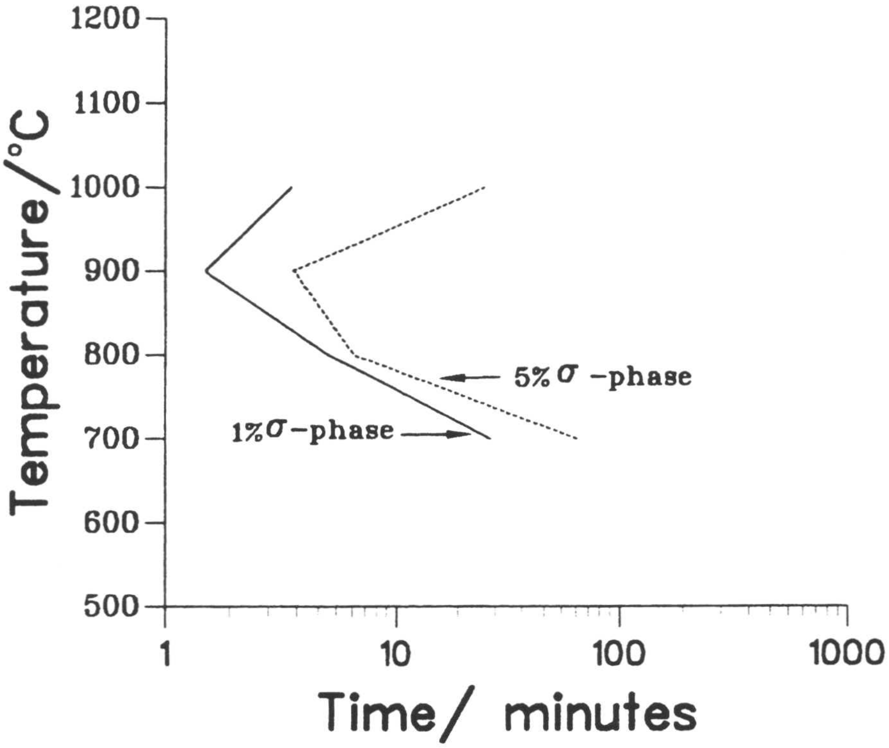

Figure 7.32. C-curves for 1 and 5 vol.% sigma-phase formation in super duplex stainless steel weld metal A219 based on measured volume fraction of sigma in the aged specimens.

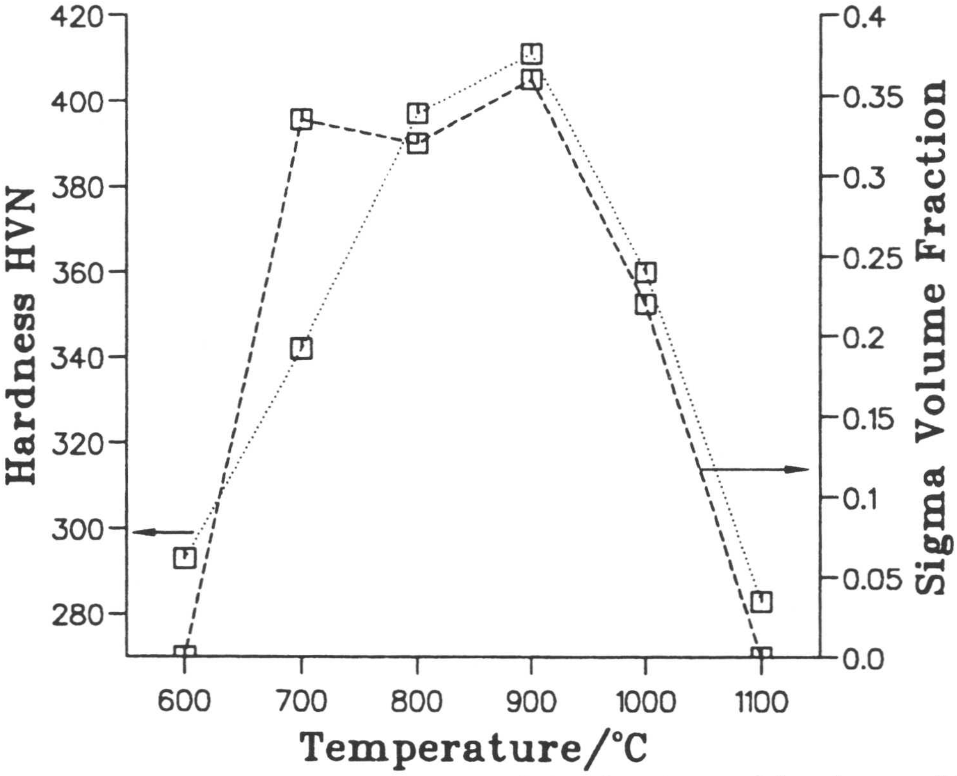

Figure 7.33. Variations of sigma phase volume fraction and hardness with temperature for specimens aged for two hours.

7.8 Partitioning of the Alloying Elements between Austenite and Sigma

The microstructures of specimens aged at 700, 800, 900 and 1000 °C for 16 hours consist mainly of austenite and sigma phase. Tables 7.6 and 7.7 show the TEM EDX data for the sigma phase and austenite respectively. These measurements show that while Cr and Mo partition into sigma phase, Ni partitions into austenite. The data are not all consistent with the thermodynamic calculations; this must be a consequence of the fact that equilibrium has not been achieved for the short time heat-treatments used.

Table 7.6. TEM EDX microanalysis of sigma phase in super duplex weld metal A219 specimens aged at different temperatures for 16 hours (all concentrations in wt.%).

Temperature °C	Fe	Cr	Ni	Mo	Mn	Si
1000	52.0±0.7	34.3±0.5	5.5±0.2	7.1±0.6	0.4±0.1	0.7 ±0.1
900	51.4±0.9	34.0±0.7	5.4±0.1	7.8±0.3	0.7±0.1	0.7 ±0.1
800	53.2±0.9	33.8±0.6	4.9±0.3	6.7±0.4	0.8±0.2	0.7 ±0.1
700	54.0±1.4	34.8±0.7	4.2±0.3	6.0±0.9	0.4±0.1	0.6 ±0.1

Table 7.7. TEM EDX microanalysis of austenite phase in super duplex weld metal A219 specimens aged at different temperatures for 16 hours (all concentrations in wt.%).

Temperature °C	Fe	Cr	Ni	Mo	Mn	Si
1000	61.0±0.3	24.4±0.4	10.5±0.4	1.9±0.2	0.7±0.2	0.5±0.2
900	61.6±0.7	23.9±0.9	10.7±0.6	1.5±0.2	0.9±0.3	0.4±0.1
800	59.2±0.5	24.2±0.4	9.6±0.4	2.8±0.5	0.6±0.1	0.5 ±0.1
700	56.9±0.9	24.7±0.7	10.6±0.4	3.4±0.2	0.9±0.2	0.5±0.1

Figures 7.34 to 7.36 show the partitioning of Cr, Ni and Mo between austenite and sigma phase respectively.

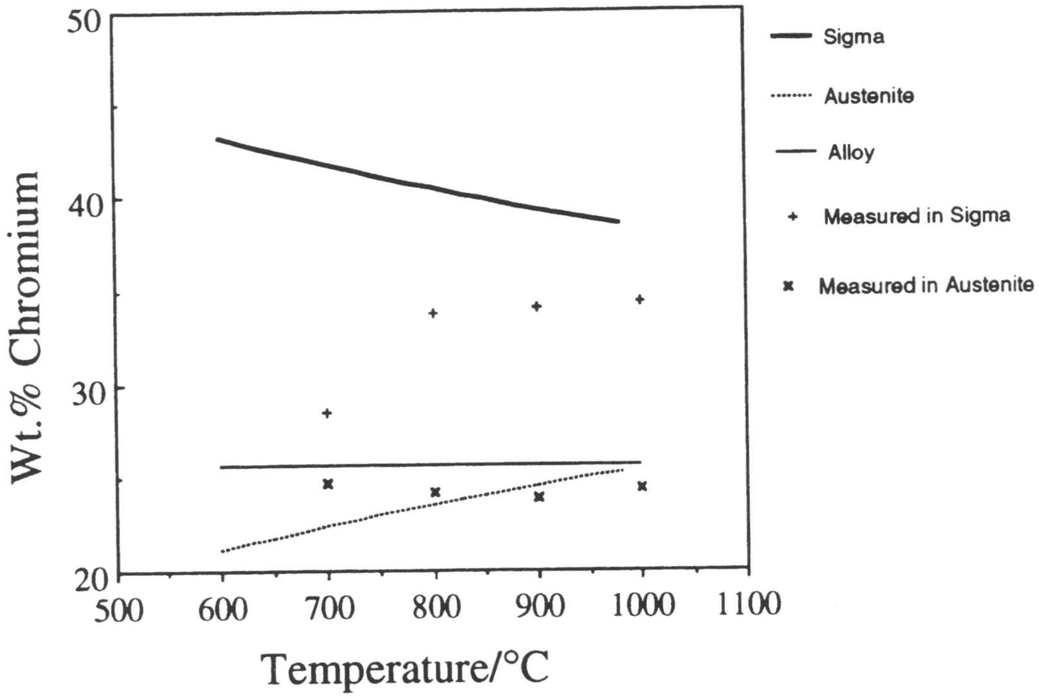

Figure 7.34. The measured partitioning of chromium between austenite and sigma phase in super duplex stainless steel weld metal A219.

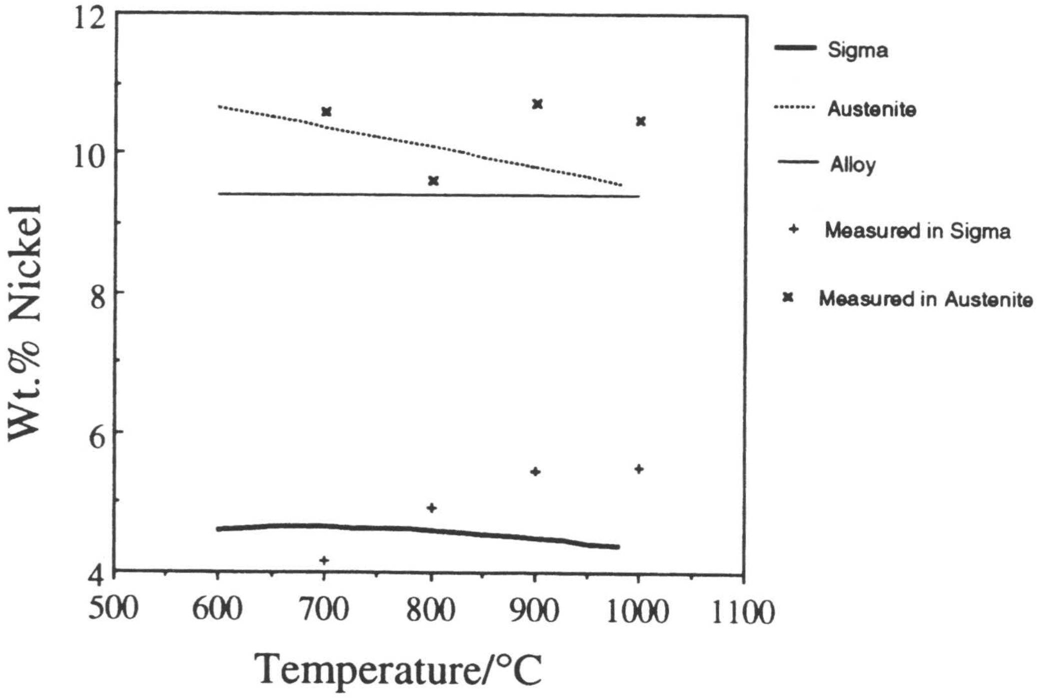

Figure 7.35. The measured partitioning of nickel between austenite and sigma phase in super duplex stainless steel weld metal A219.

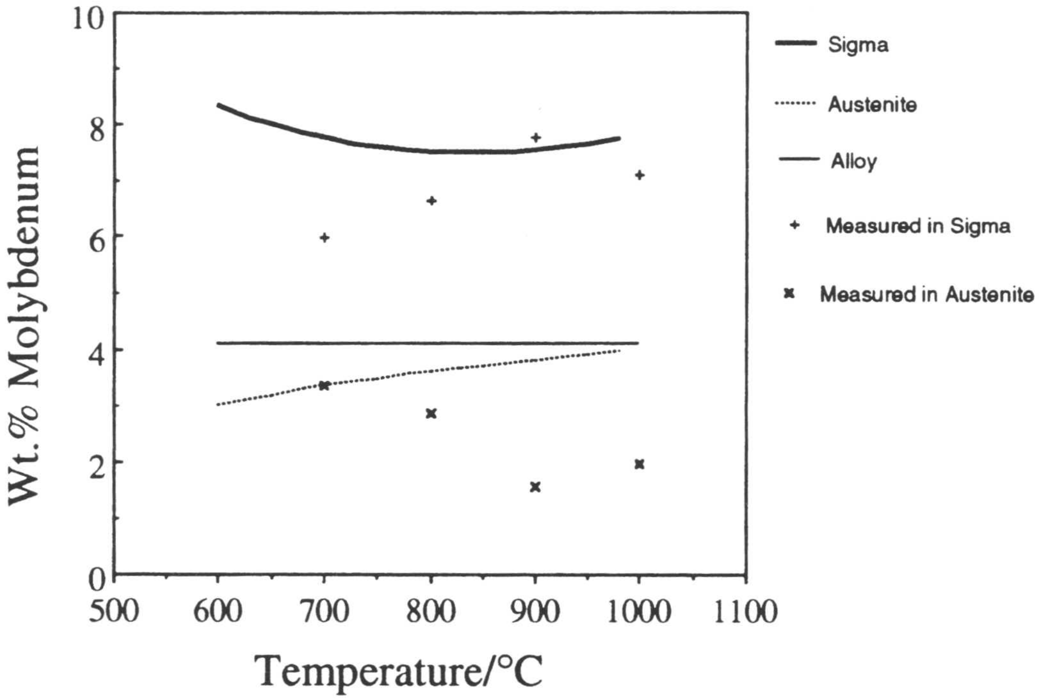

Figure 7.36. The measured partitioning of molybdenum between austenite and sigma phase in super duplex stainless steel weld metal A219.

7.9 Conclusions

1. During ageing over the temperature range 700-1050 °C, sigma phase becomes a more prominent phase than ferrite in super duplex weld metal A219.

2. The measured C-curves for sigma phase formation in alloy A219 show that the temperature range that sigma precipitate has widened for super duplex stainless steel compared with the ordinary grades. This is due to higher amount of Cr and Mo in the super grade (these two elements are very strong sigma formers).

3. Although the thermodynamic calculations show that sigma is not stable at temperatures above 980 °C in super duplex stainless steel alloy A219, it was observed in the specimens aged up to 1050 °C.

4. The hardness of the specimens aged at temperature range 700-1050 °C for enough time was much higher than the received material (in the case of specimen aged at 900 °C for four hours the hardness was found to be 1.5 times of the received material). The optical and TEM observations of the aged specimens showed a massive formation of sigma phase specially in the specimens aged at

700, 800, 900 and 1000 °C for long time. This shows that sigma phase is a hard phase and its presence will increase the hardness of the steel.

5. The TEM EDX data for the sigma phase formed in the aged specimens indicates that sigma phase is rich in Cr and Mo leaving the surrounding area low in Cr and Mo content. As these steels gain their corrosion properties from these two elements precipitation of sigma must have a detrimental consequence on corrosion properties.

Chapter 8

CONCLUSIONS AND FUTURE WORK

The microstructure of duplex stainless steels, particularly the balance between the ferrite and austenite phases can be controlled using heat treatment or alloy modification, in a way which is to a large extent predictable using phase stability calculations. This is particularly true of the trends in microstructure, which rely mostly on the thermodynamics of transformations. For example, there is no doubt that elements like chromium and molybdenum are strong ferrite stabilisers whereas nickel partitions into austenite. The concept of chromium and nickel "equivalents" also seems to work reasonably well in the sense that such parameters can represent the results of multicomponent phase diagram calculations without any major discrepancies.

Some specific results are that both thermodynamic and experimental data show that in most cases, only ferrite and austenite are the stable phases in commercial duplex and super–duplex alloys over the temperature range 1100–1300 °C, over which most of the microstructure evolves during cooling of welds. An exception is alloy A219 which reveals a tendency to form sigma–phase at about 1100 °C due to its exceptionally high chromium and molybdenum concentrations.

The formation of austenite (from ferrite) in all of the alloys is accompanied by a drop in the hardness, but this is not the case if chromium nitride also precipitates on a fine scale, as is the case with A219. Alloy A219 has an exceptionally high nitrogen concentration making it conducive to nitride formation.

Unlike duplex stainless steels, it is found that super–duplex stainless steels cannot solidify into a fully ferritic microstructure. To do so would allow the liquid phase to exist at incredibly low temperatures. Consequently, the super–duplex weld microstructure shows two major categories. The ferrite phase leads solidification, and those regions give a microstructure which is not too different from duplex steels. The trailing austenite front with the liquid leads to a microstructure which looks quite different, with rather blocky austenite. The chemical compositions of the austenite formed by solidification and that formed by solid state transformation from ferrite will also be different.

The reheated regions of multipass welds consist of two distinct zones, those regions which are ferritised and others which are tempered. The fraction of austenite in the former is always less than in the latter, since the retransformation of newly formed ferrite during cooling is somewhat sluggish. The tempering, on the other hand, causes the fraction of austenite to increase towards equilibrium.

Sigma-phase formation has also been studied. In some cases, microstructures can be produced in which all of the ferrite is replaced by austenite and sigma. This is because the formation of sigma depletes the surroundings of ferrite stabilising elements, causing an enhanced tendency for the remaining microstructure to transform into austenite. The important mechanical property of duplex stainless steels is the strength, which is enhanced by ferrite, when compared with austenitic stainless steels. An examination of the literature indicates that the achievement of toughness does not seem to be a pressing problem for duplex and super-duplex alloys.

Otherwise, the most important property of concern is the corrosion resistance, and requires the establishment of microstructure/corrosion relationships.

What is really needed is detailed kinetic theory capable of predicting the nucleation and growth rate of individual phases, so that the evolution of the microstructure can be studied. At the moment this is rather difficult because the fundamental mechanisms of transformation are not clearly established.

APPENDIX A

```
Copyright S. Sharafi and H. K. D. H. Bhadeshia, University of Cambridge
C DUPLEX STAINLESS STEELS - THERMODYNAMICS AND KINETICS 10 OCTOBER 1990
      IMPLICIT REAL*8(A-H,K-Z), INTEGER(I,J)
      DOUBLE PRECISION D(40,26),CTEMP(40,20),AUST(40,20),NI(40),CR(40),
     &                 A(40,3),CON(3),COEFFT(6,3)
C
C Typical dataset
C
C Identification number T-delta (centigrade) Number of Ctemp-%aust data
C      C  Si Mn P  S  Cr Ni Mo  W Co V
C      Nb Cu Al Sn Ti Pb As Sb Zr B  N
C      O
C  CTEMP VOL% AUST
C CTEMP VOL% AUST
C
       IN=0
       DO 1 I=1,40
          READ(5,*,END=4) D(I,1), D(I,2),IREAD
          READ(5,*)D(I,4),D(I,5),D(I,6),D(I,7),D(I,8),D(I,9),
     &             D(I,10),D(I,11),D(I,12),D(I,13),D(I,14)
          READ(5,*)D(I,15),D(I,16),D(I,17),D(I,18),D(I,19),D(I,20),
     &             D(I,21),D(I,22),D(I,23),D(I,24),D(I,25)
          READ(5,*)D(I,26)
C
                     DO 2 J=1,IREAD
                        READ(5,*)CTEMP(I,J),AUST(I,J)
2                    CONTINUE
C----------------------------------------------------------------------------
C         WRITE(6,33) D(I,1), D(I,2),IREAD
C          WRITE(6,34)D(I,4),D(I,5),D(I,6),D(I,7),D(I,8),D(I,9),
C     &             D(I,10),D(I,11),D(I,12),D(I,13),D(I,14)
C          WRITE(6,34)D(I,15),D(I,16),D(I,17),D(I,18),D(I,19),D(I,20),
C     &             D(I,21),D(I,22),D(I,23),D(I,24),D(I,25)
C          WRITE(6,34)D(I,26)
C33       FORMAT(2D10.2,I9)
C34       FORMAT(12D10.2)
C
C                     DO 22 J=1,IREAD
C                       WRITE(6,34)CTEMP(I,J),AUST(I,J)
C22                   CONTINUE
C
C----------------------------------------------------------------------------

        IN=IN+1
1       CONTINUE
4       CONTINUE
C-------------------------------------------------------------------------------.
C calculate Ni and Cr equivalents
C  NIEQ = Ni + Co + 0.5Mn + 0.3Cu + 30C + 25N all units wt.%
C                                             note that N read in ppm by wt.
C  CREQ = Cr + 2.0Si + 1.5Mo + 5.0V + 5.5Al + 0.75Nb + 1.5Ti + 0.75W wt.%
C   Ref.27 of Naseem Haddad's Thesis (1989), C, N, Mo coefficients changed
C
       DO 3 I=1,40
       NI(I)=D(I,10) + D(I,13) + 0.5*D(I,6) + 0.3*D(I,16) +
     &       15.0*D(I,4) + 13.0*1.0D-04*D(I,25)
       CR(I)=D(I,9) + 2.0*D(I,5) + 3.0*D(I,11) + 5.0*D(I,14)
```

```
     &      + 5.5*D(I,17) + 0.75*D(I,15) + 1.5* D(I,19) + 0.75*D(I,12)


3      CONTINUE
C end calculation of Ni and Cr equivalents
C-------------------------------------------------------------------------------
C
222    CONTINUE
         DO 5 I5=1,IN
                A(I5,1)=NI(I5)
               A(I5,2)=CR(I5)
               A(I5,3)=D(I5,2)
5        CONTINUE
C
C-------------------------------------------------------------------------------
      CALL MREG3(A,IN,CON,COEFFT)
      WRITE(6,103)
103   FORMAT(//10X,'STEEL',' Calculated T-delta ',' Actual   T-delta'/)
      DO 101 I=1,IN
      TDELC=CON(1) + COEFFT(1,1)*A(I,1) + COEFFT(2,1)*A(I,2)
      WRITE(6,102)I,TDELC,A(I,3)
102   FORMAT(10X,I5,2F20.0)
101   CONTINUE

      STOP
      END
C******************************************************************************:
C******************************************************************************:
C
C     Regression analysis subroutine, four variables
      SUBROUTINE MREG3(A,N,CON,COEFFT)
      IMPLICIT REAL*8 (A-H,O-Z)
      DOUBLE PRECISION A(40,3), XBAR(3), STD(3), SSP(3,3),
     *CORR(3,3),RESULT(13),
     *COEFFT(6,3),RIM(3,3), C(3,4), W(3,3), CON(3)
      INTEGER I, M, N, J, IFAIL,NI
      M = 3
      WRITE (6,99996) M, N, (J,J=1,M), (I,(A(I,J),J=1,M),I=1,N)
      IFAIL = 1
      CALL G02BAF(N, M, A, 40, XBAR, STD, SSP, 3, CORR, 3, IFAIL)
      IF (IFAIL) 20, 40, 20
   20 WRITE (6,99995) IFAIL
      GO TO 60
   40 WRITE (6,99994) (I,XBAR(I),STD(I),I=1,M)
      WRITE (6,99993) (I,I=1,M), (I,(SSP(I,J),J=1,M),I=1,M)
      WRITE (6,99992) (I,I=1,M), (I,(CORR(I,J),J=1,M),I=1,M)
   60 CONTINUE
99996 FORMAT (32H0NUMBER OF VARIABLES (COLUMNS) =, I1/10H NUMBER OF,
      * 22H CASES     (ROWS)    =, I3//17H DATA MATRIX IS:-//1H ,
      * 3I12/(1H , I3, 3D12.4))
99995 FORMAT (22H0ROUTINE FAILS, IFAIL=, I2)
99994 FORMAT (28H0VARIABLE   MEAN    ST. DEV./(1H , I5, 2D11.4))
99993 FORMAT (49H0SUMS OF SQUARES AND CROSS-PRODUCTS OF DEVIATIONS/
     * 1H , 3I12/(1H , I3, 3D12.4))
99992 FORMAT (25H0CORRELATION COEFFICIENTS/1H , 3I12/(1H , I3,
      * 3D12.4))
      NI = M - 1
      IFAIL = 1
      CALL G02CGF(N, M, NI, XBAR, SSP, 3, CORR, 3, RESULT,COEFFT, 6,
     * CON, RIM, 3, C, 3, W, 3, IFAIL)
```

```
      IF (IFAIL) 21, 41, 21
   21 CONTINUE
      WRITE (6,88885) IFAIL
      GO TO 61
   41 CONTINUE
      WRITE (6,88884) (I,(COEFFT(I,J),J=1,3),I=1,NI)
      WRITE (6,88883) (CON(I),I=1,3)
      WRITE (6,88882) (RESULT(I),I=1,13)
   61 CONTINUE
      RETURN
88885 FORMAT (22H0ROUTINE FAILS, IFAIL=, I2/)
88884 FORMAT (43H0VBLE     COEFFT       STD ERR      T-VALUE/2(1H ,
     * I3, 3D13.4/))
88883 FORMAT (6H0CONST, F11.4, 2F13.4/)
88882 FORMAT (32H0ANALYSIS OF REGRESSION TABLE :-//13H       SOURCE,
     * 55H        SUM OF SQUARES  D.F.    MEAN SQUARE     F-VALUE//
     * 18H DUE TO REGRESSION, F14.4, F8.0, 2F14.4/14H ABOUT  REGRES,
     * 4HSION, F14.4, F8.0, F14.4/18H TOTAL            , F14.4,
     * F8.0///29H STANDARD ERROR OF ESTIMATE =, F8.4/11H MULTIPLE C,
     * 18HORRELATION (R)   =, F8.4/29H DETERMINATION (R SQUARED)  =,
     * F8.4/29H CORRECTED R SQUARED        =, F8.4/)
      END
```

APPENDIX B

```
Copyright S. Sharafi and H. K. D. H. Bhadeshia, University of Cambridge
C DUPLEX STAINLESS STEELS - THERMODYNAMICS AND KINETICS 10 OCTOBER 1990
      IMPLICIT REAL*8(A-H,K-Z), INTEGER(I,J)
      DOUBLE PRECISION D(40,26),CTEMP(40,20),AUST(40,20),NI(40),CR(40),
     &                 A(40,3),CON(3),COEFFT(6,3),RESULT(13)
C
C Typical dataset
C
C Identification number T-delta (centigrade) Number of Ctemp-%aust data
C      C  Si Mn P  S  Cr Ni Mo  W Co V
C      Nb Cu Al Sn Ti Pb As Sb Zr B  N
C      O
C  CTEMP VOL% AUST
C CTEMP VOL% AUST
C
       IN=0
       DO 1 I=1,40
          READ(5,*,END=4) D(I,1), D(I,2),IREAD
          READ(5,*)D(I,4),D(I,5),D(I,6),D(I,7),D(I,8),D(I,9),
     &             D(I,10),D(I,11),D(I,12),D(I,13),D(I,14)
          READ(5,*)D(I,15),D(I,16),D(I,17),D(I,18),D(I,19),D(I,20),
     &             D(I,21),D(I,22),D(I,23),D(I,24),D(I,25)
          READ(5,*)D(I,26)
C
                     DO 2 J=1,IREAD
                        READ(5,*)CTEMP(I,J),AUST(I,J)
2                    CONTINUE
C------------------------------------------------------------------------------

        IN=IN+1
1       CONTINUE
4       CONTINUE
C---------------------------------------------------------------------------------
      AAC=4
      DO 201 IAAC=1,20
      AAN=8
      DO 202 IAAN=1,20
      AAMO=2.4
      DO 203 IMO=1,10
C calculate Ni and Cr equivalents
C  NIEQ = Ni + Co + 0.5Mn + 0.3Cu + 30C + 25N all units wt.%
C                                              note that N read in ppm by wt.
C  CREQ = Cr + 2.0Si + 1.5Mo + 5.0V + 5.5Al + 0.75Nb + 1.5Ti + 0.75W wt.%
C   Ref.27 of Naseem Haddad's Thesis (1989)
C
       DO 3 I=1,40
       NI(I)=D(I,10) + D(I,13) + 0.5*D(I,6) + 0.3*D(I,16) +
     &       AAC*D(I,4) + AAN*1.0D-04*D(I,25)
       CR(I)=D(I,9) + 2.0*D(I,5) + AAMO*D(I,11) + 5.0*D(I,14)
     &       + 5.5*D(I,17) + 0.75*D(I,15) + 1.5* D(I,19) + 0.75*D(I,12)
3      CONTINUE
C end calculation of Ni and Cr equivalents
C---------------------------------------------------------------------------------
C
222    CONTINUE
         DO 5 I5=1,IN
                 A(I5,1)=NI(I5)
```

```
                A(I5,2)=CR(I5)
                A(I5,3)=D(I5,2)
5        CONTINUE
C
C-------------------------------------------------------------------------------
      CALL MREG3(A,IN,CON,COEFFT,RESULT)
      IF(DABS(RESULT(11)) .LT. 0.891) GOTO 400
      WRITE(6,110)AAC,AAN,AAMO
110   FORMAT(' AAC, AAN, AAMO', 3F8.2)
400   CONTINUE
      AAMO=AAMO+0.5
203   CONTINUE
      AAN=AAN+2.0
202   CONTINUE
      AAC=AAC+2.0
201   CONTINUE
      STOP
      END
C********************************************************************************
C********************************************************************************
C
C     Regression analysis subroutine, four variables
      SUBROUTINE MREG3(A,N,CON,COEFFT,RESULT)
      IMPLICIT REAL*8 (A-H,O-Z)
      DOUBLE PRECISION A(40,3), XBAR(3), STD(3), SSP(3,3),
     *CORR(3,3),RESULT(13),
     *COEFFT(6,3),RIM(3,3), C(3,4), W(3,3), CON(3)
      INTEGER I, M, N, J, IFAIL,NI
      M = 3
      IFAIL = 1
      CALL G02BAF(N, M, A, 40, XBAR, STD, SSP, 3, CORR, 3, IFAIL)
      IF (IFAIL) 20, 40, 20
   20 WRITE (6,99995) IFAIL
      GO TO 60
   40 CONTINUE
   60 CONTINUE
99995 FORMAT (22H0ROUTINE FAILS, IFAIL=, I2)
      NI = M - 1
      IFAIL = 1
      CALL G02CGF(N, M, NI, XBAR, SSP, 3, CORR, 3, RESULT,COEFFT, 6,
     * CON, RIM, 3, C, 3, W, 3, IFAIL)
      IF(DABS(RESULT(11)) .LT. 0.891)GOTO 61
      IF (IFAIL) 21, 41, 21
   21 CONTINUE
      WRITE (6,88885) IFAIL
      GO TO 61
   41 CONTINUE
      WRITE (6,88884) (I,(COEFFT(I,J),J=1,3),I=1,NI)
      WRITE (6,88883) (CON(I),I=1,3)
      WRITE (6,88882) RESULT(11)
   61 CONTINUE
88885 FORMAT (22H0ROUTINE FAILS, IFAIL=, I2/)
88884 FORMAT (43H0VBLE     COEFFT       STD ERR      T-VALUE/2(1H ,
    * I3, 3D13.4))
88883 FORMAT (6H0CONST, F11.4, 2F13.4)
88882 FORMAT ('Multiple regression correlation = ',F8.5)
      RETURN
      END
```

APPENDIX C

```
Copyright S. Sharafi and H. K. D. H. Bhadeshia, University of Cambridge
C DUPLEX STAINLESS STEELS - THERMODYNAMICS AND KINETICS 10 OCTOBER 1990
      IMPLICIT REAL*8(A-H,K-Z), INTEGER(I,J)
      DOUBLE PRECISION D(40,26),CTEMP(40,20),AUST(40,20),NI(40),CR(40),
     &   A(40,3),CON(3),COEFFT(6,3),CTEMP2(500),VOLAUS(500),ARES(20)
C
C Typical dataset
C
C Identification number T-delta (centigrade) Number of Ctemp-%aust data
C      C  Si Mn P  S  Cr Ni Mo  W Co V
C      Nb Cu Al Sn Ti Pb As Sb Zr B  N
C      O
C  CTEMP VOL% AUST
C CTEMP VOL% AUST
C
       IN=0
       IALL=0
       DO 1 I=1,40
          READ(5,*,END=4) D(I,1), D(I,2),IREAD
          READ(5,*)D(I,4),D(I,5),D(I,6),D(I,7),D(I,8),D(I,9),
     &             D(I,10),D(I,11),D(I,12),D(I,13),D(I,14)
          READ(5,*)D(I,15),D(I,16),D(I,17),D(I,18),D(I,19),D(I,20),
     &             D(I,21),D(I,22),D(I,23),D(I,24),D(I,25)
          READ(5,*)D(I,26)
C
                     DO 2 J=1,IREAD
                        IALL=IALL+1
                        READ(5,*)CTEMP(I,J),AUST(I,J)
                        CTEMP2(IALL)=DLOG(D(I,2)+1.0 - CTEMP(I,J))
                        VOLAUS(IALL)=DLOG(AUST(I,J)+0.1D-1)
2                    CONTINUE
C----------------------------------------------------------------------------
C         WRITE(6,33) D(I,1), D(I,2),IREAD
C          WRITE(6,34)D(I,4),D(I,5),D(I,6),D(I,7),D(I,8),D(I,9),
C     &             D(I,10),D(I,11),D(I,12),D(I,13),D(I,14)
C          WRITE(6,34)D(I,15),D(I,16),D(I,17),D(I,18),D(I,19),D(I,20),
C     &             D(I,21),D(I,22),D(I,23),D(I,24),D(I,25)
C          WRITE(6,34)D(I,26)
C33       FORMAT(2D10.2,I9)
C34       FORMAT(12D10.2)
C
C                     DO 22 J=1,IREAD
C                       WRITE(6,34)CTEMP(I,J),AUST(I,J)
C22                   CONTINUE
C
C----------------------------------------------------------------------------

        IN=IN+1
1       CONTINUE
4       CONTINUE
C-------------------------------------------------------------------------------
      AAC=11.0D+00
      AAN=15.0D+00
      AAMO=3.0D+00
C calculate Ni and Cr equivalents
C  NIEQ = Ni + Co + 0.5Mn + 0.3Cu + 30C + 25N all units wt.%
C                                             note that N read in ppm by wt.
```

```
C  CREQ = Cr + 2.0Si + 1.5Mo + 5.0V + 5.5Al + 0.75Nb + 1.5Ti + 0.75W wt.%
C   Ref.27 of Naseem Haddad's Thesis (1989)
C
        DO 3 I=1,40
        NI(I)=D(I,10) + D(I,13) + 0.5*D(I,6) + 0.3*D(I,16) +
     &       AAC*D(I,4) + AAN*1.0D-04*D(I,25)
        CR(I)=D(I,9) + 2.0*D(I,5) + AAMO*D(I,11) + 5.0*D(I,14)
     &       + 5.5*D(I,17) + 0.75*D(I,15) + 1.5* D(I,19) + 0.75*D(I,12)
3       CONTINUE
C end calculation of Ni and Cr equivalents
C-------------------------------------------------------------------------------
C
222     CONTINUE
          DO 5 I5=1,IN
                  A(I5,1)=NI(I5)
                 A(I5,2)=CR(I5)
                 A(I5,3)=D(I5,2)
5         CONTINUE
C
C-------------------------------------------------------------------------------
       CALL MREG3(A,IN,CON,COEFFT)
       WRITE(6,103)
103    FORMAT(//10X,'STEEL',' Calculated T-delta ',' Actual   T-delta'/)
       DO 101 I=1,IN
       TDELC=CON(1) + COEFFT(1,1)*A(I,1) + COEFFT(2,1)*A(I,2)
       WRITE(6,102)I,TDELC,A(I,3)
102    FORMAT(10X,I5,2F20.0)
101    CONTINUE
       CALL MREG2(CTEMP2,VOLAUS,IALL,ARES)
       WRITE(6,104) ARES(6),ARES(7)
104    FORMAT(10X,' COEFFICIENTS ARES6, ARES7',2D12.4)
          DO  1001 I=1,IALL
              VOLA=ARES(6)*CTEMP2(I)+ARES(7)
              VOLA=DEXP(VOLA)-0.1D-1
              VOLB=DEXP(VOLAUS(I))-0.1D-1
              WRITE(6,1000)VOLA,VOLB
1000          FORMAT(2F8.1)
1001          CONTINUE



       STOP
       END
C******************************************************************************:
C******************************************************************************:
       SUBROUTINE MREG2(X,Y,N,RESULT)
       IMPLICIT REAL*8 (A-H,O-Z)
       DOUBLE PRECISION X(500), Y(500), RESULT(20)
       INTEGER I, IFAIL, N
        WRITE(6,99996)(I,X(I),Y(I),I=1,N)
       IFAIL = 1
       CALL G02CAF(N, X, Y, RESULT, IFAIL)
C
C      TEST IFAIL
C
       IF (IFAIL) 20, 40, 20
   20 WRITE (6,99995) IFAIL
       GO TO 60
   40 WRITE (6,99994) (RESULT(I),I=1,5)
       WRITE (6,99993) RESULT(6), RESULT(8), RESULT(10)
```

```
      WRITE (6,99992) RESULT(7), RESULT(9), RESULT(11)
      WRITE (6,99991) (RESULT(I),I=12,20)
   60 CONTINUE
99997 FORMAT (2F10.5)
99996 FORMAT (36H0 CASE     INDEPENDENT     DEPENDENT/10H NUMBER   ,
     * 25H  VARIABLE       VARIABLE//(1H , I4, 2F15.4))
99995 FORMAT (22H0ROUTINE FAILS, IFAIL=, I2/)
99994 FORMAT (46H0MEAN OF INDEPENDENT VARIABLE               = ,
     * F8.4/46H MEAN OF   DEPENDENT VARIABLE               = ,
     * F8.4/46H STANDARD DEVIATION OF INDEPENDENT VARIABLE = ,
     * F8.4/46H STANDARD DEVIATION OF   DEPENDENT VARIABLE = ,
     * F8.4/46H CORRELATION COEFFICIENT                    = , F8.4)
99993 FORMAT (46H0REGRESSION COEFFICIENT                     = ,
     * D12.4/46H STANDARD ERROR OF COEFFICIENT              = ,
     * F8.4/46H T-VALUE FOR COEFFICIENT                    = , F8.4)
99992 FORMAT (46H0REGRESSION CONSTANT                        = ,
     * D12.4/46H STANDARD ERROR OF CONSTANT                 = ,
     * F8.4/46H T-VALUE FOR CONSTANT                       = , F8.4)
99991 FORMAT (32H0ANALYSIS OF REGRESSION TABLE :-//13H       SOURCE,
     * 55H        SUM OF SQUARES  D.F.    MEAN SQUARE     F-VALUE//
     * 18H DUE TO REGRESSION, F14.4, F8.0, 2F14.4/14H ABOUT  REGRES,
     * 4HSION, F14.4, F8.0, F14.4/18H TOTAL            , F14.4,
     * F8.0)
      RETURN
      END

C*******************************************************************************:
C*******************************************************************************:
C
C     Regression analysis subroutine, four variables
      SUBROUTINE MREG3(A,N,CON,COEFFT)
      IMPLICIT REAL*8 (A-H,O-Z)
      DOUBLE PRECISION A(40,3), XBAR(3), STD(3), SSP(3,3),
     *CORR(3,3),RESULT(13),
     *COEFFT(6,3),RIM(3,3), C(3,4), W(3,3), CON(3)
      INTEGER I, M, N, J, IFAIL,NI
      M = 3
      WRITE (6,99996) M, N, (J,J=1,M), (I,(A(I,J),J=1,M),I=1,N)
      IFAIL = 1
      CALL G02BAF(N, M, A, 40, XBAR, STD, SSP, 3, CORR, 3, IFAIL)
      IF (IFAIL) 20, 40, 20
   20 WRITE (6,99995) IFAIL
      GO TO 60
   40 WRITE (6,99994) (I,XBAR(I),STD(I),I=1,M)
      WRITE (6,99993) (I,I=1,M), (I,(SSP(I,J),J=1,M),I=1,M)
      WRITE (6,99992) (I,I=1,M), (I,(CORR(I,J),J=1,M),I=1,M)
   60 CONTINUE
99996 FORMAT (32H0NUMBER OF VARIABLES (COLUMNS) =, I1/10H NUMBER OF,
     * 22H CASES     (ROWS)    =, I3//17H DATA MATRIX IS:-//1H ,
     * 3I12/(1H , I3, 3D12.4))
99995 FORMAT (22H0ROUTINE FAILS, IFAIL=, I2)
99994 FORMAT (28H0VARIABLE   MEAN    ST. DEV./(1H , I5, 2D11.4))
99993 FORMAT (49H0SUMS OF SQUARES AND CROSS-PRODUCTS OF DEVIATIONS/
     * 1H , 3I12/(1H , I3, 3D12.4))
99992 FORMAT (25H0CORRELATION COEFFICIENTS/1H , 3I12/(1H , I3,
     * 3D12.4))
      NI = M - 1
      IFAIL = 1
      CALL G02CGF(N, M, NI, XBAR, SSP, 3, CORR, 3, RESULT,COEFFT, 6,
     * CON, RIM, 3, C, 3, W, 3, IFAIL)
```

```
      IF (IFAIL) 21, 41, 21
   21 CONTINUE
      WRITE (6,88885) IFAIL
      GO TO 61
   41 CONTINUE
      WRITE (6,88884) (I,(COEFFT(I,J),J=1,3),I=1,NI)
      WRITE (6,88883) (CON(I),I=1,3)
      WRITE (6,88882) (RESULT(I),I=1,13)
   61 CONTINUE
88885 FORMAT (22H0ROUTINE FAILS, IFAIL=, I2/)
88884 FORMAT (43H0VBLE     COEFFT       STD ERR      T-VALUE/2(1H ,
     * I3, 3D13.4/))
88883 FORMAT (6H0CONST, F11.4, 2F13.4/)
88882 FORMAT (32H0ANALYSIS OF REGRESSION TABLE :-//13H       SOURCE,
     * 55H        SUM OF SQUARES  D.F.    MEAN SQUARE     F-VALUE//
     * 18H DUE TO REGRESSION, F14.4, F8.0, 2F14.4/14H ABOUT  REGRES,
     * 4HSION, F14.4, F8.0, F14.4/18H TOTAL            , F14.4,
     * F8.0///29H STANDARD ERROR OF ESTIMATE =, F8.4/11H MULTIPLE C,
     * 18HORRELATION (R)   =, F8.4/29H DETERMINATION (R SQUARED)  =,
     * F8.4/29H CORRECTED R SQUARED        =, F8.4/)
      RETURN
      END
```

REFERENCES

Abron, R. H. and Bain, E. C., (1930)
Trans. Amer. Soc. Steel Treating, **8**, p. 837.

Bain, E.C. and Griffiths, W.E., (1927)
Trans. AIME, **75**, p. 166.

Bechtoldt, C. J. and Vacher, H. C., (1957)
J. Res. Nat. Bur. Stand., **58**, p. 7.

Bhadeshia, H.K.D.H.; David, S.A. and Vitek, J.M., (1991)
Materials Science and Technology, **7**, p. 50.

Bowman, A.L.; Arnold, G.P.; Storms, E.K. and Nereson, N.G., (1972)
Acta Cryst. B, **28**, p. 3102.

Briggs, J.Z. and Parker, T.D., (1965)
The Super 12 wt.% Cr Steels, Climax Molybdenum Co., supplement 1983.

Bywater, K.A. and Gladman, T., (1976)
Met. Technology, **3**, 358.

Castro, R. and de Cadenet, J.J., (1968)
Welding Metallurgy of Stainless and Heat-Resisting Steels, Dunod, p. 77.

Chance, J.; Gradwell, K.J.; Coop, W. and Roscoe, C.V., (1982)
Proceeding of Inter. Conference of Duplex Stainless Steels, The USA, Paper 8201-019, p. 371.

Clark, C. A.; Gentil, P. and Guha, P., (1986)
Proceeding of Inter. Conference of Duplex Stainless Steels, The Netherlands, Paper 52, p. 109.

Climax Molybdenum Co., (1977)
Proceedings of Inter. Conference of Stainless Steel, London, p. 57.

Dawson, G.W. and Judson, P., (1982)
Second Intrn. Conf. on Offshore Welded Structure, London, p. 127.

Easterling, K., (1983)
Introduction to the Physical Metallurgy of Welding, London, p. 83.

Eriksson, S., (1934)
Jernkonttorets Annaler, **118**, p. 530.

Evans, D.A. and Jack, K.H., (1957)
Acta Cryst, **10**, p. 769.

Farrar, R. A., (1987)
J. Mat. Sci., **22**, p. 363.

Faucheur, D. and Gilbert, D., (1986)
Proceeding of Inter. Conference of Duplex Stainless Steels, The Netherlands, Paper 38, p. 83.

Folkhard, E., (1988)
Welding Metallurgy of Stainless Steels, Wein -New York, p. 25.

Geisen, W., (1909)
ISI Carnegie Scholarship Memoirs, **1**, p.1.

Gordon, G. M., (1977)
in Proc. Firminy Conf. NACE, Houston, Texas, p. 893.

Guha, P. and Clark, C.A., (1982)
Proceeding of Inter. Conference of Duplex Stainless Steels, The USA, Paper 8201-018, p. 355.

Guillet, L., (1904)
Rev. de Met., **2**, p.155.

Ha, H.C.; Pyun, S.I. and Lim, C., (1991)
Material Science and Engineering, **A131**, p. 231.

Haddad, N.I.A., (1989)
Ph.D. Thesis, University of Cambridge, Dept. of Mat. Sci. and Metallurgy, p. 28.

Hadfield, R.A., (1892)
JISI, **2**, p.49.

Hall, E.O. and Algie, S.H., (1966)
Met. Rev., **11**, p. 61.

Hammar, O. and Svensson, U, (1979)
Proceedings of Inter. Conference of Solidification and Casting of Metals, UK, p. 401.

Hansen, M. and Anderko, K., (1958)
Constitution of Binary Alloys, McGraw-Hill, p. 527.

Herbsleb, G. and Schwaab, P., (1982)
Proceeding of Inter. Conference of Duplex Stainless Steels, USA, Paper 8201-002, p. 15.

Hillert, M.; Jansson, B. and Sundman, B., (1988)
Application of the Compound-Energy Model to Oxide Systems, Zeit. Metallkde.79, p. 81-87.

Hilty, D.C. and Kaveney, T.F., (1977)
Handbook of Stainless Steels, New York, p.3.1.

Hochmann, J.; Desestret, A.; Jolly, P. and Mayound, R., (1974)
Met. Corr. Industrie, 591/592, part I, p. 390.

Hodson, S.M., (1989)
National Physic Laboratory, MTDATA Handbook, Multiphase Theory.

Honeycombe, J. and Gooch, T.G., (1985)
The Weld Inst., UK, Report 286.

Josefsson, B.; Nilsson, J.O. and Wilson, A., (1991)
Internal Report, AB SANDVIK STEEL, Sweden.

Karlsson, L. and Pak, S., (1991)
Inter. Conf. on Stainless Steel, Chiba, Japan, p. 1101.

Karlsson, L.; Pak, S. and Andersson, S.L., (1991)
Inter. Conf. on Stainless Steel, Chiba, Japan, p. 1093.

Kasper, J.S., (1954)
Acta Met., **2**, p. 456.

Kubaschewski, O., (1982)
Iron-Binary Phase Diagrams, Springer-Verlag Berlin, p. 31.

Laing, B.S.; Jones, R.L.; Randall, M.D. and Teale, R.A., (1986)
Proceeding of Inter. Conference of Duplex Stainless Steels, The Netherlands, Paper 29, p. 30.

Leach, J.C.C.; Rodgers, A. and Sheehan, G., (1978)
Secondary Steelmaking, The Metals Society (London), p.73.

Leach, J.C.C., (1982)
Steel Times, **210(10)**, p.577.

Leslie, W.C., (1981)
The Physical Metallurgy of Steels, Mc Graw-Hill, Washington.

Machara, Y., (1983)
Metal Science, **17**, p. 541.

Maehara, Y.; Ohmori, Y.; Murayama, J.; Fujino, N. and Kunitake, T., (1983)
Metal Sci., **17**, p. 541.

Marshall,P., (1984)
Austenitic Stainless Steels, Elsevier Applied Science Publishers, London.

Mundt, R. and Hoffmeister, H., (1983)
Arch. Eisenhuttenwes, **54(6)**, p. 253.

Nagano, H.; Kudo, T.; Inaba, Y. and Harada, M., (1981)
Metaux Corrosion Industrie, **No. 667**, p. 23.1.

Netzsch Company, (1989)
Instrument Manual, Germany, p. 1-6.

Nilsson J.O. and Liu, P., (1988)
AB Sandvik Steel, Internal Report, No 5603.

Nilsson J.O. and Liu, P., (1991)
Inter. Conf. on Stainless Steel, Chiba, Japan, p. 1109.

Noble, D.N. and Gooch, T.G., (1986)
The Weld. Inst., UK, Report 321.

Olsson, J. and Nordin, S., (1986)
Proceeding of Inter. Conference of Duplex Stainless Steels, The Netherlands, Paper 48, p. 219.

Perteneder, E.; Tosch, J.; Reiterer, P. and Rabensteiner, G., (1986)
Proceeding of Inter. Conference of Duplex Stainless Steels, The Netherlands, Paper 21, p. 48.

Pickering, F.B., (1984)
Conf. Proc. Stainless Steel '84, Paper 2, p. 2.

Redmond, J.D. and Miska, K.H., (1982)
Chemical Engineering, October, p.79.

Rideout, S.; Manly, W.D.; Kamen, E.L.; Lement, B.S. and Beck, P.A., (1951)
Trans. AIME, **2**, p. 872.

Rivlin, V.G. and Raynor, G.V., (1980)
Inter. Metals Reviews, **1**, p. 21.

Roscoe, C.V. and Gradwell, K.J., (1986)
Proceeding of Inter. Conference of Duplex Stainless Steels, The Netherlands, Paper 34, p. 126.

Roscoe, C.V.; Gradwell, K.J. and Lorimer, G.W., (1984)
Proceeding of Inter. Conference of Stainless Steels, Sweden, p. 563.

Rouault, A.; Herpin, P. and Fruchart, R., (1970)
Ann. Chim, **5**, p. 461.

Sakai, J.; Matsushima, I.; Kamemura, Y.; Tanimura, M. and Osuka, T., (1982)
Proceeding of Inter. Conference of Duplex Stainless Steels, The USA, Paper (8201-010), p. 211.

Schaeffler, A.L., (1949)
Metal Progress, **56**, p. 680.

Schuller, H. J., (1965)
Arch. Eisenhuttenwes, **34**, p. 61.

Schweitzer, P.A., (1983)
Corrosion and Corrosion Protection Handbook, Second Edition, p. 69-84.

Sedriks, A.J., (1979)
Corrosion of Stainless Steels, Wiley, p.50-67.

Sedriks, A. J., (1983)
Inter. Metal Reviews, **28**, p. 295.

Seferian, D., (1959)
Metallurgie de la Soudure, Dunod, Paris.

Skuin, K. and Kreyssing, T., (1978)
Neue Hutte, **23(1)**, p. 22.

Smith, R. and Nutting, J., (1957)
British Journal of Applied Physics, **7**, p. 214-217.

Solomon, H.D. and Devine, T.M., (1979)
Mi Con 78, ASTM STP, p.430.

Southwick, P. D., (1978)
Ph.D. Thesis, University of Cambridge, Dept. of Mat. Sci. and Metallurgy.

Southwick, P.D., and Honeycombe, R.W.K., (1980)
Met. Sci., **14**, p. 253.

Strangwood, M. and Druce, S.G., (1990)
Material Science and Technology, **6**, 237.

Strutt, A.J.; Lorimer, G.W.; Roscoe, C.V. and Gradwell, K.J., (1986)
Proceeding of Inter. Conference of Duplex Stainless Steels, The Hague, The Netherlands, Paper 3, p. 310.

Sully, A.H. and Brandes, E.A., (1967)
Chromium, 2nd Edition, p. 77.

Sump, C. H. and Bodine, G. C., (1982)
Proceeding of Inter. Conference of Duplex Stainless Steels, The USA, Paper 8201-004, p. 71.

Suutala, N., (1983)
Third Scandinavian Symposium in Material Science, Finland, p. 53.

Suutala, N.; Takalo, T. and Mosio, T., (1979)
Met. Trans., **10A**, p. 513.

Thorvaldsson, T.; Erickson, H.; Kutka, J. and Salwen, A., (1985)
Proceeding of Inter. Conference of Stainless Steels, The Institute of Metals, p. 101.

Truman, J.E., Coleman, M.J. and Pirt, K.R., (1977)
Br. Corros. J., **12**, p. 236.

Truman, J.E., (1979)
Stainless Steel Industry, **7(39)**, p.3.

Truman, J.E., (1980)
The Metallurgist and Materials Technologist, **2**, p.75.

Wilde, B. E., (1977)
U.S. Patent, No. 4002510, Issued January 11th 1977.